BABEŞ-BOLYAI UNIVERSITY
CLUJ-NAPOCA

GHENT UNIVERSITY

Luminescence dating of Romanian loess using feldspars

ŞTEFAN VASILINIUC

Thesis submitted in fulfillment of the requirements

for the degree of Doctor (PhD) of Science:

Physics at Babeş-Bolyai University

Geology at Ghent University

Promotors:

Prof. Dr. Constantin Cosma

(Babeş-Bolyai University)

Prof. Dr. Peter van den haute

Dr. Dimitri Vandenberghe

(Ghent University)

Academic year: 2010-2011

The research results discussed in the present thesis have been obtained through the joint PhD collaboration between Babeş-Bolyai University in Cluj Napoca and Ghent University. Ştefan Vasiliniuc performed a total of 14 months of study stay at Ghent University as a PhD student.

The financial support provided by (1) The SECTORAL OPERATIONAL PROGRAMME HUMAN RESOURCES DEVELOPMENT, Contract POSDRU 6/1.5/S/3 – Doctoral studies: through science towards society and (2) Ghent University – Special Research Fund – co-funding for joint doctorate students is highly acknowledged.

Luminescence research of European loess at Ghent University is financed by the Fund for Scientific Research – Flanders (FWO Vlaanderen).

This work contains 48 figures, 9 tables and 151 references

TABLE OF CONTENTS

Chapter III
Luminescence characteristics of silt-sized and sand-sized quartz: a comparison on the Mostiştea loess-palaeosol sequence (SE Romania)

Chapter IV
Combined IRSL and post-IR OSL dating of Romanian loess using single aliquots of polymineral fine grains

Chapter V
Conventional IRSL dating of Romanian loess using single aliquots of polymineral fine grains

INTRODUCTION

Introduction

The major importance of loess deposits as records of climate change has led to an increased number of research studies worldwide. Especially in the past two decades, considerable efforts have been made in refining methods for establishing the chronological framework of loess deposition. Among the several methods applied in the study of loess, luminescence dating provides absolute depositional ages directly, measuring the mineral constituents of the sediment itself. The aeolian nature of loess makes it the perfect material luminescence for the development and testing of luminescence dating methods.

Some of the thickest loess deposits in Europe occur in South-Eastern Romania. These are believed to form the link between the glacial loess deposits of West and Central Europe and the non-glacial loess deposits that extend all the way to China. However, an absolute chronology is generally lacking, the main methods in Romanian loess studies being proxy-based methods (such as pedostratigraphy and magnetic susceptibility).

The establishment of a luminescence research group at Babeş-Bolyai University five years ago took advantage of the latest developments in luminescence dating, namely optically stimulated luminescence (OSL) from quartz corroborated with the single-aliquot regenerative-dose (SAR) protocol. This was successfully applied by Timar et al. (2010) using silt-sized quartz extracted from the loess sequence at Mircea Vodă (Dobrogea). Their results allocated the formation of the uppermost well-developed palaeosol (S1) to the last interglacial period, in agreement with previous studies of similar loess deposits in Romania, Serbia and Bulgaria. Another important outcome of the study of Timar et al. (2010) is the change in loess accumulation rate observed to have happened during the last glacial period. This change in sedimentation rate was correlated with a Marine Isotope Stage (MIS) 3 interstadial during which a weakly developed palaeosol was formed.

A further study of material collected from the sequence at Mircea Vodă was performed using sand-sized quartz grains (Timar Gabor et al., 2011). The OSL ages obtained in this study were intriguingly different from those obtained previously using silt-sized quartz. Although both sets of ages allocate the uppermost well-developed palaeosol (S1) to the MIS 5 interglacial, the attribution of the chronological position of the weakly-developed palaeosol observed in the loess unit L1 to either MIS 3 or MIS 5 is disputed. Furthermore, comparison with independent age

control (pedostratigraphy and palaeomagnetism) also indicates that the dating procedure underestimates the true burial age from the penultimate glacial period onwards. Both the age underestimation and the age-discrepancy are not yet understood.

Due to the lack of an independent and absolute age control for Romanian loess, it cannot be evaluated whether any of the quartz-based ages is accurate. This corroborated the need for examining the luminescence characteristics and age of an alternative dosimeter, such as feldspar. Feldspars have the attractive properties of emitting bright luminescence signals that continue to grow up to larger doses. At least in principle, this would allow dating over a larger age range. The advantages, however, may be offset by anomalous fading, a phenomenon that generally affects luminescence signals from feldspars and leads to age underestimation. However, recent studies using modern and alternative procedures have shown that this drawback may be overcome.

Within the framework of this thesis, two directions have been followed. The first direction was to investigate whether the quartz-based OSL ages obtained at Mircea Vodă, reflect a general characteristic of loess deposits in SE Romania. For this, we extended the OSL investigation to the loess sequence near Mostiştea Lake (Danube Plain; SE Romania), by documenting the luminescence characteristics of silt (4-11 μm) and sand-sized (63-90 μm) quartz using the SAR-OSL technique. The second and major research direction adopted in this work was to investigate infra-red stimulated luminescence (IRSL) signals obtained from feldspars extracted from Romanian loess. The investigations included an in-depth study of the luminescence signals from feldspars together with investigations on whether or not it is possible to minimize anomalous fading using newly-reported experimental conditions (e.g. a higher stimulation temperature). Various methodologies for IRSL signals were used, from 'conventional' IRSL and the 'double-SAR' to the most recently developed post-IR IRSL method.

Objectives

The main objective of this work is to establish an accurate and precise chronology for some of the most important loess sequences in Romania. For this, we investigate the potential of modern and alternative luminescence dating procedures, with the emphasis on feldspar as

dosimeter. This is aimed at providing insights into the age discrepancy that the quartz-based OSL studies have shown and also to extend the chronology of these deposits further back in time, beyond the last interglacial/glacial cycle.

Thesis outline

The thesis is composed of six chapters.

Chapter 1 presents a general description of loess and loess deposits and their potential in providing climate change information. A definition of loess and the generally accepted processes that lead to the formation of loess accumulations is given and the variety of information that may be obtained from loess research is briefly reviewed. A geographical perspective is also provided, discussing loess distribution worldwide and in Romania in particular including the study area covered by this work. The previous studies using proxy-based methods are discussed together the chronological interpretation proposed. In addition, this chapter presents the potential of luminescence dating as an absolute method for dating loess deposits together with the previous studies using this method for Romanian loess.

Chapter 2 presents an overview of luminescence dating in short descriptions of the essential concepts: luminescence phenomenon, age equation, dose rate and equivalent dose determination. A general description of feldspars is also included covering mineralogy, advantages for luminescence dating and stimulation and emission spectra. In addition, the IRSL model proposed by Hutt et al. (1988) is presented together with the more recent contributions of Poolton (2002a,b) and Jain and Ankjaergaard (2011). This chapter also includes an overview of anomalous fading covering aspects such as: currently accepted mechanism, detection and correction. In addition, the chapter contains a description of IRSL signals used for dating with respect to thermal stability and measurement procedures applied in dating applications.

Chapter 3 provides an extensive analysis of the luminescence characteristics obtained from both silt-size (4-11µm) and sand-sized (63-80 µm) quartz from the loess section at Mostiştea. The first part presents the general behavior of the two fractions using a single-aliquot regenerative-

dose (SAR) protocol. Equivalent dose and age results are discussed in comparison with the ones previously obtained for the section at Mircea Vodă. The second part of the chapter contains additional investigatins on the reliability of SAR-OSL equivalent doses obtained for quartz samples displaying dose response curves with more than one component.

The following chapters apply different stimulation techniques aimed at investigating signals from feldspar. Polymineral fine grains extracted from samples collected at Mircea Vodă are used as study material.

Chapter 4 presents the application of the double-SAR protocol. The two types of signal obtained using this procedure (IRSL and post-IR OSL) are documented using typical laboratory tests and fading measurements. Age results are compared with the previously ages obtained using silt-sized quartz. A discussion of the advantages and limitations of this procedure is provided.

Chapter 5 presents the investigation of IRSL signals in a conventional approach, involving a stimulation temperature of 50 ^{o}C. The signals are documented using a SAR protocol in terms of thermal stability, initial sensitivity changes and fading. The obtained results are discussed in comparison with previous studies.

Chapter 6 presents the application of the recently reported post-IR IRSL procedure, aimed at obtaining IRSL signals from feldspars that are not affected by anomalous fading. Two types of signal are documented in terms of dose response curve, ability to recover a known given dose and fading. The potential of this procedure is further discussed by comparing age results with the available quartz-based ages and independent age control.

CHAPTER I

Loess deposits and their palaeoclimate significance

I. Loess deposits and their palaeoclimate significance

I.1. General aspects of loess and loess deposits

Loess deposits are considered some of the most important terrestrial archives of palaeoclimate during the Quaternary. It took a long period of time and many researchers in order to understand the origin and formation of loess deposits (Codrea, 1998; Smalley et al., 2001). It has been a well-debated subject in the last century, but nowadays, a clear picture is available. During glacial periods, when the climate was cold and dry, ice formation processes generated silt-sized particles through glacial erosion. A "great ice mill", as Hardcastle described at the end of the nineteen century (Smalley, 1995). The great energy of ice masses allowed for glacial grinding of rocks up to silt-sized particles. Sufficiently strong winds were then needed in order to blow these particles and deposit them over a suitable area (Pye, 1995) forming loess deposits. Consequently loess formation took place in periglacial areas where the lack of a well developed vegetation allowed for intense deflation and long-distance transport. Aeolian transport and means of deposition are considered vital in the formation of loess deposits (Smalley et al., 2011 and references therein). Thus, loess is a clastic sedimentary rock formed by the accumulation of wind blown dust. According to Pecsi (1995) loess is homogenous, porous, pale yellow and predominantly coarse silt (10-50 μm), relatively well sorted and slightly diagenetically altered. The predominant mineral in loess is quartz followed by feldspars, calcite and dolomite.

Considerable advances in the study of this material have been made, especially in the past five decades since it has been demonstrated that loess deposits represent detailed archives of climate change (Smalley et al., 2001). A multitude of information may be obtained by studying loess deposits. They mainly characterize the link between aerosols and palaeoclimate and may provide information on palaeowind direction and strength, rates of dust transport and deposition, and even indicate the average element composition of the upper continental crust (see e.g. Pye, 1995; Buggle et al., 2008; Maher, 2011; Stevens et al., 2007).

Furthermore, loess deposits contain intercalated palaeosols that formed during the warm and humid periods when soil formation was favourable (Porter, 2001 and references therein). Such loess-palaeosol sequences represent records of climate change and, by correlation of these

deposits with other climatic records such as the marine oxygen isotope records that primarily record global climate signals (Kukla et al., 2002), a global picture may be obtained on the duration and intensity of the glacial or interglacial periods.

I.2. Distribution of loess deposits: world-wide and Romania

Loess deposits are distributed throughout the world, but mainly in the Northern hemisphere (Fig. I.1) ranging from Northwest and Central Europe through Southeast Europe and the Russian Plain (Fig. I.2), Central Asia to China and Japan and North America. The deposits in Central Asia and China are by far the most detailed and extensive records of Quaternary climate and environmental change (Frechen, 2011). These can reach heights of several hundreds meters and their deposition may be tracked back to the Early Pleistocene or even before. At present, the Chinese loess stratigraphy is acknowledged as the only complete terrestrial stratigraphy of the Quaternary (Zöller, 2010).

Figure I.1: *The global distribution of loess deposits (Maher, 2011)*

In Western and Central Europe, refined loess stratigraphies have been known for up to four decades whereas detailed studies in Southeast Europe have only begun to appear in the last decade (Frechen et al., 2003). In the lower Danube Basin, loess accumulated on plateau uplands

and fluvial terraces in Serbia, Bulgaria and Romania (Fig. I.2; Haase et al., 2007). Thick loess-palaeosol sequences are also exposed along the Black Sea coast (see e.g. Balescu et al., 2010).

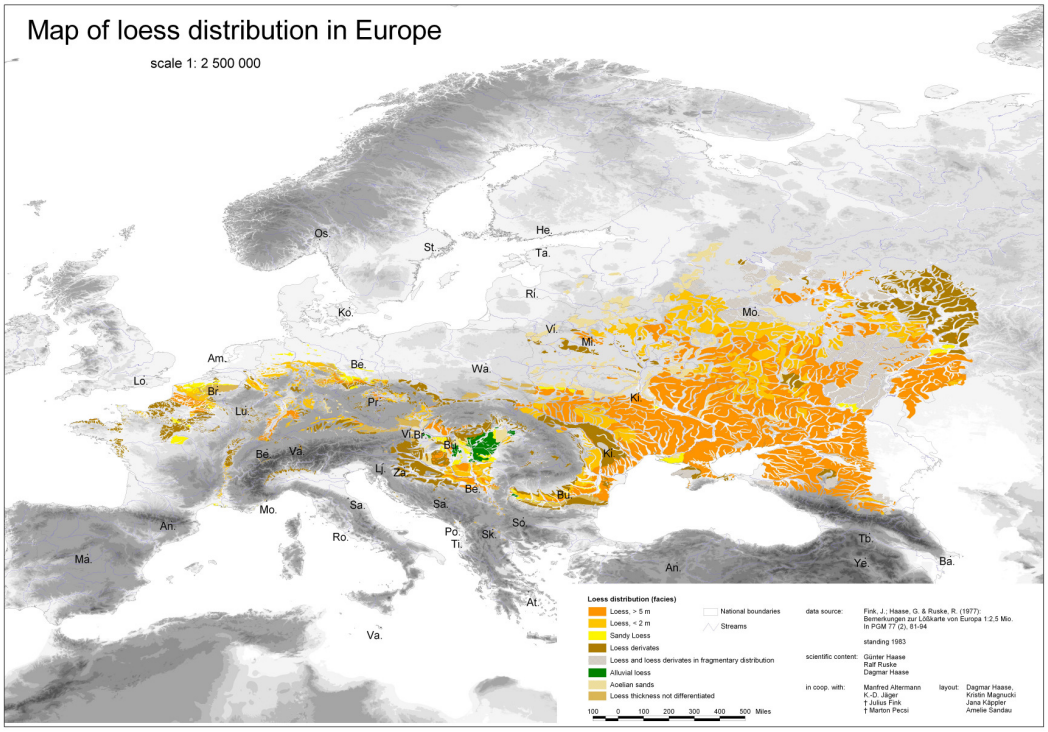

Figure I.2: *Loess distribution in Europe by Haase et al. (2007)*

The loess-palaeosol sequences of the Carpathian Basin-Lower Danube region (Romania, Serbia, Bulgaria) are thought to represent the most continuous and high resolution archives of regional climate and environmental change during the Late and Middle Pleistocene, in this part of Europe and provide a link between similar deposits in central Europe and Asia (Marković et al., 2009; Zöller, 2010).

In Romania, there are both loess and loess-like deposits the latter being predominant (Codrea, 1998). Loess accumulations may have thicknesses of more than 70 m and they are spread over a surface of 40,000 km^2. The most representative regions for loess accumulations are Dobrogea (Southeast; including the coast of the Black Sea), the Romanian Plain (South) and the Moldavian Plateau (East). They also occur in the western part of the country, in the Western Plain (Fig. I.3)

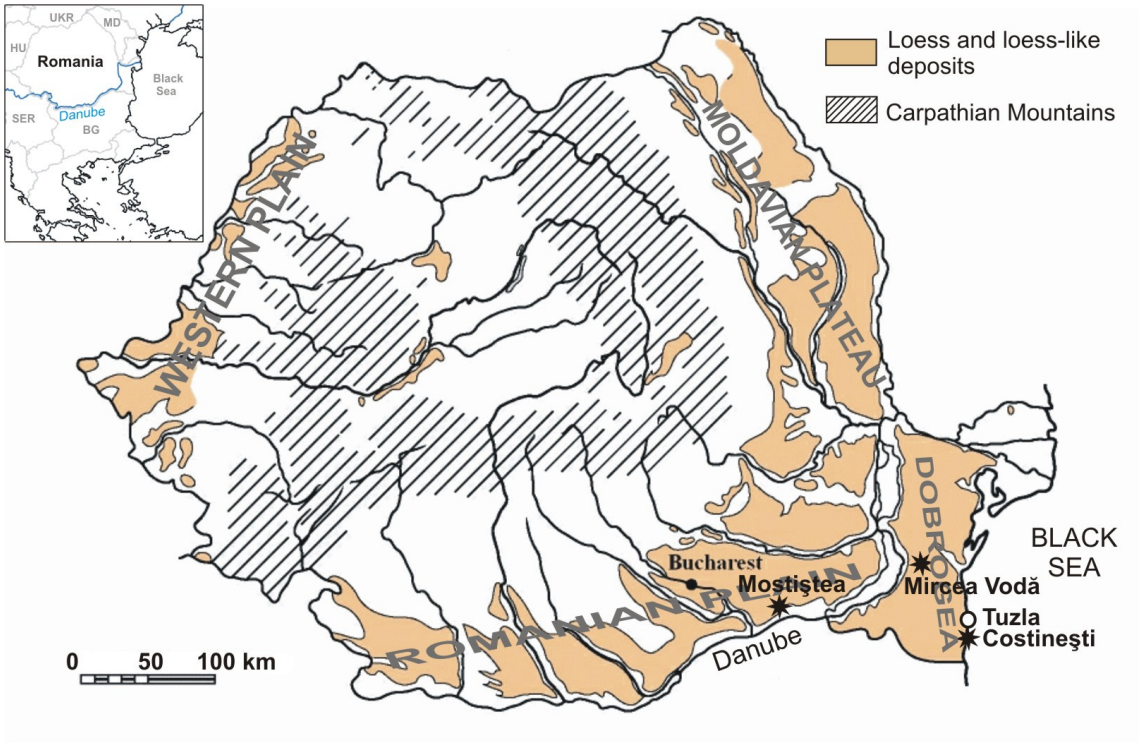

Figure I.3: *Distribution of loess and loess-like deposits in Romania showing the location of the study sites and the location of the Tuzla loess section.*

I.3. Previous studies of Romanian loess deposits using relative methods

The work of Ana Conea is representative in being the first to systematically describe these formations (Conea, 1969; 1970). Using relative pedostratigraphic methods she proposed a chronology of the formation of these deposits. Seven loess units and six intercalated palaeosols sections were identified, reaching more than 20 m height. Based on geomorphological, lithological and pedostratigraphical characteristics, she ascribed the uppermost red-brown palaeosol complex (currently nominated as S3) to the last interglacial period (Riss-Würm). Moreover, the two well developed palaeosol units above (S1 and S2) were interpreted as Würmian interstadials. The later investigations of Panaiotu et al. (2001) and Buggle et al. (2009) used magnetic susceptibility as a proxy-based method to demonstrate the potential of magnetic susceptibility as a climatic proxy. The correlation of the magnetic susceptibility records with the marine oxygen isotope records was used to compare local loess profiles and inter-regional loess profiles. This allowed the correlation not only of the palaeosol units in sequences from Romania, Serbia and Bulgaria, but also a chronostratigraphical correlation with a sequence in China

(Panaiotu et al., 2001; Buggle et al., 2009; Marković et al., 2009). These studies allocate the formation of the uppermost three well developed palaeosol units (S1, S2, S3) to interglacial periods corresponding to Marine Isotope Stages 5, 7 and 9, respectively. Therefore, the 'short chronology' proposed Conea (1969, 1970) may not be valid.

Regarding the origin of Romanian loess deposits, Conea (1970) suggests that the material was transported from different sources. One of them is the glacio-fluvial deposits of the Bug and Dnieper from where sediments were transported by north-eastern winds. The same winds probably acted also on sediments from the river valleys in the Romanian plain. The mechanical composition of loess in Dobrogea indicates that the material in the upper two loess units has also an alluvial component from the Danube. Marine sediments from the Black Sea are also suggested as a source for these deposits, based on the finer texture of the upper loess from the Black Sea coast and the low sea level during the last glacial period. Furthermore, the alteration of consolidated rocks in this region, uncovered by Quaternary deposits, is suggested to have contributed to the formation of loess but mostly loess-like deposits.

The more recent study of Buggle et al. (2008) supports the interpretations of Ana Conea. Their geochemical characterization of Southeastern and Eastern European loess indicates that the loess in Dobrogea (loess sequence at Mircea Vodă) has a significant contribution from the Danube alluvial sediments. The element composition of the Danube sediments suggest that their initial source is the Carpathian mountain range (drained mainly by the Tisa River) and the Eastern Alps (drained by the Drava river). Futhermore, indications of palaeowind direction in the region, led them to include additional contributions either from glaciofluvial sediments related to the Fennoscandianavian ice sheet and local sand dunes.

I.4. The potential of luminescence dating

In comparison to other loess sequences elsewhere in Western, Central and Eastern Europe, the deposits in Romania have been much less extensively studied (Frechen et al., 2003). These deposits preserve a potentially important and detailed archive of Pleistocene climate change; however, their significance can only be fully understood once a reliable and absolute chronology is available (Roberts, 2008). For the Romanian loess deposits, such a chronological framework is largely lacking. Indeed, age information for Romanian loess is mainly based on

relative methods (such as pedostratigraphy and magnetic susceptibility) and correlation of sequences with comparable features (see Section I.3). The major difficulty with these approaches is that they assume that the terrestrial record is complete (i.e. no erosive hiatuses present) and/or that loess deposition occurs at a constant rate. Application of newly developed absolute dating methods (notably luminescence dating), however, yields convincing evidence for both varying accumulation rates and erosive hiatuses (Stevens et al., 2007). This contests some fundamental ideas regarding the nature, formation and significance of loess records, and questions the stratigraphic position of several palaeosols and the way in which they should be correlated. Consequently, absolute dates are essential to determine (i) the timing of climate events that are reflected in the loess, (ii) the rate of processes such as sedimentation and pedogenesis and (iii) the correlation between the Eurasian loess sequences.

Luminescence dating allows the direct determination of depositional ages for sediments from a wide variety of depositional environments, especially aeolian sediments (Murray and Olley, 2002). The method uses the mineral constituents of the sediment itself (and not associated material); it typically covers an age range of a few years to ~100 ka, and has the potential to go even further back in time. Luminescence dating has undergone major technological developments over the past ten years. These resulted in a significant improvement in the achievable precision and accuracy, as a result of which the technique is now considered as one of the most important chronometers in the study of the recent Quaternary (Wintle, 2008). Luminescence dating is, at present, the only method that allows the establishment of an absolute chronology for loess deposits. Moreover, the characteristics of loess make it an ideal material for developing, testing and applying luminescence techniques. Indeed, luminescence dating uses grains of quartz and/ or feldspar, which are both typically abundant in loess, and the windblown nature of loess ensures that the luminescence clock was completely reset prior to deposition. New developments in luminescence dating intrinsically offer the opportunity to establish a new, precise and accurate absolute chronology for a considerable fraction of the stratigraphic European loess record; however, the dating of loess deposits in Romania by luminescence methods is just beginning. There is thus a clear need for a systematic and detailed chronometric investigation in which modern luminescence dating procedures are applied and/or further developed to establish a detailed and reliable chronological framework for these significant terrestrial records of climate change.

I.5. Previous luminescence dating studies of Romanian loess deposits

During the past decade, several studies attempted to establish a chronological framework for the most representative sequences by means of luminescence dating. Balescu et al. (2003) performed an exploratory study on a section along the Black Sea coast – at Tuzla. They used infrared stimulated luminescence (IRSL) signals from K-feldspar separated from four samples. Despite the limited dataset, the obtained age results indicates that the uppermost palaeosol in the section was formed during MIS 5 and that the first three loess layers accumulated during the last three glacial periods (MIS 4, MIS 6, respectively MIS 8). This broad chronology was later extended to the loess sequences near Mostiştea and Mircea Vodă (Fig. I.3.; Balescu et al., 2010).

The collaboration of Dr. Alida Timar-Gabor with the luminescence research laboratory at Ghent University, followed by the establishment of a luminescence dating laboratory in Cluj Napoca, has resulted in more detailed investigations. Timar et al. (2010) were the first to report a study of quartz-based luminescence age results for a loess/palaeosol sequence in Romania. These investigations used silt-sized quartz (4-11 μm) and indicate that the uppermost well-developed palaeosol unit (S1) formed during the last interglacial period. This result agrees with the study of Balescu et al. (2010) and also with a palaeomagnetic time-depth model that Timar et al. (2010) developed for the section at Mircea Vodă. Furthermore, the large number of samples collected from the uppermost loess unit L1 allowed the observation of a change in loess accumulation rate during the last glacial period. This change in sedimentation rate was correlated with a MIS 3 interstadial during which a weakly developed palaeosol was formed (Timar et al., 2010).

The same samples (collected from the section at Mircea Vodă by Timar et al., 2010) were then investigated using sand-sized quartz (63-90 μm) by Timar Gabor et al. (2011). The age results obtained using this fraction were between 20 to 70 % higher than the ages obtained using silt-sized quartz. Since OSL signals from both fractions were documented as suitable for optical dating, the age discrepancy is not understood. Chronologically, the formation of the S1 palaeosol during the last interglacial period is supported by both fractions investigated. However, the coarser fraction indicates that the weakly developed palaeosol was also formed during MIS 5, the change in sedimentation rate thus reflecting the transition from MIS 5 to MIS 4. Furthermore, the OSL ages obtained using both grain size fractions of quartz were interpreted as underestimates from the penultimate glacial period onwards (Timar et al., 2010 and Timar Gabor et al., 2011).

No clear explanation of both age discrepancy and age-underestimation has yet been found. A speculative explanation of the age discrepancy is based on the fact that the two quartz fractions investigated may have originate from different sources, as indicated by several studies (Conea, 1970; Buggle et al, 2008; Timar Gabor et al. 2011). This was correlated with possible effects that artificial irradiation may have on the luminescence processes leading to different characteristics of the dose-response curve observed for the two quartz fractions (Timar Gabor, 2010). Since the internal structure of crystals is strongly related to the formation processes, it is expected that different luminescence characteristics occur for the two grain-sizes of quartz investigated. However, given the complexity of the mechanism that give rise to luminescence signals in quartz, and in natural minerals in general, these speculations remain to be proved. As it is less common that dating studies are performed on different grain sizes of the same mineral, the results obtained by Timar et al. (2010) and Timar Gabor et al. (2011) point to unknown aspects regarding the SAR-OSL dating method. Therefore luminescence dating of loess deposits may be less straightforward than generally accepted and suggest that quartz-based OSL ages should be interpreted with caution. If the grain-size dependence of the age results is a general feature of loess sequences in the region, it can only be found by studying other sites.

I.6. Study area

For the purpose of this work, three of the most representative loess-palaeosol sequences in SE Romania (Fig. I.3) were selected for luminescence investigations. The loess sections are located near Mostiştea and Costineşti; the third site is Mircea Vodă, which has been the subject of previous work.

I.6.1. Costineşti

The sequence is located on the coast of the Black Sea (Fig. I.4) shore, north of Costineşti village. It comprises at least five loess units (L1-L5) and intercalated palaeosols (S1-S5) plus the Holocene topsoil (S0). L1 has a thickness of ~ 1.10 m and L2 ~ 2.15 m.

A high resolution sampling (10 - 20 cm vertical intervals) was performed for the first two loess layers and S1 unit (see Fig. I.5). The samples collected from the sequence near Costineşti were

prepared for the separation of sand-sized (63-90 μm) quartz grains using conventional techniques (see Chapter III).

Figure I.4: *Photo with the exposed loess-palaeosol sequence near Costineşti.*

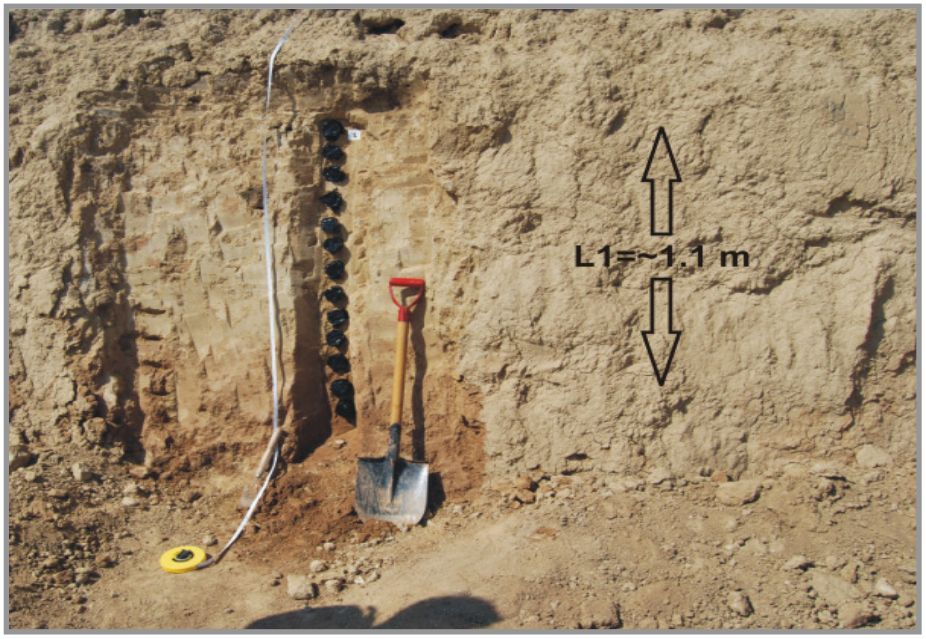

Figure I.5: *Sample collection from the L1 unit at Costineşti.*

I.6.2. Mostiştea

The loess-palaeosol sequence near Mostiştea is located on the border of Mostiştea lake (~20 km in length and 56.7 km^2 of water surface, Danube Plain, SE Romania; Fig. I.3). It is about 21 m thick and consists of four loess-palaeosol units (L1, S1 etc.) and the Holocene topsoil (S0). The two upper palaeosols (S1,S2) are chernozemic while S3 and S4 are brown-reddish palaeosols (Fig. I.6; Panaiotu et al., 2004). The sequence has previously been investigated using magnetic susceptibility (MS) and IRSL techniques (Panaiotu et al., 2001; 2004; Necula and Panaiotu, 2008; Balescu et al., 2010). Both the MS and the IRSL results indicate that the uppermost three palaeosols (S1, S2, S3) formed during MIS5, MIS 7 and MIS 9, respectively.

In this work state of the art luminescence dating is performed using quartz as luminescence dosimeter. OSL signals from two grain-size fractions (4-11µm and 63-90 µm) are documented in Chapter III.

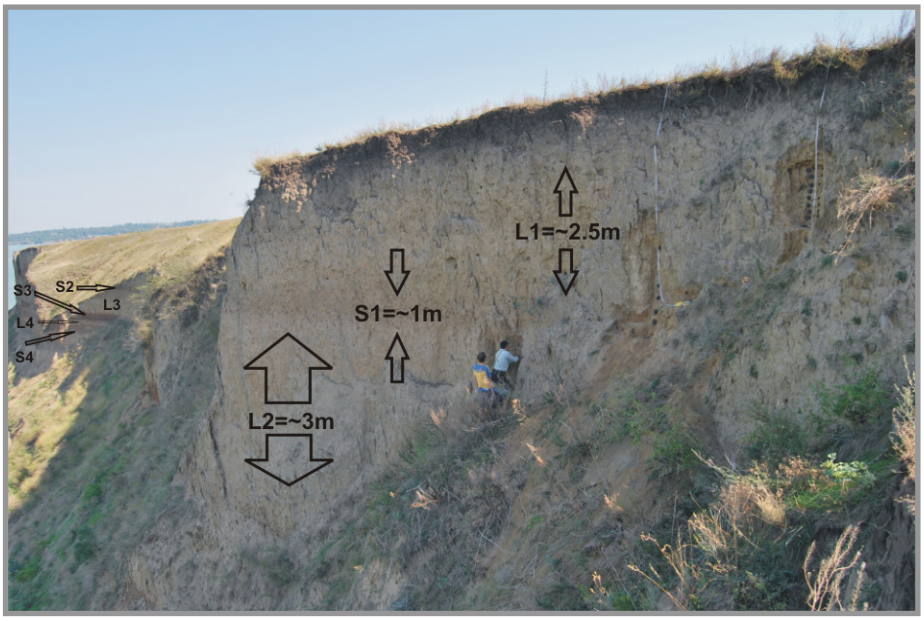

Figure I.6: *General view of the Mostiştea loess palaeosol sequence with indications of the loess units and intercalated palaeosols.*

I.6.3. Mircea Vodă

The sequence at Mircea Vodă is located near the village of Mircea Vodă, in the Dobrogea-plateau (SE Romania) at about 15 km from the River Danube (Fig. I.3). It is one of the

most complete palaeoclimate archives in Romania. This sequence was the subject of previous luminescence investigations performed by Timar et al. (2010) and Timar Gabor et al. (2011). It encompasses six loess units (L1-L6), five well-developed palaeosol units (S1-S5) and the Holocene topsoil (S0). In addition, a weakly-developed palaeosol was observed in the L1 loess unit (Timar et al., 2010).

We extend our previous investigations of this sequence (see Sections I.3 and I.5) by using luminescence signals from feldspars. These investigations are presented in Chapters IV, V and VI and include both conventional and alternative and/or modern methods.

CHAPTER II

Overview of Luminescence Dating

II. Overview of Luminescence Dating

II.1. Introduction

Luminescence dating is a chronological method that exploits the property of natural minerals to store energy during exposure to nuclear radiation. The radiation comes mainly from the decay of uranium, thorium and potassium together with the cosmic radiation (Aitken, 1985). Due to the ionizing effect of nuclear radiation, electrons are trapped at defects in the structure of crystals. The number of electrons is proportional to the radiation dose that the mineral received over a period of time. When the minerals are stimulated by heat or light, recombination of the trapped electrons takes place within the crystal leading to a release of energy. Some of this energy is released as light and is called luminescence. The light signal is called thermoluminescence (or thermally stimulated luminescence; TL) if heat is used for stimulation or optically stimulated luminescence (OSL) if the minerals are stimulated using light. Depending on the stimulation wavelength, different terms may be used such as infrared stimulated luminescence (IRSL) or blue light stimulated luminescence (BLSL or BSL).

For sediments, the latent luminescence (in the form of trapped electrons) that accumulates from the formation of the minerals is removed during transport and deposition when they are exposed to sunlight. This process is usually termed bleaching or zeroing. When the mineral grains are covered by other sedimentary minerals deposited on top, the luminescence signal builds up again. These luminescence signals are measured in the laboratory and they reflect the total radiation dose (or equivalent dose - D_e) that the minerals received after the last zeroing event. If the rate of dose delivered by exposure to radiation is further determined, the depositional age may be computed as follows:

$$Age = \frac{Equivalent\ dose\ (Gy)}{Dose\ rate\ (Gy\ /\ ka)} \qquad (2.1)$$

II.2. Dose rate determination

Dose rate measurements are usually performed using spectrometric methods that quantify the sources of radioactivity in the immediate environment of the sampled sediments and inside the mineral grains themselves. The concentrations of the natural radionuclides and their daughters are converted into dose rates using conversion factors (e.g. the factors tabulated by Adamiec and Aitken, 1988). In addition, the contribution from cosmic radiation is also considered. The cosmic dose rate is usually used from the literature (see e.g. Prescott and Hutton, 1994). The penetration power efficiency of nuclear radiations in inducing luminescence is also included in the calculation of the dose rate. While beta and gamma radiation have the same efficiency in inducing luminescence, the efficiency of the alpha radiation is one order of magnitude lower. This difference is important since the equivalent dose is determined usually using beta radiation. For coarse-grain investigations, this is avoided by physically removing any significant contribution of the alpha particles to the total dose. This is performed by chemical etching (Lang et al., 1996). Furthermore, when coarse grains are used, the attenuation of alpha and beta particles together with the effect of etching must also be considered (Aitken, 1985, Appendix C). An estimation of the moisture content in the sediments is of major importance because water absorbs a part of the radiation that would otherwise reach the mineral grains. The water content in the sediments is either measured using bulk material or taken from literature.

II.3. D_e determination

The equivalent dose is obtained by comparing natural luminescence signals with artificially regenerated signals obtained using a calibrated radioisotope source (usually a $^{90}Sr/^{90}Y$ beta source). The irradiation may be performed either before the measurement of the natural luminescence signal, adding an artificial dose on top of the natural dose (additive methods), or after the natural signal has been zeroed (regenerative methods). For an overview on the methods used for D_e determination the reader is referred to Wintle (2008).

In OSL studies, the most commonly used method for D_e determination is the single-aliquot regenerative-dose (SAR) protocol (Murray and Wintle 2000; Wintle and Murray, 2006). This protocol was initially proposed for quartz investigations, but it has been also applied to feldspars

(Wallinga et al., 2000; Huot and Lamothe, 2003; Blair et al., 2005; Buylaert et al., 2011). It allows the determination of the equivalent dose using single aliquots of the investigated material. After the measurement of the natural signal, the same grains are given different laboratory doses and a dose-response curve (growth curve) is constructed. The equivalent dose is obtained by interpolating the natural response on the dose-response curve. Thermal treatments (preheats) are used in order to isolate the thermally stable signals. In order to correct for sensitivity changes occurring after repeated irradiation, preheating and stimulation, the response to a constant laboratory dose (test dose) is used. Therefore the dose-response curve is constructed using the L_x/T_x ratio, where L_x is the OSL signal obtained using the regenerative doses, and T_x is the corresponding signal obtained from the test dose.

Several tests have been proposed to check the performances of the SAR measurements (Murray and Wintle, 2000; Wallinga et al., 2000). The repeated measurement of a regenerative dose (usually the lowest) is used to calculate the recycling ratio. A ratio within 10 % from unity is considered to indicate that sensitivity changes occurring throughout the SAR cycles are accurately corrected for. Furthermore, the measurement of a zero dose is used to detect residual signals that may influence the accuracy of the D_e measurement. The dependence of the equivalent dose on the preheat treatment, also known as the plateau test, is used to check that the signals used for dating are thermally stable. The final test is the dose recovery test. In this test, a known dose is given to samples that have been bleached either by daylight or using a light source. This dose is then measured as if it is an unknown dose. The recovered/given dose ratio is then determined and used to assess the performances of the protocol. Detailed descriptions of the SAR protocol are given by Wintle and Murray (2006)

The SAR protocol has been shown to provide accurate age results for samples from different depositional contexts (Murray and Olley, 2002; Buylaert et al., 2007). The protocol has been extensively used in the past decade and various versions have appeared since it was initially proposed (e.g. Banerjee et al., 2001; Roberts and Wintle, 2001; Buylaert et al., 2009).

II.4. Feldspars as luminescence dosimeters

The most used minerals for dating sediments are quartz and feldspars. These two minerals are found abundantly in sedimentary rocks. The development of the SAR protocol led to an

extensive use of quartz for OSL dating. The predominant use of quartz as opposed to feldspars is mainly related to the anomalous fading observed to affect luminescence signals from feldspars (Wintle, 1973; Huntley and Lamothe, 2001). IRSL signals from feldspar were also observed to bleach slower than quartz OSL signals (Godfrey-Smith et al., 1988; Thomsen et al., 2008a). This allowed the development of a large body of knowledge regarding the characteristics of luminescence signals from quartz (Preusser et al., 2009) while the luminescence signals from feldspars are still poorly understood.

II.4.1. Mineralogical background of feldspars

The term feldspar refers to a group of aluminosilicates that form three dimensional framework structures with corner shared (AlO_4) and (SiO_4) tetrahedral. Charge compensating cations occupy large irregular cavities in the tetrahedral framework. These are mainly potassium (K), sodium (Na) and calcium (Ca). A range of chemical compositions exists including $KAlSi_3O_8$ (orthoclase), $NaAlSi_3O_8$ (albite) and $CaAl_2Si_2O_8$ (anorthite). These are the end-members of a solid-solution series that is conventionally represented as a ternary diagram (Fig. II.1). The intermediate species are defined in terms of the mole percent of the three end-members.

The chemical composition is not the only criterion used to classify feldspars. Their structure may also be used in identifying different characteristics, that may be used to describe luminescence signals obtained from feldspars. For more details on the relationship between the structure of feldspars and luminescence the reader is referred to Duller (1997 and references therein).

II.4.2. Advantages of feldspars for luminescence dating

Feldspars have a series of advantages that make them attractive for luminescence studies. One of the most important features of feldspars is that they generally exhibit luminescence signals that saturate at higher doses than those obtained from quartz. In principle, this would allow for older depositional ages to be obtained using signals from feldspars. Moreover, feldspars may be preferentially stimulated using infrared (IR) light from aliquots that contain also quartz (Bøtter-Jensen et al., 2003). This allows (i) a broader detection window of the signals

and (ii) IRSL investigations of polymineral samples, without the need for sample preparation procedures to separate the two minerals (Roberts, 2008).

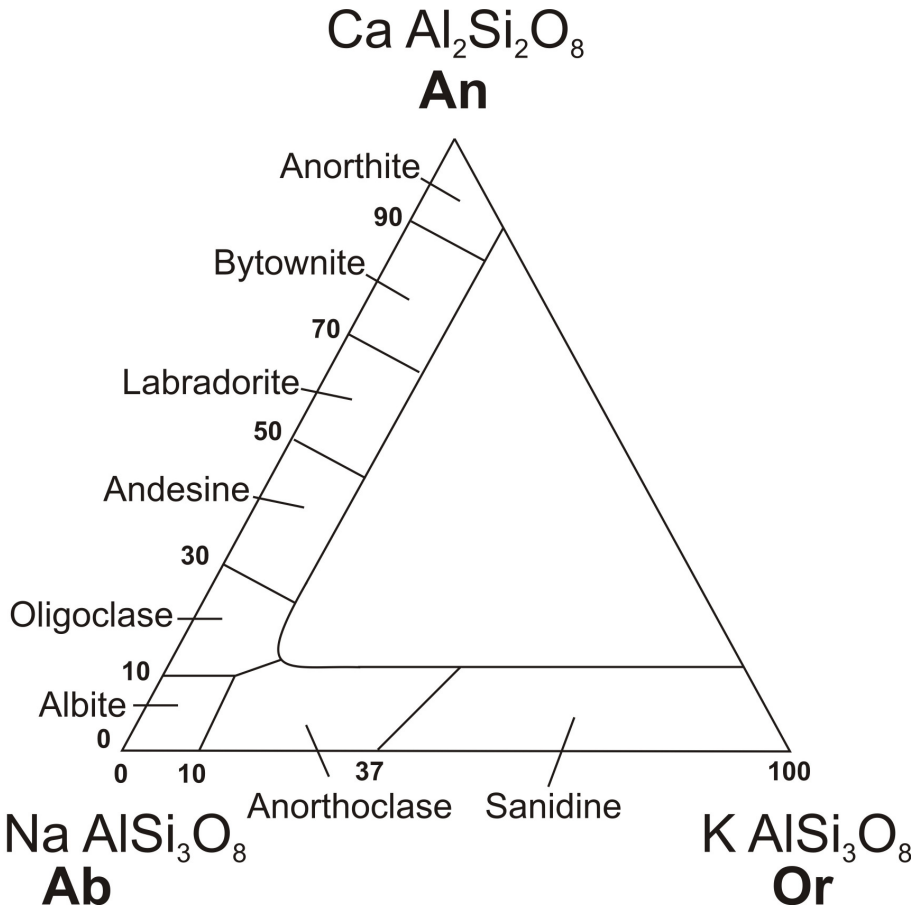

Figure II.1. *The ternary diagram of feldspars (redrawn from Duller, 1997).*

In contrast, OSL signals from quartz may be measured only after the removal of any OSL contribution from feldspars (Wintle, 2008). This may be done optically, through an initial IR stimulation of the polymineral aliquots that is aimed to reduce the OSL signal from the feldspathic component. This is followed by a blue stimulation that stimulates a [post-IR] OSL signal which should be dominated by quartz. This method has been applied in a 'double-SAR' protocol; an overview of this method may be found in Roberts (2008). An application of the double-SAR protocol for dating Romanian loess is presented in Chapter IV. The other method to isolate a signal from quartz is the chemical removal (etching) of feldspar grains.

Feldspars are observed to be brighter than quartz (Aitken, 1998). Therefore, feldspars may be useful for dating young sediments, allowing for a smaller detection limit. From the

dosimetry perspective, due to the high internal radioactivity of sand-sized K-feldspars the equivalent dose is less susceptible to changes in their environment (e.g. moisture content; Wintle, 2008).

II.4.3. Stimulation and emission spectra

By choosing the appropriate wavelength, stimulation of the most sensitive luminescence signals in a crystal may be performed. This is one of the important advantages of OSL over TL. For quartz, conventional stimulation of luminescence signals is performed using blue light (470 nm) at a constant stimulation power. The selection of this wavelength is based on studies that document the stimulation spectra (Krbetschek et al., 1997 and references therein). The emitted luminescence from quartz has a peak intensity at ~ 365 or 380 nm (Preusser et al., 2009 and references therein). Therefore quartz OSL is detected in the UV region of the spectrum. On the other hand, luminescence signals from feldspars have been shown to be sensitive to stimulation wavelengths ranging from visible (blue-green) to IR (Bøtter-Jensen et al., 2003). This broad range is due to the multitude of mineralogical forms of feldspar existing in nature. Nevertheless, a main peak in stimulation spectra appears at ~ 855 nm (IR) has been observed for various feldspar species. This is considered a common feature of feldspars irrespective of their chemical composition (Duller, 1997). The emitted luminescence is also varied, clustered in bands from 280 to 570 nm (Krbetschek et al., 1997). IR stimulation allows the observation of the emission spectrum; the main emission bands are in the blue or UV regions and these are the typical detection windows used for dating studies.

II.4.4. Models of feldspar luminescence

The first stimulation spectrum from feldspars was published by Hütt et al. (1988). They observed a large stimulation peak in the near infrared (1.4 eV) and demonstrated that the charge thereby evicted comes from traps which are stable enough to permit dating. The mechanism they proposed to explain their observations is represented in figure II.2. The model involves a two stage detrapping process. In the first stage, photons of infrared raise electrons from the ground

state into an excited state. In the second stage, some electrons are raised from the excited state into the conduction band thermally, i.e. by lattice vibrations, and then by diffusion some reach luminescence centres. This is a resonant process, as supported by the fact that the peak in the stimulation spectrum was observed to have a Gaussian shape. The model allows for stimulation in the visible region as well, in which case the transition is a direct one into the conduction band.

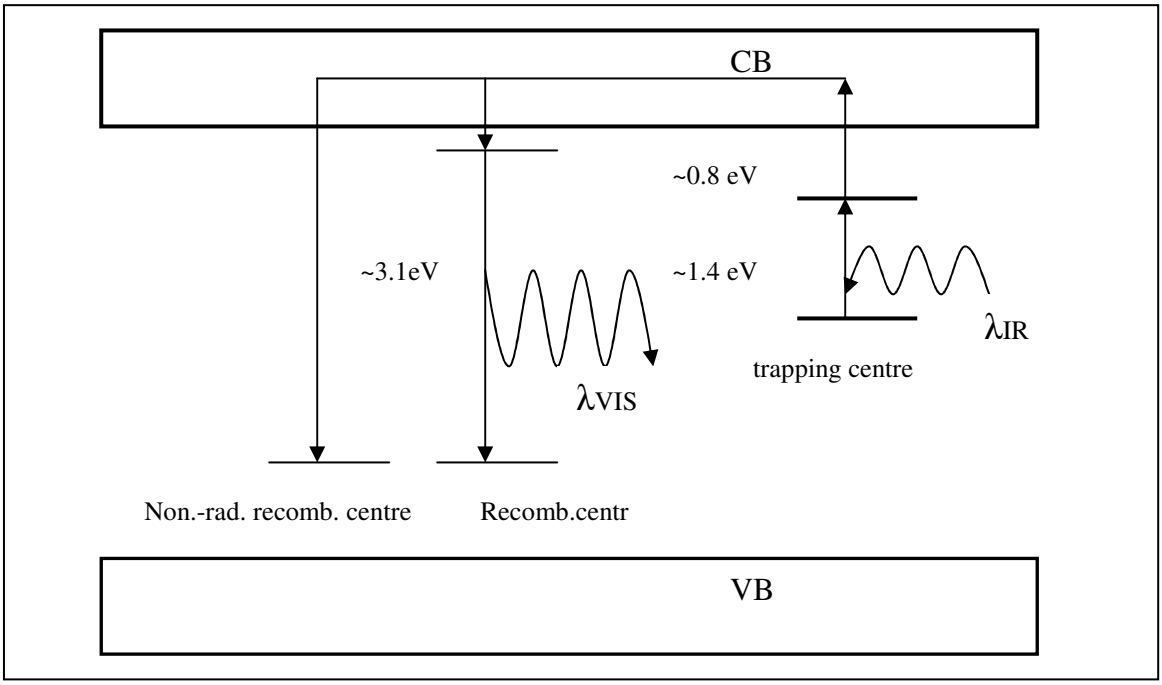

Figure II.2: *Two stage detrapping process (photon-phonon) of IRSL production in feldspars as suggested by Hütt et al. (1988). The figure is redrawn from L. Bøtter-Jensen, S.W.S. McKeever and A.G. Wintle (2003).*

Other explanations of the phenomenon have been given more recently. The work of Poolton et al. (1995; 2002a,b; 2009) is considered to have significantly contributed understanding luminescence production in feldspars. Poolton et al. (2002a,b) suggest that IRSL signals from feldspars result from a combination of two processes: (1) tunnelling from the excited state of the IRSL trap to a recombination centre and (2) transfer of electrons from the excited state into low mobility band-tail states lying beneath the conduction band. The existence of band tail states is caused by random fluctuations in bond length and angles in disordered crystals (Poolton et al., 2002b, 2009). The tunnelling component requires no thermal assistance, the recombination probability depending on the distance between the electron trap and the

recombination centre. On the other hand, the chances of luminescent recombination through band tail states increase with temperature.

The most recent contribution regarding charge recombination in feldspars is the study of Jain and Ankjaergaard (2011). Using time-resolved optically stimulated luminescence (TR-OSL) they document the recombination routes for different types of feldspar mineral specimens. A new and more detailed model is proposed which extends the work of Poolton et al. (2002a,b). The model is based on a single dosimetric trap and emphasizes the role of band tail states in luminescence generation. Several paths of charge transport are suggested with strong dependence on the energy of stimulation. Following optical stimulation, a fast and a slow recombination are observed. The fast recombination is suggested to occur either from the excited state of the trap (<100 μs; when resonant IR at ~ 1.4 eV, excitation is used) or from the conduction band (<1 μs; for non resonant blue and green excitations at 2.63 and 2.36 eV respectively). The slow recombination (up to several milliseconds) takes place from the band tail states at a rate independent of the excitation photon energy. For non-resonant excitation, the band-tail states are populated by direct sub conduction band electrons. The band-tail transport includes two main thermally competing pathways: a relatively efficient sub conduction band transport assisted by strong lattice vibrations corresponding to 0.05-0/06 eV phonons, and a slow tunnelling recombination from localized deep lying, disconnected band tails. The tunnelling recombination can be observed for several ms and follows a power law. Thermal stimulation is considered to lead to the same localised recombination routes as after optical excitation. In other words, luminescence can be produced following different routes: conduction band, thermally assisted hopping through band tail states, tunnelling from the basal, disconnected band tail states and tunnelling from the excited state of the trap.

The model of Jain and Ankjaergaard (2011) suggests that luminescence production is governed by the availability of luminescence centres in the volume accessible by the excited electron. Therefore, a decrease in the luminescence intensity of IRSL or TL signals reflects a decrease in the local hole population and not the electron population. There is also a competition between recombination and retrapping during both thermal and optical stimulation. This competition may be varied by changing the stimulation energy (thermally or optically) in order to control the number of recombination centres that may be accessed.

II.4.5. Thermal stability of luminescence signals from feldspars

Luminescence signals from feldspars were initially obtained by thermal stimulation (TL). TL signals are obtained by gradually increasing the temperature of the sample. Their shape indicates the thermal depth of the traps that are emptied, identified through the peaks of the glow curves. Two components (peaks) were generally observed in the natural TL signals from K-feldspars, centred at 250-280 and 330 ^{o}C. Regenerated TL signals were observed to exhibit additional low temperature components represented by a broad peak at 150-180 ^{o}C (Duller, 1997; Murray et al., 2009). These components were shown to represent different traps that are probed during the stimulation (Strickertsson, 1985). This distribution of traps was observed to vary, probably reflecting mineralogy variations.

While for quartz it is generally accepted that the OSL signals originate from the trap corresponding to the 325 ^{o}C TL peak (Murray and Wintle, 2000), more than one trap may contribute to the IRSL signal from feldspars. One way to relate TL components to IRSL is by comparing TL signals recorded after different IRSL stimulation durations. Duller (1997) shows that all TL components are reduced by prior IR stimulation for various types of feldspar. Duller and Bøtter-Jensen (1993) investigate the effect that IR and green stimulation have on TL, IRSL and a green light stimulated signal (GLSL). They observed that after 1000s of IR stimulation, a significant GLSL signal remains which was removed by 1000 s of green stimulation, indicating that there may be traps that can only be probed using green stimulation.

Another technique that provides information of the relation between the TL components and IRSL signals is pulse annealing. Pulse anneal measurements investigate IRSL signals following different heat treatments. An indication is obtained concerning the relationship between thermally evicted and optically evicted charge. The experiments involve repeated IRSL measurements and annealing the sample at successively higher temperatures between each IRSL measurement (Duller, 1997). Duller (1994) shows that between 200 and 270 ^{o}C K-feldspar samples that were irradiated exhibit an additional loss of IRSL signal in comparison with unirradiated samples. This was correlated with a contribution from thermally unstable, low temperature traps which affects regenerated signals. Removal of the unstable components was advocated by preheating (at 220 ^{o}C for 10 min) the samples before measuring the IRSL signals. A similar conclusion was also reached by Li (1991) or Buylaert et al. (2011-submitted).

However, there are also studies that show that preheating may not be necessary in order to isolate the IRSL signal corresponding to thermally stable traps (Duller and Bøtter-Jensen, 1993; Li and Wintle, 1992; Murray et al., 2009).

As previously discussed the characteristics of luminescence signals from feldspars are significantly influenced by their mineralogy. This is also observed in the thermal stability of the traps that contribute to the luminescence signals. K-feldspars were found to be more stable than Na-feldspars (Duller, 1997). Furthermore, IRSL signals from polymineral fine and medium loess grains were shown to have a similar stability as the signals from Na-feldspar (Li and Wintle, 1992).

According to the luminescence model of Jain and Ankjaergaard (2011), the pulse annealing technique is not expected to give correct indications of the trap depth. The thermal stimulation leads to recombination via band tail states and by increasing the preheat temperature recombination takes place in more distant recombination centres (delocalised recombinations). This leads to an increase in the distance between the donor (electron trap) and the available acceptor (recombination centre). Therefore the decrease in IRSL signal with increasing preheat does not reflect a decrease in electrons but a decrease in recombination probability due to the consumption of the holes in the neighbouring recombination centre by the thermal pre-treatment.

II.5. Anomalous fading

II.5.1. Introduction

The term fading is used to denote an observed loss of luminescent signal. This loss can be due to many causes. It can, for instance, be thermally or optically induced. For some minerals, however, fading is observed even after storage in the dark and at low temperatures. This phenomenon is termed anomalous fading, as the signal loss exceeds that predicted from the lifetime of the traps.

Wintle (1973) was the first to note the effect for volcanic feldspars. Subsequently, the phenomenon has been observed and investigated in a number of studies, such as those by Wintle (1977) and Spooner (1992, 1994), to name a few. More recent studies report that anomalous fading is ubiquitous for sedimentary feldspars from different geographic regions (Huntley and Lamothe, 2001; Huntley and Lian, 2006).

In the context of dating, the consequence of anomalous fading is an underestimation of the equivalent doses, especially when the measurements are performed shortly after irradiation (Wintle, 2008). This has been reported in several dating studies using either TL or IRSL signals from feldspars or polymineral fine grains. For this reason, it is necessary to test for the presence of anomalous fading whenever the dating involves the use of feldspars. It can be pointed out here that samples showing age shortfall do not always show loss during laboratory tests. As a result, a number of authors associate the term anomalous fading with samples showing such loss and class as "long term fading" whatever effects are responsible for shortfall in samples which do not show laboratory loss (Aitken, 1998, Appendix D).

II.5.2. Mechanism

Tunnelling has been the favoured explanation since the first observations of anomalous fading. Figure II.3. shows the possible escape routes of an electron from a trap.

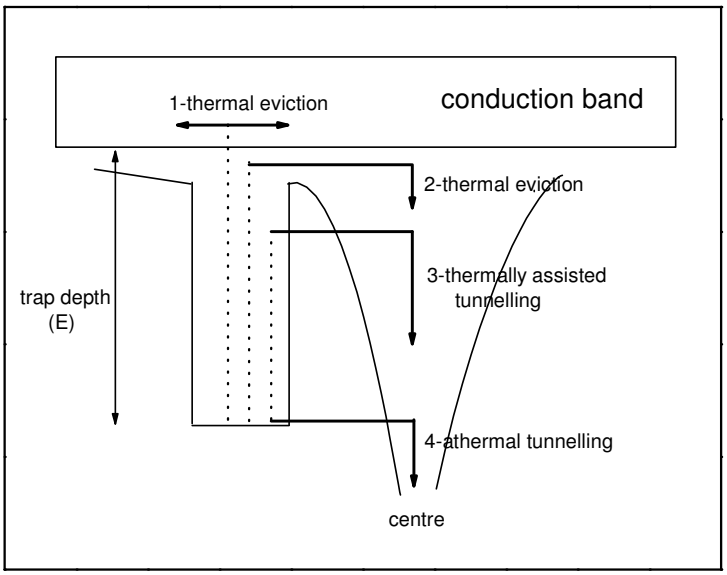

Figure II.3: *Escape routes from a trap (redrawn from Aitken 1985).*

Routes 1 and 2 represent thermal eviction, the probability of detrapping being a function of temperature of Arrhenius type. Routes 3 and 4 represent escape by tunnelling. The difference between 3 and 4 is that in the case of 4 the electron tunnels the barrier from its bottom (ground state tunnelling), while in the case of 3 the particle hops first into an excited level by receiving

thermal energy and then tunnelling occurs. Tunnelling is a quantum mechanical effect which cannot be explained in classical terms. It basically represents the fact that there is a finite probability for the particle to escape the potential barrier even if it does not have the necessary kinetic energy.

In the case of trapped electrons and recombination centres in a crystal the probability of recombination via quantum mechanical tunnelling is given by the overlapping of the two wave functions of the pair trap-centre. For a trap and a recombination centre separated by a distance R the tunnelling rate (meaning the probability per unit of time for the transition to occur) can be written as:

$$P(R) = s \cdot \exp(-R / a) \qquad (2.1)$$

Where s is the frequency factor and a is a constant, roughly half the Bohr radius of the electron in the trap. So the probability of decay is an exponential function of the barrier thickness, temperature not being involved in the dependence anymore. That is why fading by tunnelling is generically called athermal fading.

There is a very important implication of this formula: the critical dependence on the separation distance of the traps and recombination centres. This means that even for electrons with the same trap depth the probability of recombination via quantum mechanical tunnelling can vary dramatically. The closest pairs will recombine first, and as time passes it will be more and more difficult for recombination to occur. This leads to a slow decrease in the detrapping rate, with roughly hyperbolical time dependence (1/t) as was observed experimentally.

The dependency on the proximity of centres implies that if they are randomly distributed then high concentrations are required. This leads to the idea that bright minerals are more likely to be affected (and this is easily observed, feldspars being brighter than quartz); then the state of crystallization seems also to be a factor (Aitken 1985). It is expected that crystals with more structural defects like the ones that come from volcanic rocks will suffer more from fading than the ones nicely crystallized such the case of plutonic rocks. Still, as a note it must be added that the study of Huntley and Lian (2006) concluded by analyzing 77 K-feldspar extracts that the fading rates of K-feldspars from sediments derived largely from volcanic bedrock are not higher than those from non-volcanic bedrock.

The dependency on the trap/centre distance leads to the prediction that the rate of detrapping is proportional to t^{-1}, t being the time elapsed since irradiation. The number of electrons lost through tunnelling is then proportional to log t. It can be shown (Aitken, 1985; Appendix F) that the number of electrons detrapped and, therefore, the luminescence L_i lost in the time between t_1 and t_2 owing to tunnelling is given by

$$\frac{L_2 - L_1}{L_1} \approx \ln^2(st_1)\ln(t_2 / t_1) \qquad (2.3)$$

as long as the number of electrons detrapped is small compared to the number trapped at time t_1. A logarithmic signal decay has been observed experimentally, and these observations lend strong support to an explanation of fading in terms of tunnelling.

Besides tunnelling, other mechanisms have been put forward to explain fading. For more details on these, and other suggested causes of age shortfall, reference is made to Aitken (1985, Appendix F; 1998, Appendix F) and Bøtter-Jensen et al. (2003).

For the sake of completeness the most important ones will be outlined below:

- Localized transitions model (Templer ,1986)
- Erroneous trap parameters
- Enhanced trapping efficiency for laboratory irradiation due to high dose rate.
- Absorption of UV within large grains of K-feldspar (Duller, 1997, Wallinga and Duller, 2000)
- Decay of effective luminescent centres

These mechanisms can be operable to a certain extent in certain synthetic or natural crystals and can lead to age shortfall but in the case of feldspars quantum mechanical tunnelling explanation is highly sustained by the correlation with low temperature phosphorescence or tunnelling afterglow (Visocekas, 2002).

II.5.3. Detection

Strong support for quantum mechanical tunnelling as an explanation for anomalous fading is provided in measurements of phosphorescence when recently irradiated samples are taken down to liquid nitrogen temperature (LNT). This phosphorescence was called “tunnelling afterglow” by Visocekas (1985). It can be observed in the wavelength region of 590-890 nm, but not in the region from 305-590 nm.

A typical afterglow observed for feldspar is represented in figure II.4. The sample was irradiated at room temperature and the luminescence was measured. At first the signal results from recombination due to thermal eviction at room temperature. As the temperature is lowered, the signal decreases as the traps can no longer be thermally emptied. However the signal does not reach zero, indicating another source of luminescence. This is the tunnelling afterglow, a phenomenon which cannot be explained in terms of other auxiliary effects such as retrapping or competition (Visocekas, 2002). On storage at LNT, the luminescence emission decays with time. Finally, the sample is heated. The luminescence observed first decreases owing to thermal quenching, and then takes the shape of a TL glow curve.

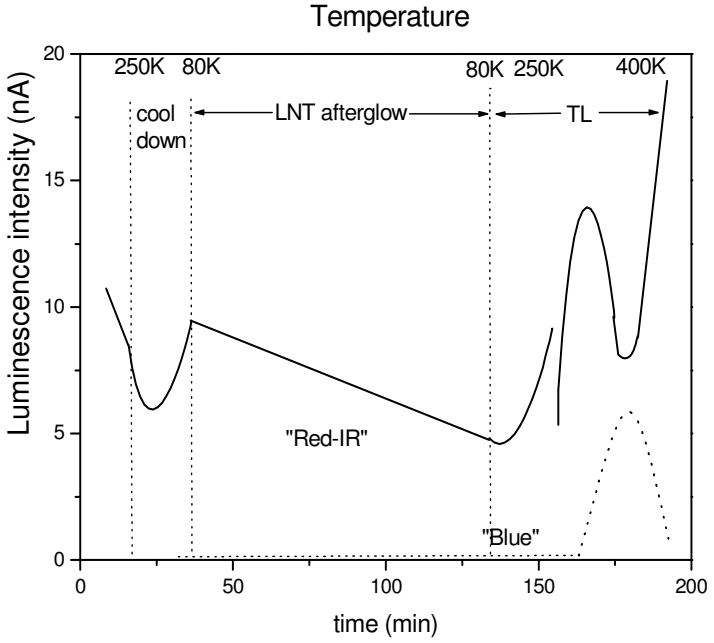

Figure II.4: *Typical afterglow for feldspars. Redrawn from Visocekas et al. (1994)*

Visocekas et al. (1994) observed the tunnel emission from 23 feldspar samples and compared the presence or absence of afterglow with the measured fading behaviour. They found a close correlation between the samples that showed tunnelling afterglow and those for which anomalous fading was detected. Spooner (1994) also concluded that the dominant mechanism governing anomalous fading is tunnelling. As tunnelling-type fading is largely immune to thermal effects, and hence cannot be circumvented by any existing laboratory procedure, monitoring for anomalous fading is essential. A second consequence of this mechanism is that the data obtained from the monitoring should be plotted using a logarithmic time scale. The use of a linear representation of remanent luminescence versus storage time is misleading, as it gives the impression that the fading reaches a stable level (Spooner, 1994).

In essence, the clear conclusion is that in the case of feldspars anomalous fading cannot be circumvented by any existing laboratory procedure such as preheating, because it is a quantum mechanical tunnelling process and largely immune to thermal effects (Prescott and Robertson, 1997 and references therein).

This means that testing for it is the ultimate solution. Rejection of certain samples or correction for the effects is the final step. Detection can be made either by monitoring the afterglow i.e. observing the luminescence emitted by recombination via tunnelling either by conducting storage test in which the luminescent signal is measured at different time intervals i.e. quantifying the loss in the signal which occurred due to ground state tunnelling.

However, new perspectives into isolation of a stable signal from feldspars are provided by Jain and Ankjaergaard (2011). As discussed in section II.4.4., they used TR-OSL in order to investigate electron recombination pathways during optical and thermal stimulation. Their results suggest that once the closest electron-holes pairs are consumed through localised recombinations, the signal obtained by recombination of distant pairs is less affected by fading. This is based on the fact that ground-state tunnelling (which leads to fading) consumes the nearest electron-hole pairs. According to the model of Jain and Ankjaergaard (2011), three methods may be used to isolate a stable signal in feldspars: (i) preheating the sample at a sufficiently high temperature ensuring that the remaining distant pairs have a low fading probability in nature; a minimum preheat at 350 ^{o}C is advocated; (ii) using a low energy optical or thermo-optical pre-conditioning of the sample or (iii) by directly examining the distant pair recombination through TR-IRSL signals and pulsed IR stimulations.

It must be noted that these methods are based on the assumption that there exist isolated traps with distant centres (acceptor sites), such that it is not possible to trap any holes in the vicinity during burial irradiation (Jain and Ankjaergaard, 2011). This is in contradiction with the random distribution model of Huntley (2006), where every electron trap has a similar surrounding distribution of hole trapping centres. Further investigations are required to better understand the nature of the electron-hole trapping, in order to evaluate the existence of geologically stable electrons. Nevertheless, the initial applications of the methods suggested by Jain and Ankjaergaard (2011) to circumvent anomalous fading have been shown to lead promising results (see Section II.6).

II.5.4. Implications of logarithmic signal decay

If the loss of luminescence is proportional to log (t), then the loss between 1 h and 10 h is the same as the loss between 10 h and 100 h and between 100 h and 1000 h and so on. The fading (the percentage of signal loss) occurring between two times differing by a factor of ten is denoted by the symbol *g* (Aitken, 1985). Figure II.5 shows the signal loss as a function of storage time for several theoretical fading rates (Visocekas, 2002). It can be seen that if a sample has g = 5% per decade, this would lead to an age underestimation between 40 and 60% for samples in the range from 1 ka to 1 Ma, whereas samples showing a fading rate of ~20% cannot be dated.

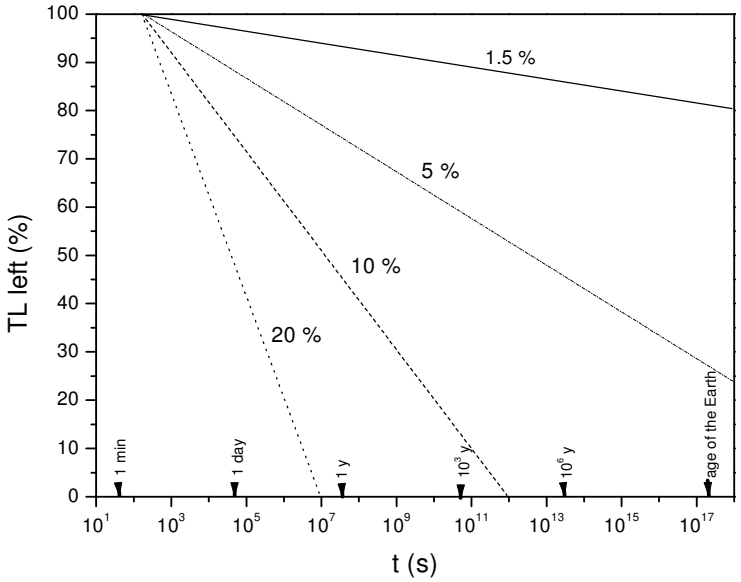

Figure II.5: *Percentage TL left after anomalous fading as a function of storage time in semi-logarithmic coordinates for different theoretical fading rates. Redrawn from Visocekas 1985.*

II.5.5. Correcting for anomalous fading

Several methods to deal with anomalous fading in dating studies have been proposed. According to Huntley and Lamothe (2001), they can be classified into three categories: circumvention, variability and correction.

Circumvention involves the use of a signal that does not exhibit fading. Combinations of heating, storage and/or exposure to low energy photons have been tried with the purpose of eliminating the fading signal component(s). Other approaches involve the use of deeper traps or of a luminescence emission that exhibits a long-term stability (such as the far-red TL emission).

Variability methods are based on the observation that different grains from a deposit have different fading rates. Grain to grain variability in fading behaviour has been demonstrated by Lamothe and Auclair (1997) and Huot and Lamothe (2003). A plot of the equivalent doses as function of the fading rates for individual grains, when extrapolated to zero fading rate, should yield the correct equivalent dose. This is the "Fadia "method developed by Lamothe and Auclair (1999, 2000) and they showed that extrapolation can result in the correct age.

The correction approach is based on the idea that if one can measure the fading rate in the laboratory, one might be able to make a correction for the age. This approach was tested by Huntley and Lamothe (2001) and they obtained very promising results. The model put forward by Huntley and Lamothe (2001) for correcting optical ages for anomalous fading was also applied in this work (see Chapters IV, V and VI), and it can be summarized as follows.

Following from the tunnelling model (see Eq. 2.3), the luminescence intensity I measured at a time t after a short radiation dose can be described by:

$$I = I_c(1 - \kappa \ln(\frac{t}{t_c})) = I_c(1 - \frac{g}{100}\log(\frac{t}{t_c})) \qquad (2.4)$$

where I_c corresponds to the intensity at an arbitrary time t_c, and κ and g are constants representing fading rates. The relation between g and κ is:

$$g = 100\kappa \ln(10) \qquad (2.5)$$

The actual value of κ and g depends on the choice of t_c as can be seen from equation 2.3.

It is then assumed that the effect of any particular radiation is independent of that of any other radiation dose. This assumption is expected to hold in the low-dose linear-response region. The luminescence intensity is built-up by a continuous exposure to radiation over a time T. To find this luminescence intensity, Eq. 2.5. must be written in differential form and integrated. Choosing a time scale such that t' =0 at the beginning of the irradiation and t'=T at the end of irradiation, the luminescence intensity contributing at measurement due to the irradiation during a time interval δt' can be written as:

$$\delta I_f = (I_0 / T)\delta t' \left[1 - \kappa \ln\left(\frac{T + T_L - t`}{t_c}\right) \right] \tag{2.6}$$

Where I_0 is the intensity owing to irradiation in time T if there was no fading, and T_L is a time interval during which there was no irradiation. T_L can be understood as the time between sample collection and measurement. Integrating Eq. 2.6. from t' = 0 to t' = T, and assuming that $T_L << T$ yields:

$$I_F = I_0 \left\{ 1 - \kappa \left[\ln\left(\frac{T}{t_c}\right) - 1 \right] \right\} \tag{2.7}$$

We now choose t_c to be the time between laboratory irradiation and luminescence measurement for the equivalent dose determination. However, the laboratory irradiation is continuous, starting at t_2 and finishing at t_1, with both t_1 and t_2 being time before measurement. To take this into account, it can be shown (Aitken, 1985) that t_c is given by

$$t_c = \frac{1}{2.7} \frac{{t_2}^{t_2/(t_2 - t_1)}}{{t_1}^{t_1/(t_2 - t_1)}} \tag{2.8}$$

Subsequently, we evaluate κ (or *g*) appropriate for this t_c (using Eq. 2.4). As intensity, equivalent dose, and age are all proportional, the formula for correcting an optical age affected by anomalous fading is obtained from 2.7 as:

$$\frac{T_F}{T} = \frac{D_f}{D_e} = \frac{I_f}{I} = 1 - \kappa \left[\ln\left(\frac{T}{t_c}\right) - 1 \right] \tag{2.9}$$

Where T is the true age, and D_e and I are the equivalent dose and luminescence intensity, respectively, that would be obtained in the absence of fading. The subscript f indicates a value affected by fading. To obtain the true age T, Eq. 2.9 must be rewritten as:

$$0 = T\left\{1 - \kappa\left[\ln(\frac{T}{t_c}) - 1\right]\right\} - T_F \qquad (2.10)$$

from which T is obtained using an iterative procedure

The correction proposed by Huntley and Lamothe (2001) has been shown to work for young sediments (typically younger than 20-50 ka) where the dose-response curve is linear. However, the logarithmic approximation of decay of the IRSL signal is not valid for very short and very long delay times (Huntley and Lamothe, 2001).

A more recently proposed method by Kars et al. (2008) is suggested to correct for fading in the case of older material. It is based on modelling natural (faded) dose-response curves using laboratory fading measurements and dose response as input parameters. Initial results obtained by Kars and Wallinga (2009) indicate that the method can provide reliable age results. However, the general applicability of this method has not yet been tested.

II.6. IRSL signals used for dating

Conventionally, IRSL signals are measured while holding the sample at 50 ^{o}C as this ensures fixed stimulation temperatures for measurement protocols that include a preheat after irradiation (Bøtter-Jensen et al., 2003). As these signals were observed to generally suffer from anomalous fading, their application for dating required age correction. Although increasing the stimulation temperature was observed to cause a significant increase of the luminescence intensity (Duller and Wintle, 1991; Duller and Bøtter-Jensen, 1993), it was only recently that this characteristic was studied with respect to anomalous fading. Jain and Singhvi (2001) show that IR stimulation at elevated temperature (220 ^{o}C) depletes a residual signal that was observed by stimulation with green light. Thus, elevated temperature IR stimulation is shown to probe more BGSL traps than the 'conventional' (low temperature) stimulation. Jain and Singhvi (2001) speculated that the charge observed to be measured using elevated temperature IR stimulation

may show less fading. However Poolton et al. (2002b) suggested that stimulation at elevated temperatures may lead to overestimating age results due to accessing traps that are difficult to bleach in nature. Thomsen et al. (2008a) carried on this direction performing fading-rate measurements as a function of stimulation temperature. Using sodium and potassium feldspar-rich feldspars, they observed a decrease in fading-rate with increasing stimulation temperature. A double IR stimulation was further investigated, performing a first IR stimulation at 50 ^{o}C followed by a second one (post-IR IR) at 225 ^{o}C. The first stimulation was aimed to remove the unstable signal while the second stimulation targeted the more stable trap suggested by Jain and Singhvi (2001). This stimulation configuration appeared to provide a post-IR IRSL significantly brighter than the signal stimulated at 50 ^{o}C and also showing a reduced fading rate. These observations are consistent with the recent model proposed by Jain and Ankjaergaard (2011; see section II.4.4 and II.5.3.).

Bleaching experiments using both K- and Na-rich samples indicated that IRSL signals stimulated at 225 ^{o}C bleach at a similar rate as the IRSL signals stimulated at 50 ^{o}C (Thomsen et al., 2008a). Furthermore, residual doses of a few grays were obtained on modern samples indicating that this type of stimulation is suitable for old samples where such residual levels are negligible. Similar conclusions were drawn by Buylaert et al. (2009) who tested the post-IR IRSL signals (stimulated at 225 ^{o}C) using K-feldspars extracted from sediments with different depositional contexts. Post-IR IRSL signals were observed to exhibit less fading than the signal obtained by stimulation at 50 ^{o}C, thus allowing for age results that are less dependent on the fading correction. A good agreement was obtained between post-IR IRSL ages and independent age control.

Different studies subsequently used the post-IR IR stimulation at different temperatures and obtained reliable age results (Thiel et al., 2010; 2011a; 2011b; Schmidt et al., 2011; Stevens et al., 2011). Moreover, using a post-IR IR stimulation at 290 ^{o}C and polymineral fine grains extracted from an infinitely old sample below the Brunhes/Matuyama boundary), Thiel et al. (2011b) obtained natural signals in saturation indicating that these signals may not fade over a period of ~ 750 ka. Moreover, besides having a lower fading rate, post-IR IRSL signals appear thermally more stable than IRSL signal obtained using a single IR stimulation at 50 ^{o}C (Thomsen et al., 2011; Li and Li, 2011).

In Chapter VI, the post-IR IRSL approach is tested for polymineral fine grains extracted from Romanian loess.

CHAPTER III

Luminescence characteristics of silt-sized and sand-sized quartz: a comparison on the Mostiştea loess-palaeosol sequence (SE Romania)

Chapter based on:

Vasiliniuc, S., Timar-Gabor, A., Vandenberghe, D.A.G., Panaiotu, C.G., Begy, R.Cs., Cosma, C., 2011. *A high resolution optical dating study of the Mostiştea loess-palaeosol sequence (SE Romania) using sand-sized quartz*. Geochronometria 38, 34-41.

Timar Gabor A., **Vasiliniuc, S.**, Vandenberghe, D.A.G., Cosma, C., Wintle, A.G., submitted. *Investigations on the reliability of SAR-OSL equivalent doses obtained for quartz samples displaying dose response curves with more than one component*. Radiation Measurements, proceedings of LED 2011.

III. Luminescence characteristics of silt-sized and sand-sized quartz: a comparison on the Mostiştea loess-palaeosol sequence (SE Romania)

III.1. General characteristics and age results

III.1.1. Introduction

As discussed in Chapter I, the chronology of Romanian loess has been documented mainly by relative methods while absolute age information was obtained only from a few applications (see Sections I.3 and I.5). Because an absolute timeframe is lacking, there is great uncertainty about the stratigraphic position of several palaeosols and the way in which they should be correlated. This strongly hampers interpreting the sequences in terms of the signatures of palaeoclimatic and environmental changes.

The most robust luminescence dating procedure currently available involves the use of optically stimulated luminescence (OSL) signals from quartz, in combination with the single-aliquot regenerative-dose (SAR) protocol (Murray and Olley, 2002; Wintle and Murray, 2006). This procedure was applied in the first optical dating applications on Romanian loess, performed by Timar et al. (2010) and Timar Gabor et al. (2011) on the loess-palaeosol sequence at Mircea Vodă (Dobrogea, see section I.6.3). Their results show a dependency of the age results on the two grain-size fractions of quartz, despite both fractions passing all SAR-procedural tests (i.e. recycling ratio, recuperation and dose recovery; see Timar et al., 2010; Timar Gabor et al., 2011).

In this work we extend the luminescence dating investigations of different grain-size fractions of quartz to the loess-palaeosol sequence at Mostiştea (SE Romania; Section I.6.2). Our main objective is to determine whether there are any discrepancies similar with the results reported by Timar Gabor et al. (2011).

III.1.2. Samples and analytical facilities

The profile investigated here is located at a distance of ~ 50 m from the sections previously studied using magnetic susceptibility (MS) and IRSL techniques (Panaiotu et al., 2001; 2004; Necula and Panaiotu, 2008; Balescu et al., 2010). Our study focused on the uppermost loess-palaeosol unit (L1/S1) and the top of the second loess unit (L2). Due to intense bioturbation in the form of root casts and the difficult access to the upper part of the L1 unit, the samples were collected starting from a depth of 2.1 m. Nineteen samples in total were collected, at relatively closely spaced vertical intervals (~ 10 – 25 cm; Fig. III.1a). The sampling was performed by hammering stainless steel cylinders into freshly cleaned exposures. The sediment surrounding each tube was collected for dose rate determination. To correlate our sections with those from the previous studies, the magnetic susceptibility was measured using a MS2B Magnetic Susceptibility System (Bartington Instruments) on a subsample of the sediment surrounding each OSL tube (Fig. III.1b).

Conventional sample preparation techniques (Lang et al., 1996; Frechen et al., 1996) were applied for the extraction of sand-sized (63 – 90 μm) quartz grains and polymineral fine grains (4-11 μm). The silt-sized quartz was further isolated etching in hydrofluorosilicic acid (35%) (H_2SiF_6) for 10 days.

Sand-sized quartz aliquots were prepared by spreading a monolayer of quartz grains was spread out on the inner 9 mm of 9.7 mm-diameter stainless steel discs; silicone oil was used as adhesive. The silt-sized quartz aliquots were prepared by settling of a 2 mg/ml suspension on aluminium discs. The purity of the quartz was confirmed by the absence of a significant IRSL response at 60^{o}C to a large regenerative dose (>35 Gy); the sensitivity to infrared stimulation was defined as significant if the OSL IR depletion ratio deviated more than 10% from unity (Duller, 2003). The test was performed for each aliquot that was measured; no aliquots had to be rejected on the basis of this criterion.

All luminescence measurements were made with a Risø TL/OSL DA-20 reader equipped with blue diodes emitting at 470 ± 30 nm and IR LEDs emitting at 870 nm; luminescence signals were observed through a 7.5 mm thick Hoya U-340 UV filter. Details on the measurement apparatus can be found in Bøtter-Jensen et al. (2003) and Thomsen et al. (2008b). Irradiations have been carried out using a ^{90}Sr-^{90}Y beta source. The source was calibrated using calibration

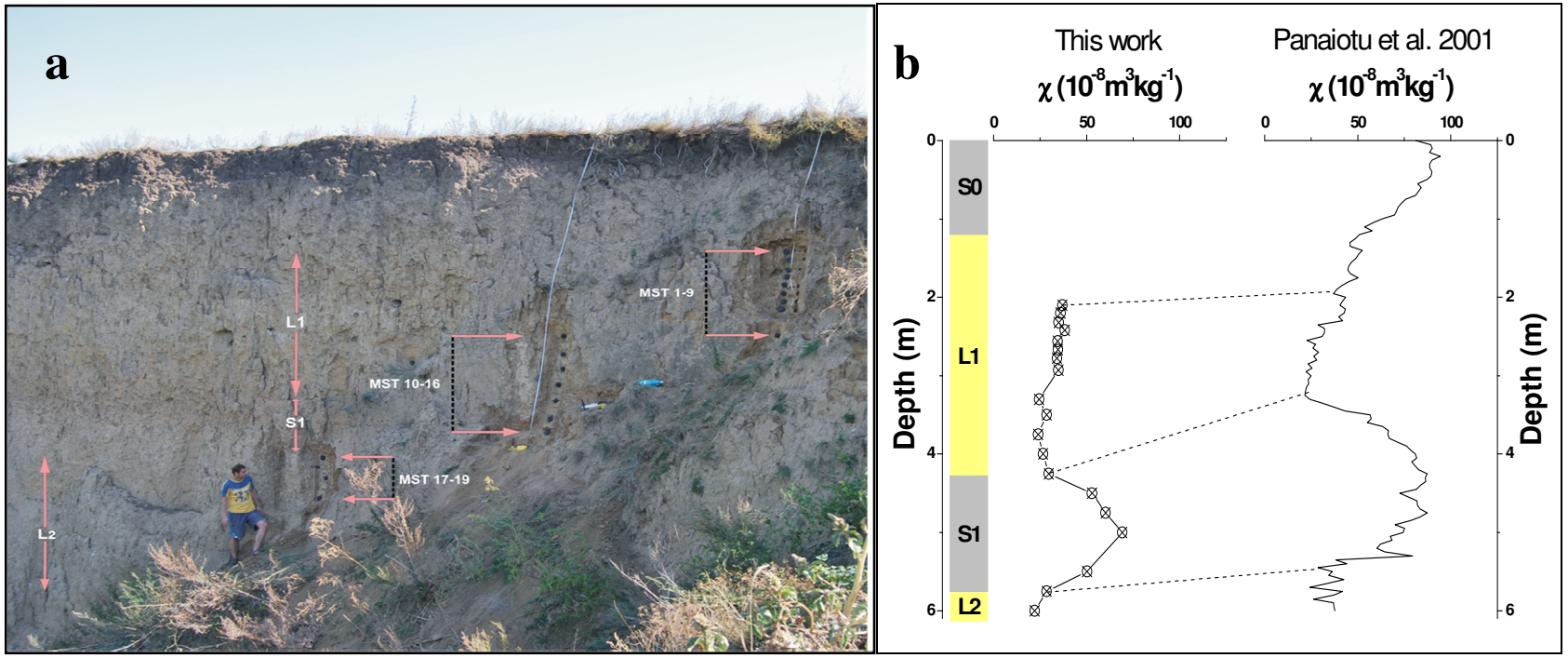

Figure III.1*: (a) Collection of samples for OSL. The sampling was performed at a high resolution for the L1 and the upper part of L2 and the intercalated palaeosol S1. (b) Schematic representation of the sampled section. The upper lithology is sketched indicating soil (dark layers) and loess (light layers) units. The variation of the magnetic susceptibility measured for subsample of the sediment surrounding each OSL tube (left) is correlated with the previously investigated section by Panaiotu et al. (2001) (right). The dashed lines (eye guide) correlate the two sections.*

quartz supplied by Risø National Laboratory. The dose rate determined for coarse grains deposited on stainless steel disks was 0.161 Gy/s, and 0.127Gy/s for fine grains deposited on aluminium disks (reference date August 2011).

The luminescence characteristics of the samples were investigated using the single-aliquot regenerative-dose (SAR) protocol (Murray and Wintle, 2000). Stimulation with the blue diodes was for 40 s at 125°C. The first 0.32 s of the decay was used in the calculations, minus a background evaluated from the 1.60 s to 2.88 s interval.

Moving the background interval closer to the initial signal is more effective in reducing the contribution from slower components (see e.g. Ballarini et al., 2007), but we observed no dependence of the results on the interval chosen for background evaluation. Unless indicated otherwise, natural and regenerated signals were measured after a preheat of 10 s at 220°C; the response to the test dose (17 Gy) was measured after a cutheat to 180°C. Timar et al. (2010) and Timar Gabor et al. (2011) used the same thermal pretreatments in their optical dating studies of the loess section near Mircea Vodă. After the measurement of the response to the test dose, a high-temperature bleach was performed by stimulating with the blue diodes for 40 s at 280°C (Murray and Wintle, 2003).

For the determination of the annual dose, the sediment from the surroundings of the OSL tubes was dried, powdered and packed in sealed containers. The sediment samples were stored for at least one month before being measured using high-resolution gamma-ray spectrometry.

III.1.3. General behaviour in the SAR protocol

For all samples, the OSL signals obtained from both quartz grain-size fractions are bright and decay rapidly with stimulation time (Fig. III.2). The decay is typical for quartz that is dominated by a fast component. This was confirmed by examining the LM-OSL signals of samples from different depths. The natural and regenerated signals show a well-defined peak early in the curve; the position of the peak matches that observed for calibration quartz and is not dependent on the preheat treatment (insets to Fig. III.2, for sample MST1; samples MST2, -7, -8, and -12 exhibit the same LM-OSL characteristics). It is generally accepted that the OSL signal of calibration quartz is dominated by the fast component.

To asses the suitability of the SAR protocol employed for measuring the dose in our samples, we performed a dose recovery test. At least two aliquots per sample were bleached at room temperature by stimulating twice for 40 s with the blue diodes; the two bleaching treatments were separated by a 10 ks pause.

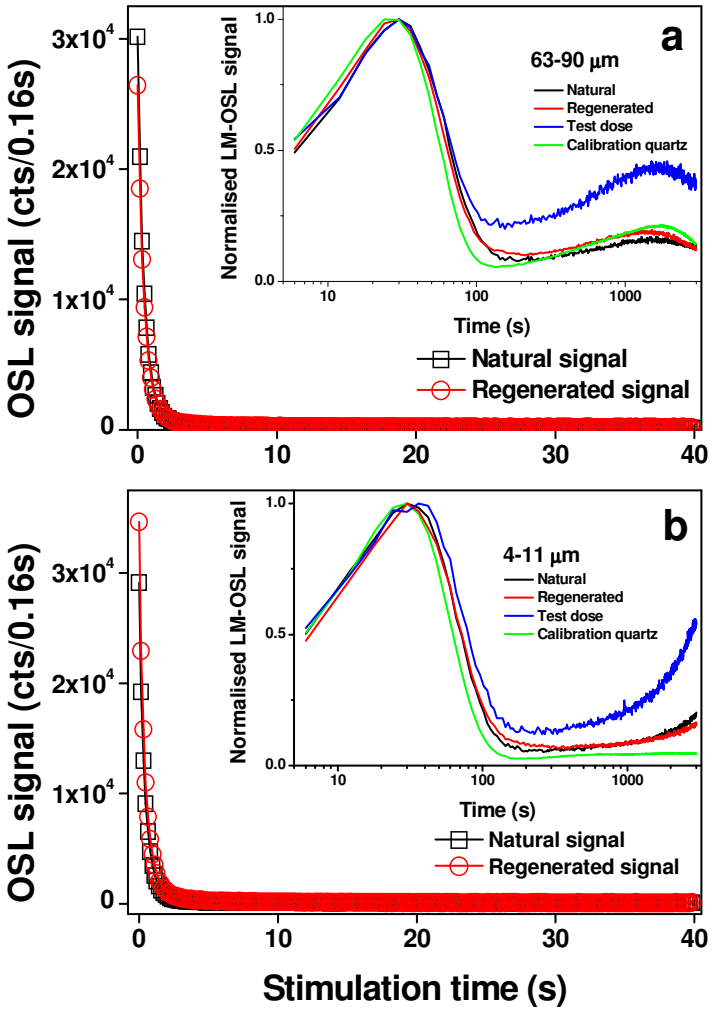

Figure III.2: *Examples of natural and regenerated OSL decay curves using sand-sized quartz (a) and silt-sized quartz (b). The signals are measured using aliquots of sample MST2. The insets show natural and regenerated LM-OSL signals obtained using sample MST1 in comparison with calibration quartz. Stimulation power was ramped from 0 to 100% in 3000 s. The natural, regenerated and calibration quartz luminescence signals were measured at 125°C, following a preheat of 10 s at 220°C. The test dose signal was measured at 125°C, following a cutheat at 180°C.*

The aliquots were then given a laboratory dose, which was chosen to be equal to the estimated equivalent dose (D_e), and measured using the SAR protocol. The dose recovery data are summarized in Fig. III.3 for both sand-sized (circles) and silt-sized (squares) quartz.

For sand-sized quartz, considering 1σ level, the recovered per given dose is within 10 % from unity for all investigated samples except MST9 and MST13. For the latter sample the recovered per given dose is within 10 % from unity only at 2σ level.

However, for sample MST9, the measured to given dose ratio is 2.5 ± 0.3; at present, it is not understood as to why this particular sample behaves so differently from the other samples and yields such a poor dose recovery. Excluding sample MST9, the overall average measured to given dose ratio (± 1 standard error) is 1.06 ± 0.01 (n = 76).

For all the investigated samples, the silt-sized quartz gave a recovered to given dose ratio within 10 % of unity (considering 1 standard error) and the overall average recovered to given dose ratio is 1.03 ± 0.01 (n = 47). Unfortunately, due to an insufficient amount of material, we were not able to perform the dose recovery test for silt-sized material from sample MST9.

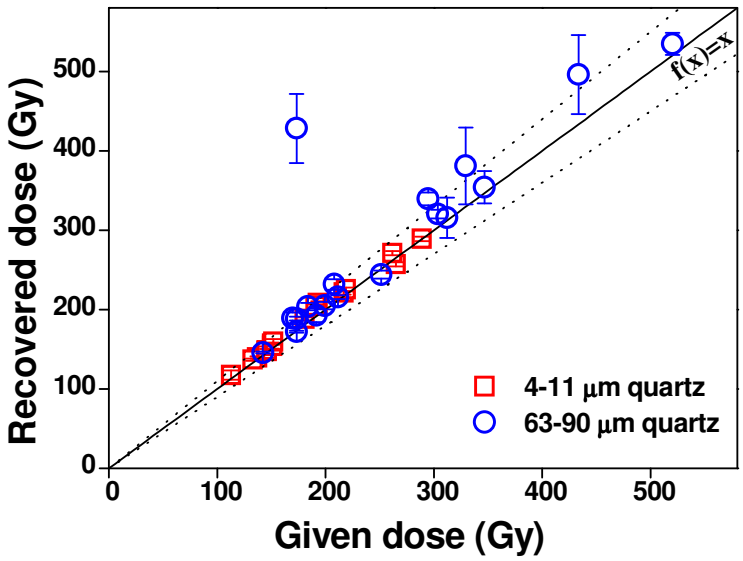

Figure III.3: *Results of the dose recovery test obtained using both fine and coarse quartz for the samples collected from Mostiştea. Error bars represent one standard error. The solid and dashed lines are the 1:1 relation and brackets of 10% deviation from unity, respectively.*

The dependence of equivalent dose (D_e) on preheat treatment was further investigated for various samples over the 200-280 ^{o}C range. Figs. III.4a and b present the results obtained for sample MST2 for sand-sized and silt-sized grains, respectively. No dependence on preheat

temperature may be observed across the investigated temperature range. D_e values from both grain sizes appear consistent with the average (± 1 standard error) of 143 ± 11 Gy for sand-sized grains and 104 ± 2 Gy for silt-sized grains respectively. The corresponding recycling ratios and recuperation are shown in Fig. III.4c and d. The recycling ratio shows no variation with preheat temperature, but it has a tendency to lie below unity; the overall average value (± 1 standard error) is 0.92 ± 0.01 for sand-sized grains and 0.955 ± 0.008 for silt-sized grains respectively.. The recuperated signal is negligible (as compared to the corrected OSL signal) across the entire investigated temperature range. Similar observations were made for samples MST 3, -9 and -13 for coarse grains and MST 10 and 13 for fine grains. No influence of the cutheat temperature on the equivalent dose was observed for a fixed preheat of 10 s at 220 °C (data not shown).

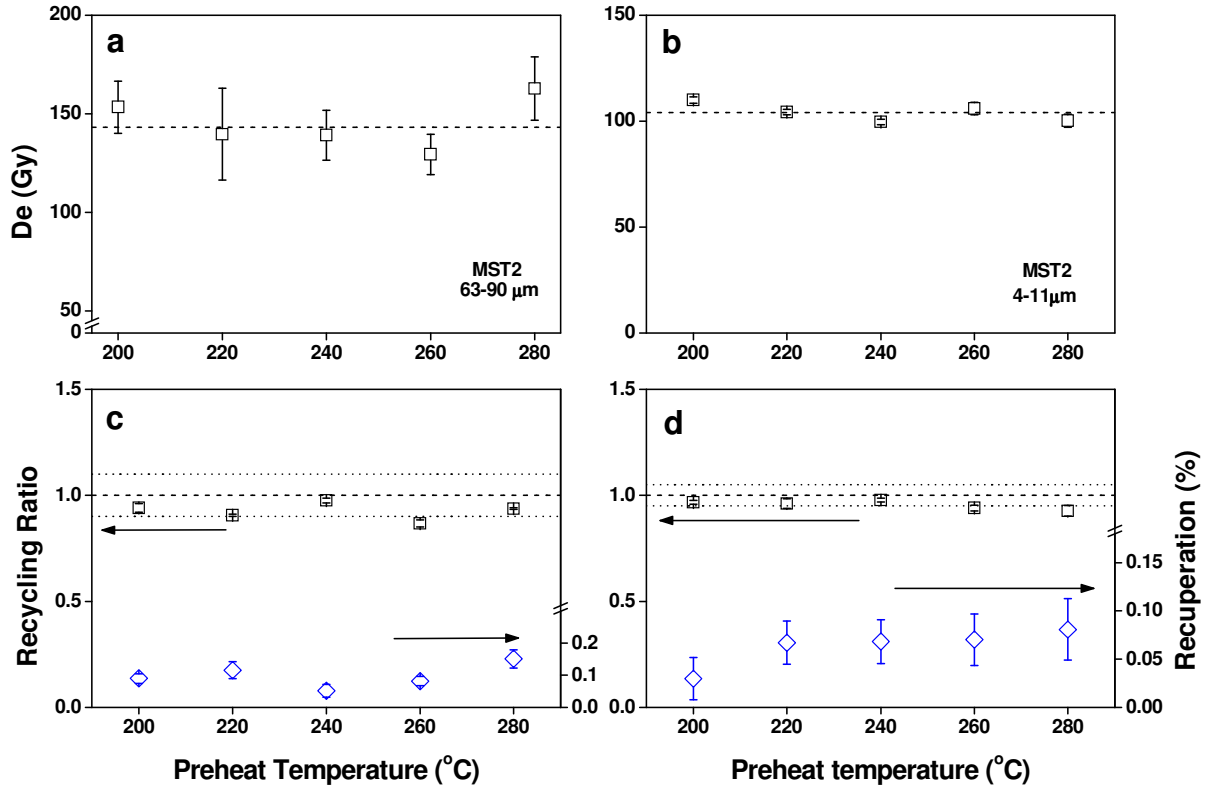

Figure III.4: *Equivalent dose as a function of preheat temperature for sample MST2, sand-sized grains (a); silt-sized grains (b). A minimum of three aliquots was used per preheat temperature and the error bars represent one standard error. The dashed line (eye guide) highlights the average value across the 200-280°C preheat temperature interval. (c) and (d) present recycling ratios and recuperation as a function of preheat temperature for the same aliquots as in (a) and (b). Error bars represent one standard errors. The dashed and dotted lines (eye guide) highlight the ideal recycling ratio of unity and a ± 10% (c) and ± 5% (d), respectively.*

The values obtained in the three tests (recycling ratio, recuperation and dose recovery) are usually considered as acceptable in the literature. Therefore, equivalent dose measurements were subsequently performed. Table III.1 summarizes the average D_e values (± 1 standard error) that were obtained using the same SAR protocol as previously used to date the section near Mircea Vodă (Timar et al., 2010; Timar Gabor et al., 2011). For each sample, in between 4 and 18 replicate measurements of D_e were made. A value was accepted if both the recycling ratio and the IR depletion ratio were within 10% of unity, and if recuperation did not exceed 5% of the corrected natural signal. No aliquots had to be rejected on the basis of recuperation or feldspar contamination. Some aliquots, however, had to be rejected on account of a poor recycling but only for the coarse grains. Especially for sample MST9, the correction for sensitivity changes appears rather problematic, as more than half of the aliquots had to be excluded from the analysis. The aberrant and poor luminescence behaviour of this particular sample had also been identified through the dose recovery test.

III.1.4. Dosimetry

Radionuclide activity concentrations were obtained through high-resolution gamma-ray spectrometry and converted to dose rates using the conversion factors calculated from the data presented by Adamiec and Aitken (1998). For 63-90 μm grains the external beta dose rates were corrected for the effects of etching and attenuation using a factor of 0.94 (± 5 % relative uncertainty (Mejdahl, 1979). Moreover, an internal dose rate of 0.013 ± 0.003 Gy/ka was assumed (Vandenberghe et al., 2008). In the case of 4-11 μm grains, an a-value of 0.04 ± 0.02 was adopted to allow for the lower efficiency of alpha radiation in inducing luminescence. A water content of 20 ± 5% was used to account for the effect of moisture (Balescu et al., 2003) and the contribution from cosmic radiation was calculated following Prescott and Hutton (1994). Table III.1 summarizes the dosimetric information. It can be seen that there is little variation in dose rate with depth and the values are spread around a mean value (± 1 standard error) of 2.84 ± 0.02 Gy/ka and 3.26 ± 0.02 Gy/ka for coarse and fine grains respectively.

Sample	Depth (cm)	Grain size (μm)	^{226}Ra (Bq kg^{-1})	^{232}Th (Bq kg^{-1})	^{40}K (Bq kg^{-1})	Total Dose Rate (Gy / ka)	De (Gy)	Age (ka)	σ_r (%)	σ_{sys} (%)	FG/ CG
MST 1	**210**	**63-90** **4-11**	33 ± 1	40 ± 1	594 ± 8	2.85 ± 0.03 3.31 ± 0.03	**175 ± 8** (n=17/18) **138 ± 2** (n=7/7)	**61 ± 8** **42 ± 6**	5 2	13 14	0.69
MST 2	**220**	**63-90** **4-11**	32 ± 1	41 ± 1	591 ± 8	2.84 ± 0.03 3.29 ± 0.03	**130 ± 10** (n=7/10) **113 ± 2** (n=8/8)	**46 ± 7** **34 ± 5**	7 2	13 14	0.74
MST 3	**232**	**63-90** **4-11**	35 ± 1	41 ± 1	606 ± 8	2.93 ± 0.03 3.40 ± 0.03	**153 ± 4** (n=9/11) **151 ± 4** (n=7/7)	**52 ± 7** **44 ± 6**	3 3	13 14	0.85
MST 4	**242**	**63-90** **4-11**	32 ± 1	40 ± 1	625 ± 6	2.91 ± 0.02 3.36 ± 0.02	**162 ± 18** (n=8/8) **134 ± 2** (n=8/8)	**56 ± 9** **40 ± 6**	11 1	13 14	0.71
MST 5	**256**	**63-90** **4-11**	33 ± 1	41 ± 1	609 ± 8	2.90 ± 0.03 3.36 ± 0.03	**169 ± 9** (n=6/8) **146 ± 1** (n=8/8)	**58 ± 8** **44 ± 6**	5 1	13 14	0.76
MST 6	**267**	**63-90** **4-11**	32 ± 1	39 ± 1	612 ± 9	2.86 ± 0.03 3.30 ± 0.04	**185 ± 9** (n=15/15) **147 ± 2** (n=7/7)	**65 ± 9** **44 ± 6**	5 2	13 14	0.68
MST 7	**278**	**63-90** **4-11**	32 ± 1	41 ± 1	603 ± 8	2.86 ± 0.03 3.32 ± 0.03	**191 ± 17** (n=7/8) **149 ± 3** (n=6/6)	**67 ± 11** **45 ± 6**	9 2	13 14	0.67
MST 8	**293**	**63-90** **4-11**	34 ± 1	41 ± 1	605 ± 8	2.90 ± 0.03 3.36 ± 0.03	**186 ± 12** (n=10/13) **152 ± 2** (n=8/8)	**64 ± 9** **45 ±6**	6 2	13 14	0.70
MST 9	**330**	**63-90** **4-11**	31 ± 1	37 ± 1	593 ± 8	2.76 ± 0.03 3.18 ± 0.03	**260 ± 28** (n=5/17) **X**	**94 ± 16** **X**	11 X	13 X	x
MST 10	**350**	**63-90** **4-11**	31 ± 1	38 ± 1	576 ± 6	2.72 ± 0.02 3.15 ± 0.03	**210 ± 16** (n=5/5) **X**	**77 ± 11** **X**	7 X	13 X	x
MST 11	**375**	**63-90** **4-11**	32 ± 1	37 ± 1	591 ± 8	2.76 ± 0.03 3.19 ± 0.03	**232 ± 33** (n=7/11) **178 ± 4** (n=7/7)	**84 ± 16** **56 ± 8**	14 3	13 14	0.66
MST 12	**400**	**63-90** **4-11**	32 ± 1	39 ± 1	606 ± 8	2.83 ± 0.03 3.27 ± 0.03	**237 ± 22** (n=11/13) **193 ± 2** (n=8/8)	**84 ± 13** **59 ± 8**	9 2	13 14	0.70
MST 13	**425**	**63-90** **4-11**	33 ± 1	41 ± 1	601 ± 8	2.86 ± 0.03 3.31 ± 0.03	**277 ± 15** (n=11/13) **X**	**97 ± 14** **X**	6 X	13 X	x
MST 14	**450**	**63-90** **4-11**	32 ± 1	40 ± 1	621 ± 8	2.88 ± 0.03 3.32 ± 0.03	**273 ± 25** (n=8/8) **191 ± 2** (n=8/8)	**95 ± 15** **58 ± 8**	9 1	13 14	0.61
MST 15	**475**	**63-90** **4-11**	32 ± 1	40 ± 1	618 ± 9	2.86 ± 0.03 3.31 ± 0.04	**253 ± 38** (n=3/6) **217 ± 1** (n=8/8)	**88 ± 18** **66 ± 9**	15 1	13 14	0.75
MST 16	**500**	**63-90** **4-11**	31 ± 1	40 ± 1	589 ± 8	2.77 ± 0.03 3.23 ± 0.03	**275 ± 51** (n=6/10) **219 ± 5** (n=6/6)	**100 ± 22** **68 ± 10**	19 2	13 14	0.68
MST 17	**550**	**63-90** **4-11**	29 ± 1	38 ± 1	557 ± 7	2.63 ± 0.02 3.03 ± 0.03	**279 ± 28** (n=5/6) **265 ± 5** (n=7/7)	**107 ± 18** **87 ± 12**	10 2	13 14	0.81
MST 18	**575**	**63-90** **4-11**	30 ± 1	38 ± 1	585 ± 6	2.70 ± 0.02 3.11 ± 0.03	**391 ± 28** (n=5/6) **252 ± 3** (n=11/11)	**144 ± 21** **81 ± 12**	7 2	13 14	0.56
MST 19	**600**	**63-90** **4-11**	29 ± 1	38 ± 1	585 ± 7	2.69 ± 0.02 3.10 ± 0.03	**288 ± 57** (n=4/4) **289 ± 9** (n=6/6)	**107 ± 26** **93 ± 14**	20 3	13 14	0.87

Table III.1: *Summary of radionuclide activities, calculated total dose rates, equivalent doses (D_e), optical ages, and random (σ_r) and systematic (σ_{sys}) uncertainties. The number of accepted aliquots out of the total measured is indicated in the subscript to the D_e-data. Uncertainties mentioned with the D_e and dosimetry data are random; all uncertainties represent one sigma. The uncertainty associated with the water content (20 ± 5 %) is dominant in the overall systematic uncertainty. The ratio of the age results obtained using the fine grains (FG) to the coarse grains (CG) is given in the last column.*

III.1.5. Optical ages

All information relevant to the optical age and uncertainty calculation is summarized in Table III.1. Uncertainties on the optical ages were calculated following the error assessment system proposed by Aitken and Alldred (1972) and Aitken (1976). In general, the systematic uncertainty is dominant in the overall uncertainty on the ages, which amounts to 13-14 % for coarse quartz and ~ 14 % for fine quartz. The systematic error is dominated by the error associated with the effect of the uncertainty in water content. The overall contribution from random sources of uncertainty varies between ~3 and 20 % for coarse quartz and between 1 and 3 % for fine quartz. Within this uncertainty, most of the optical ages are consistent with the stratigraphic position of the samples and they increase smoothly with depth. At 3σ level, only the age result of sample MST1, obtained using coarse quartz, appears irreconcilable with the results obtained for the underlying samples. It is therefore concluded that all sources of random uncertainty have been identified and properly accounted for, and that the observed variability is not much larger than expected from the individual uncertainties. An increase in random uncertainty is observed for samples MST 10-19 compared to MST 1-8. This is probably related to the small number of aliquots used for D_e determination but also due to the high value of the natural OSL on the dose-response curve which increases the uncertainty in equivalent dose (see Fig. 4 of Murray and Funder, 2003).

For all investigated samples, the ages obtained using the 4-11 μm quartz appear systematically younger than the ages obtained using the 63-90 μm quartz, with an age difference ranging from ~ 13 to 44 % (see Table III.1).

Fig. III.5 presents the two sets of OSL ages obtained using sand-sized (63-90 μm) and silt-sized (4-11 μm) quartz grains in comparison with the magnetic age depth model established by Necula and Panaiotu (2008). No confidence limits can be defined for the time-depth model,

but we incorporated a depth error of ± 10 cm for the correlation between the sequence investigated here and the one for which the model was established. Within analytical uncertainty, the time-depth model appears consistent with both sets of optical ages for the uppermost eight samples. For the remainder of the samples, this agreement remains only for the coarse quartz age results. Some spread can be observed in the OSL ages obtained for samples taken from the S1 unit (MST 13-18). As discussed above, the observed spread is not higher than expected from the random uncertainties associated with these age estimates, which range from ~6 to ~19%. This behaviour might be the effect of pedogenic processes such as bioturbation (see e.g. Bateman et al., 2007) as S1 is a palaeosol.

According to the sand-sized quartz ages, palaeosol S1 formed during the last interglacial period, commonly identified with the Marine Isotope Stage 5 (MIS 5; ~ 130-70 ka; Lisiecki and Raymo, 2005); this is also in accordance with the IRSL chronology established by Balescu et al. (2010) at this locality. However, the silt-sized quartz ages indicate that the soil formation started during the latest part of MIS 5, namely MIS 5a (Shackleton et al., 1990), and continued also during the MIS 4 glacial. This is in contradiction with the chronostratigraphy established for the loess-palaeosol sequences in this region based on magnetic susceptibility data (Panaiotu et al., 2001; Buggle et al., 2009). The lack of an independent age control does not allow us to constrain the depositional chronology for this profile.

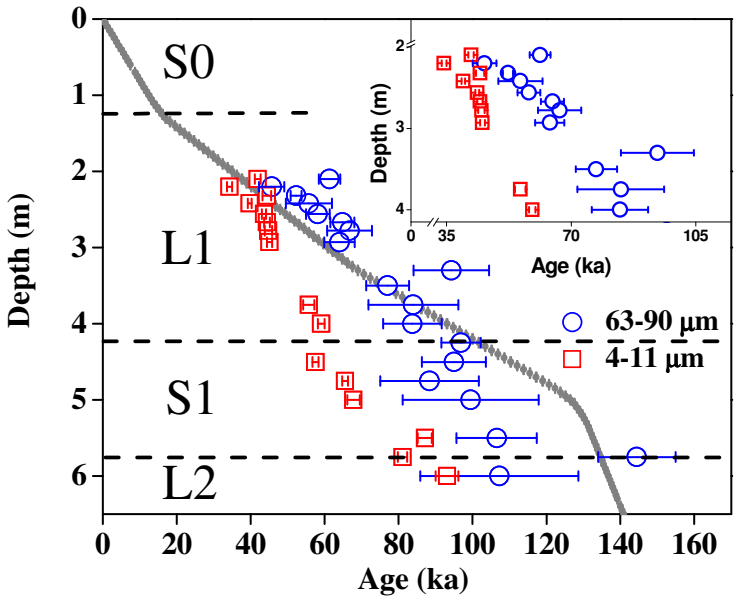

Figure III.5: *Plot of optical ages (1 sigma total uncertainties) from silt-sized (open squares) and sand-sized (open circles) quartz grains. The magnetic age-depth model is shown by the dotted line with error bars incorporating a depth error of ± 10 cm for the correlation between the section investigated here and the one for which the model was established (Necula and Panaiotu, 2008). The dashed lines (eye guide) highlight the boundaries of the stratigraphic units. The inset shows the optical ages (1 sigma random uncertainties) obtained for the L1 unit.*

The age discrepancy appears to be related to the difference in D_e values obtained using the two quartz fractions. The D_e values obtained for sand-sized quartz are systematically higher than the values obtained for the silt-sized quartz with no apparent dependence on the stratigraphic position of the samples (Fig. III.6a). Timar Gabor et al. (2011) obtained similar results for the loess sequence Mircea Voda section. For the sake of completeness the ratio of the equivalent doses obtained for the latter section is presented in Fig. III.6b. These results are very concerning as the equivalent doses obtained on coarse-grained etched quartz should be smaller than those obtained on the fine grains when considering the effective dose rates.

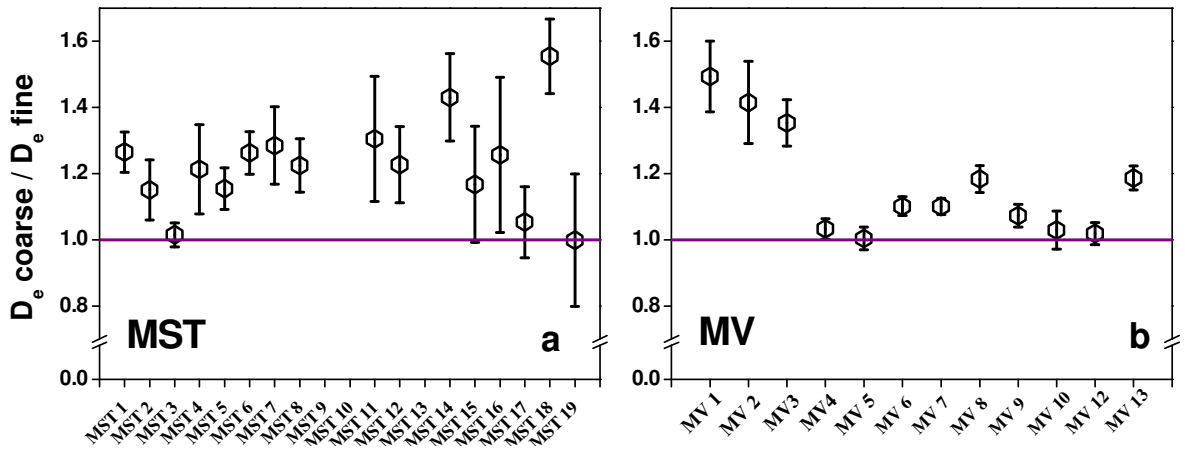

Figure III.6: *Summary of the ratios between the equivalent doses obtained on coarse quartz to the equivalent doses obtained on the fine quartz for Mostiştea (a) and Mircea Vodă (b). Error bars represent one standard error.*

III.2. An investigation into the reliability of SAR-OSL equivalent doses obtained for quartz samples displaying dose response curves with more than one component

III.2.1. Introduction

Dose response curve construction is an essential part of equivalent dose determination in luminescence dating. The development of the single aliquot regenerative dose (SAR) protocol (Murray and Wintle 2000, 2003) allowed for the construction and study of dose response characteristics of quartz of different grain sizes and origins. Assuming first order kinetics and a single electron trap/recombination centre involved in OSL production in quartz, a single saturation exponential (SSE) function would be expected to fit a growth curve. A single component will increase with dose according to

$$I(D) = I_0(1 - \exp(-D / D_0)),$$

where *I(D)* is the intensity of the signal for a given dose *D*, I_0 is the limit of saturation (for an infinite dose) and D_0 the dose that characterises the rate of onset of saturation with dose, also named characteristic dose in literature.

Wintle and Murray (2006) reviewed values reported in literature for the characteristic dose for the mathematically separated fast component of coarse quartz and concluded that reported values ranged from 55 to 190 Gy. However, as pointed out by Preusser et al. (2009), it is not yet established whether these differences relate to different intrinsic properties of the investigated quartz or whether some variability relates to the choice of the value of the largest regenerative dose used.

However, increasingly presented in literature are quartz samples with OSL signals dominated by a fast component for which the dose response curve at high doses was reported not to be satisfied by a single saturating exponential regression model. In their attempt to construct a standardised growth curve (SGC) for coarse quartz grains, Roberts and Duller (2004) reported that for doses higher than 125 Gy an additional linear term has to be added to the dose response and reported higher scatter of data in this region. The scatter was attributed to causes such as the small number of grains used or possible feldspar inclusions and the potential use of the SGC was

restricted to 40 Gy. This approach was applied to medium size quartz (45-63 μm) from 4 locations on the Chinese Loess Plateau (Lai, 2006) and extended to 15 loess samples of the same grain size but different origins (Lai et. al., 2007). Growth curves constructed up to 200 Gy showed similar dose response characteristics and a SSE+linear regression was used. Medium size quartz OSL growth curves constructed up to 600 or 700 Gy and fitted with a single saturating exponential function and a linear component have been presented for loess samples from Yanbao (Lai et al., 2008) as well as Luochuan (Lai, 2010). In the latter study a value of 128 Gy was quoted for the characteristic dose of the exponential function. A similar characteristic dose (117 Gy) was reported based on a SSE+linear fit for doses up to 1000 Gy by Buylaert et al. (2008), in their study on 63-90 μm quartz of Chinese loess, while Murray et al. (2008) reported lower saturation characteristics (67 Gy) for their fluvial sandy quartz (180-250 μm) based on the same regression model and a dose response constructed up to 800 Gy. OSL dose response curves for fine quartz (4-11μm) have been reported to follow the same pattern, a SSE+linear regression model as presented in several studies for doses up to 700 Gy (Lowick et al., 2010a; Sugisaki et al., 2010; Schmidt et al., 2011; Shen and Mauz, 2011; Timar et al., 2010).

By constructing the dose response up to higher doses, some authors suggested that a double saturating exponential model (DSE) would more closely fit their data. Murray et al. (2007) took this approach for coarse (180-250 μm) quartz and by constructing the dose response up to 1000 Gy reported characteristic doses of 44 and 450 Gy, respectively for the two components, while Pawley et al. (2010) applied a maximum dose of 1200Gy and reported similar characteristic doses for their coarse (180-250 μm) quartz (50 and 320 Gy, respectively). Lowick and Preusser (2011) used a DSE model for the dose response constructed on fine (4-11 μm) quartz, while Lowick et al. (2010b) extended their dose range investigations up to 4200 Gy quoting characteristic higher characteristic doses of 128 and 1680 Gy, respectively for their fine grains. In this work they have also shown that the linear term observed up to 1000 Gy represents the early expression of a second and later saturating exponential. This result seems logical as a linear growth at high doses is unlikely to be the true representation of the dose response as the source of the signal should be finite and eventually lead to saturation.

It has been recently shown (Berger and Chen, 2011) that in the dose range useful for dating the equivalent doses obtained using a SSE+linear or a DSE fit are not statistically different; thus there would not be much case for concern regarding the precision of the different

regression models. However, the accuracy of the equivalent doses obtained using the growth resulting from the second function remains questionable and requires further investigations (Wintle, 2010).

The previous investigations on fine (4-11μm) and coarse (63-90 μm) grained quartz samples from the loess section near Mircea Vodă (SE Romania), showed a higher than exponential pattern of growth for the dose response (Timar et al., 2010; Timar Gabor et al., 2011). As very different patterns of growth were observed for the two grain sizes for regenerative doses applied up to 700 Gy, the present work aims at deepening these investigations by analysing the dose response pattern in the very high dose region 5000-10000 Gy. Luminescence characteristics of fine and coarse quartz extracted from Mostiştea section will be documented along with new data from Mircea Vodă in order to gain more insight into the equivalent dose discrepancy obtained for the two fractions.

For samples collected from the Mircea Voda (MV) section, this study uses archived material of samples from the previous studies by Timar et al. (2010) and Timar Gabor et al. (2011). For the sake of clarity, for all samples presented in this work the field codes will be used. An additional sample (CSTinf) has been collected from Costinesti section (see Section I.6.1). The sampling location is very close to Tuzla section (Fig. I.3) which has been previously investigated by Balescu et al. (2003, 2010). This sample was taken from below S6 soil and is expected to have an age of at least 800 ka (for additional details, the reader is referred to the work of Balescu et al., 2010).

III.2.2. Thermal stability

From the ratios of D_e values shown in Figure III.6(b), a leading concern would be related to a thermal instability of the OSL signal from the fine fraction. This could be caused either by contamination of the signal with an unstable medium OSL component (see e.g. Choi et al. (2003); Li and Li (2006); Steffen et al. (2009)), or by instability of the fast OSL component itself (Fan et al., 2011). A high resolution pulse anneal measurement was therefore performed for sample MST5 using a single aliquot from each grain size. This sample has an equivalent dose of approximately 150 Gy (Table III.1). The natural signals from each aliquot were first measured using the same SAR protocol that was applied for D_e measurement (see Section III.1.2). The

aliquots were then given a 200 Gy dose, preheated for 10 s to a temperature between 160 and 400 °C (in a 10 °C step) and measured to give L_x; this was followed by a measurement of the response to a 17 Gy test dose after a fixed cutheat at 180 °C. Figures III.6a and b show the sensitivity-corrected signals for the coarse and fine quartz respectively. The reproducibility of the measurements was confirmed by repeating the measurements for preheat temperatures of 240 and 300 °C (Fig III.7a and b; triangles). The same type of experiment was also performed for a calibration quartz aliquot of 63-90 µm (see Fig. III.7b – solid circles); the only difference was that the regenerative and test doses were 3.4 and 1.7 Gy respectively.

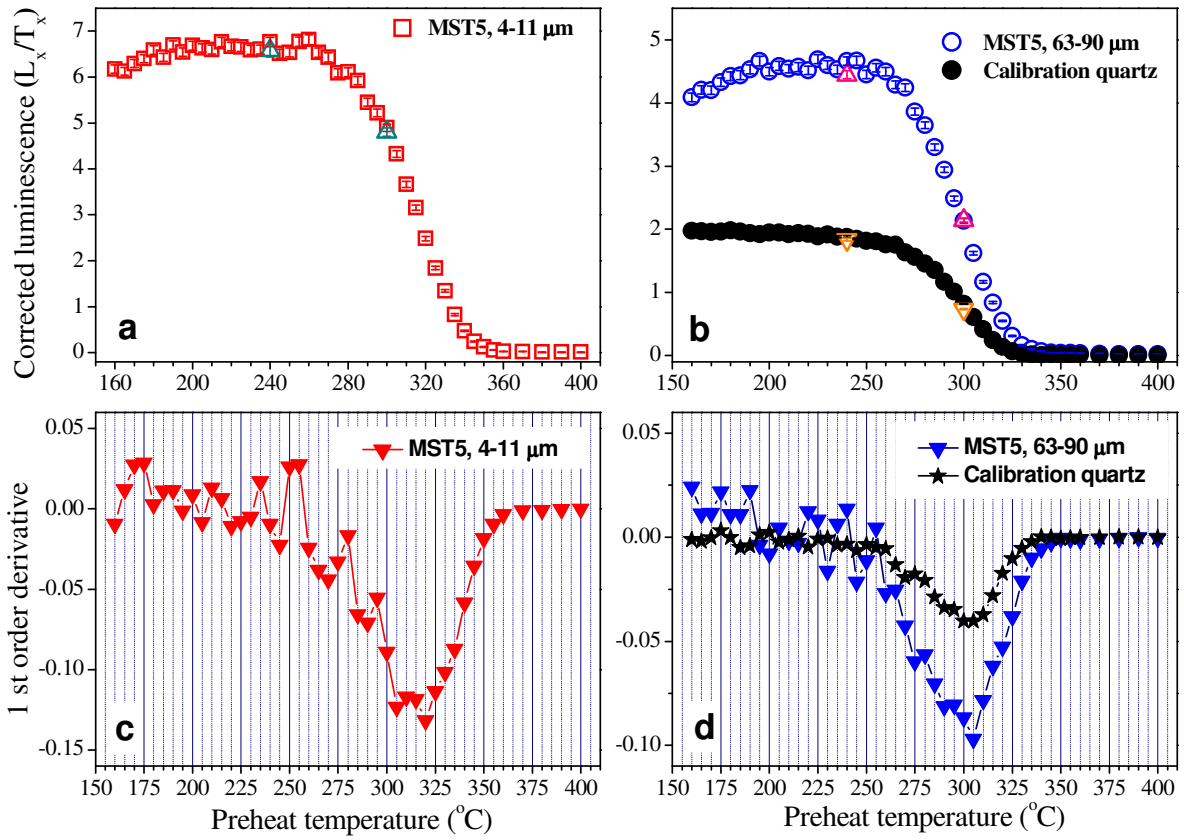

Figure III.7: *(a) Pulse annealing curves for OSL signals for an aliquot of silt-sized (a) and sand-sized (b) quartz grains for sample MST 5. Pulse anneal characteristics obtained for calibration quartz are also shown in (b). (c) and (d) present the first order derivatives of the data in (a) and (b) respectively.*

A very consistent pattern is observed for between the three types of quartz investigated. There is no decrease in the sensitivity corrected OSL when heated up to ~ 260°C for 10 s and the signals are fully eroded by a thermal treatment of 10 s at 330-350 °C. Fig. III.7c and d plot the first derivative for the pulse anneal data in Fig. III.7a and b, respectively. It is used as an

indicator of the thermal removal of the fast component with increasing preheat temperature. The single peak at ~ 300 ^{o}C occurring in all three graphs suggests that the stability of the fast component for both grain sizes is the same and thus the long term stability of the signal should not be a problem. The slight difference in the peak temperature between the fine grain (Figure III.7c) and coarse grain (Figure III.7d) is most likely to be related to the different heat transfer for the aluminium and stainless steel discs, and this could be checked by deposition of fine grains on a stainless steel discs and repeating the experiment.

III.2.3. Dose response

Dose response characteristics were investigated using samples collected from both Mircea Vodă and Mostiştea loess sequences. Fig. III.8 shows extended dose response curves using regenerative doses up to 10 kGy obtained for two samples from the loess sequence at Mircea Vodă. A test dose of 17 Gy was used for both fine and coarse grains. Fitting was carried out using either a single saturating exponential function (SSE) or a double saturating exponential (DSE) function. In both cases, the fits were best with a DSE function as indicated by the reduced chi square values as well as the residual sums of squares (see Table III.2). However, it can also be seen that the saturation characteristics of the two grain sizes are very different, the coarse grains saturating much earlier. This explains why the L_x/T_x for low preheat temperatures for coarse grains of MST5 (Fig III.7b) is smaller than that for the fine grains (Fig. III.7a) when the doses used to obtain L_x and T_x were fixed at 200 and 17 Gy, respectively. Sensitivity changes appear accurately corrected as indicated by recycling ratios measured for different regenerative doses (Fig.III.8a,b; grey-filled triangles). Furthermore, the dose response curves pass close to the origin, demonstrating that recuperation is negligible.

Regression model	Data points used	Degrees of freedom	Reduced χ^2	Residual sums of squares
MV 10 4-11 µm				
SSE	14	11	0.92	10
DSE	14	9	0.085	0.76
MV 8 63-90 µm				
SSE	14	11	0.162	1.8
DSE	14	9	0.05	0.5

Table III.2: *Comparison between the goodness of fit using a SSE and a DSE regression model for dose-response curves constructed up to 10000 Gy for samples collected from the loess sequence at Mircea Vodă.*

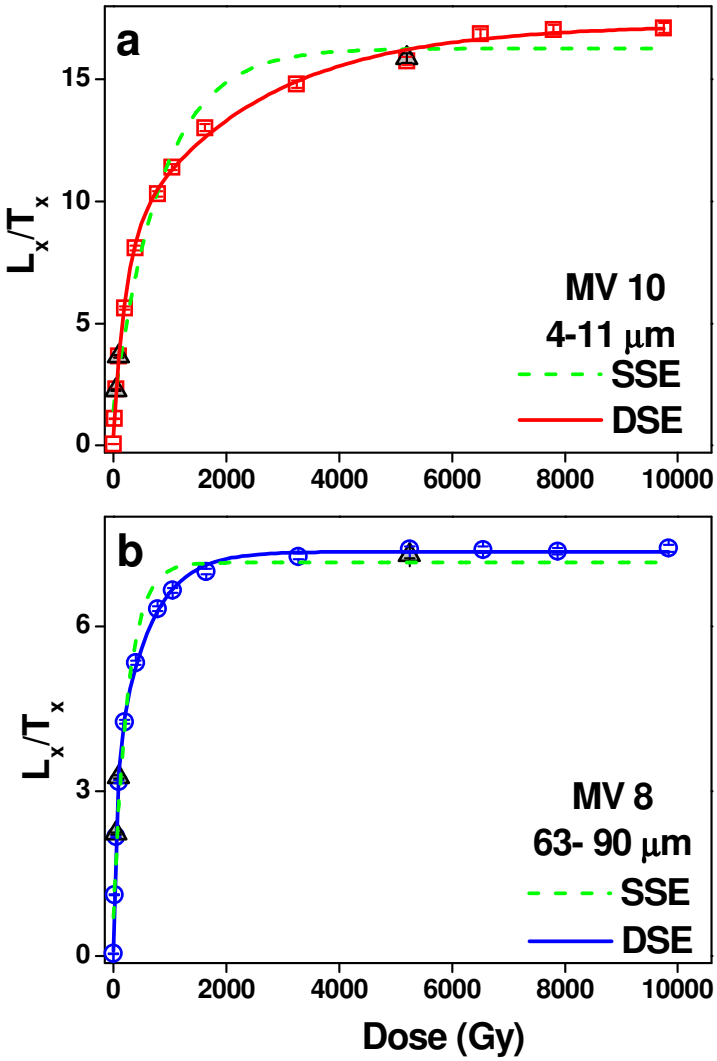

Figure III.8: *Comparison between sensitivity-corrected growth curves constructed using silt-sized quartz (a) and sand-sized quartz (b) extracted from samples collected from Mircea Vodă. The L_x/T_x data are fitted with either a single saturating exponential (SSE) or a double saturating exponential (DSE) function. Recycled points are shown as grey-filled triangles.*

It is important to note that the above mentioned behavior is a characteristic of the fast OSL component. Dose response curves for the LM-OSL signals up to just over 1 kGy have been constructed for both fine and coarse grains of sample MV9 (Fig. III.9). It was observed that the position of the first peak of the LM-OSL does not change with irradiation dose. The fact that the

integrated signal used to construct the dose response is indeed the fast component was confirmed as well by the fact that this signal is reduced to a negligible level after an 8000 s IR bleach at 160 ^{o}C (Jain et al., 2003; Fig. III.10).

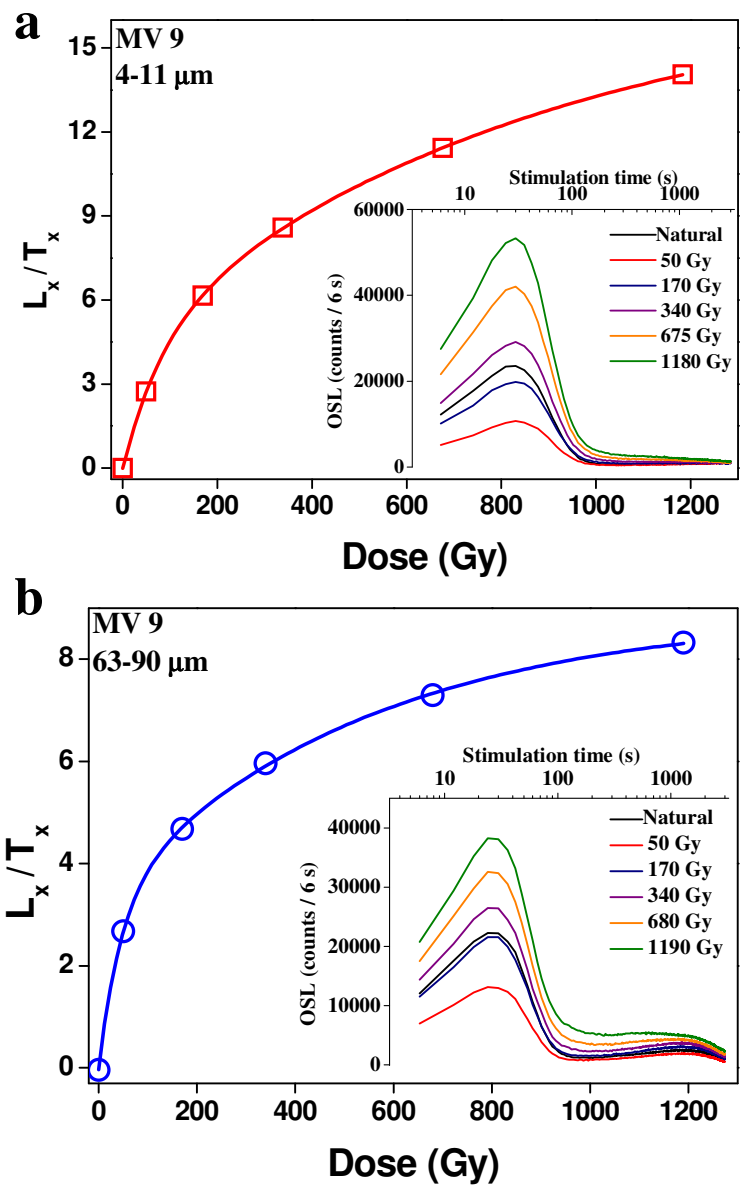

Figure III.9: *Dose response curves constructed using LM-OSL signals for fine (a) and coarse (b) quartz of sample MV9. The insets show the LM-OSL for the natural and regenerated signals.*

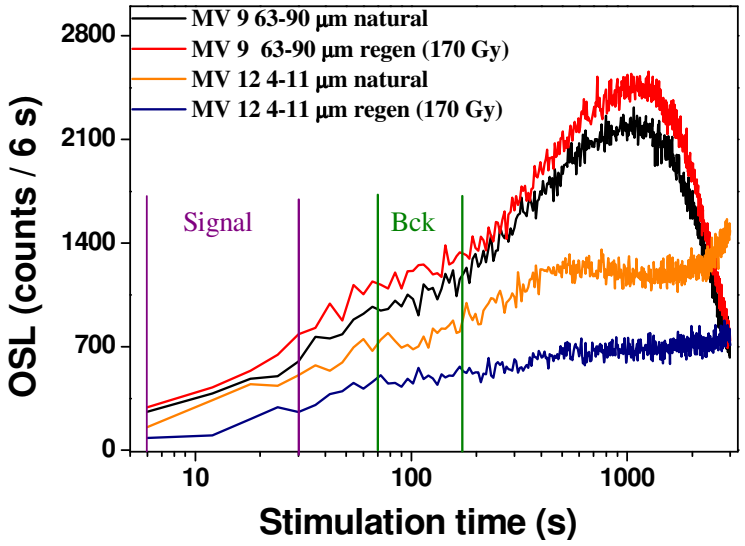

Figure III.10: *Natural and regenerated LM-OSL signals obtained using MV12 fine quartz and MV9 coarse quartz, respectively. The signals were measured following IR stimulation at 160 ^{o}C for 8000 s. The vertical lines indicate the integration region of the OSL signal (the first 30 s of stimulation) and the region used for background evaluation (between 60 and 180 s of stimulation).*

Dose response curves were obtained up to 5000 Gy for both coarse and fine grains from a number of samples from site MST (Fig. III.11). The growth of the signal with dose is best represented by the sum of two saturating exponential functions for all samples investigated. The coarse grain samples (MST 3, 7 and 19) show negligible growth when doses above 1000 Gy are used. This is in contrast to the continuing growth shown by the fine grain samples (MST2, MST6, MST 13, MST 19). There appears to be a fundamental difference in response between fine and coarse grained quartz when doses up to 5000 Gy are used to construct dose response curves.

The saturation characteristics for all the data plotted in Fig. III.11 is summarized in Table III.3. The values for the characteristic doses D_{01} and D_{02} do not seem to vary with the stratigraphic depth of the sample but are very different for the two different grain size fractions. Timar Gabor et al. (2011) made the same observation for samples collected at Mircea Vodă.

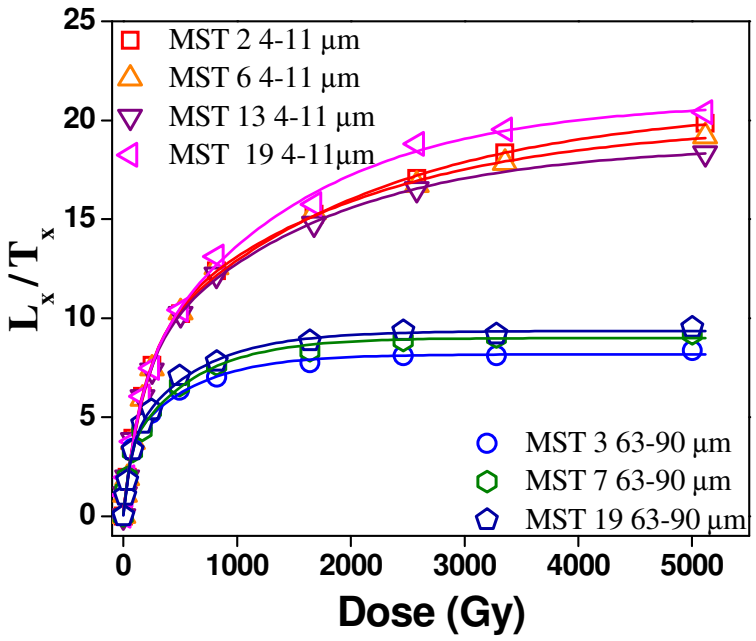

Figure III.11: *Dose response curves constructed using silt- and sand-sized quartz extracted from different samples from Mostiştea. The solid lines represent the best fit to the sum of two saturating exponential functions.*

SAMPLE	I_0	A	D_{01}	B	D_{02}	Red. χ^2	RSS
MST 2 4-11 µm	0.2±0.1	7.7 ± 0.5	168 ± 16	12.9 ±0.4	2031 ± 202	0.032	0.22
MST 6 4-11 µm	0.3±0.2	8.3 ± 0.7	200 ± 24	11.3 ± 0.5	1917 ± 280	0.047	0.33
MST 13 4-11 µm	0.2 0.1	7.3 ± 0.6	164 ±18	11.2 ± 0.5	1588 ±163	0.003	0.19
MST 19 4-11 µm	0.2±0.2	6.5 ± 1.0	154 ± 35	14.3 ± 0.8	1500 ± 216	0.109	0.76
MST 3 63-90 µm	0.1±0.1	3.5 ± 0.3	53 ± 9	4.6 ± 0.3	576 ± 69	0.019	0.14
MST 7 63-90 µm	0.1±0.2	3.1 ± 0.4	49 ± 12	5.8 ± 0.4	586 ± 64	0.036	0.25
MST 19 63-90µm	0.1±0.1	3.6 ± 0.4	66 ± 13	5.7 ± 0.4	600 ± 72	0.024	0.17

Table III.3: *Fitting parameters for OSL dose response of samples of different ages from Mostistea*

The continuing growth of the signals up to very high doses might be attributed to feldspar contamination or small feldspar inclusions inside the quartz grains that would be unable to be removed by HF etching. Nonetheless, this possible explanation was discarded by observing the IR response of both fine and coarse grains after an irradiation with a very high dose (2600 Gy). The IRSL signal (integration of counts collected in the first seconds of stimulation) amounts to less than 1% of the OSL signal recorded for the same disk during OSL stimulation for both grain sizes investigated (Fig. III.12).

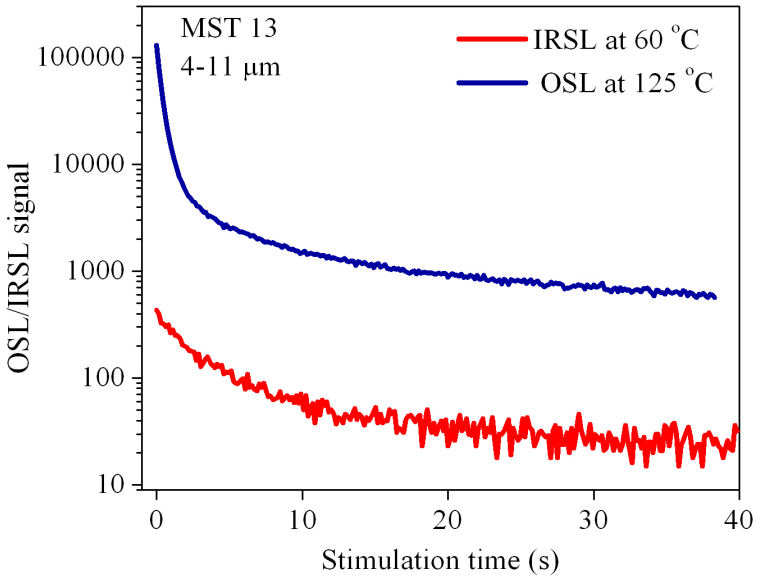

Figure III.12: *Comparison between OSL and IRSL signals measured following the administration of a 2600 Gy dose. The stimulation temperatures are indicated in the legend. Note the logarithmic scale of the signal intensity axis.*

Considering this systematic difference between the saturation characteristics obtained for the two quartz fractions investigated, one should ask oneself the question whether these differences are related to the unexpected results obtained for the D_e values of fine and coarse grains at both Mircea Vodă and Mostiştea. Also, what causes the difference in saturation characteristics seen in Fig. III.11?

III.2.4. Different bleaching history?

A fundamental difference that exists in nature between the coarse grains and the fine grains is the fact that the latter suffer multiple cycles of bleaching and irradiation. In order to see whether this may be reflected in the dose response saturation characteristics, an experiment was performed for nine aliquots of coarse quartz from three different samples collected from three different loess sequences (Mircea Vodă, Mostiştea and Costineşti). The samples were first optically zeroed using a double blue stimulation at room temperature for 100 s with 10 ks pause inbetween. The aliquots were then given a 170 Gy dose and the OSL signal was measured using blue stimulation at 125 °C for 40 s. This was repeated for five times in order to accumulate a dose of ~ 1000 Gy, though the OSL is removed by bleaching. A dose response curve was then built using seven regenerative doses up to ~ 1050 Gy. Fig. III.13a shows the saturation characteristics (D_{01}, D_{02})

obtained in this experiment compared with the values obtained when the measurement was performed following the measurement of the natural signal. Fig III.13b presents the change in sensitivity that occurred following each bleach-dose cycle in which 170 Gy was given. A sensitization of all aliquots with bleaching and dosing was noticed, as also reported in other studies (e.g. Moska and Murray, 2006) but there was no noticeable change in the dose response curve shape constructed for the aliquots that were subjected to this treatment compared to aliquots from the same samples on which the dose response curve was constructed following the measurement of the natural (Fig. III.13.a). A further experiment with alpha irradiation would be of great interest.

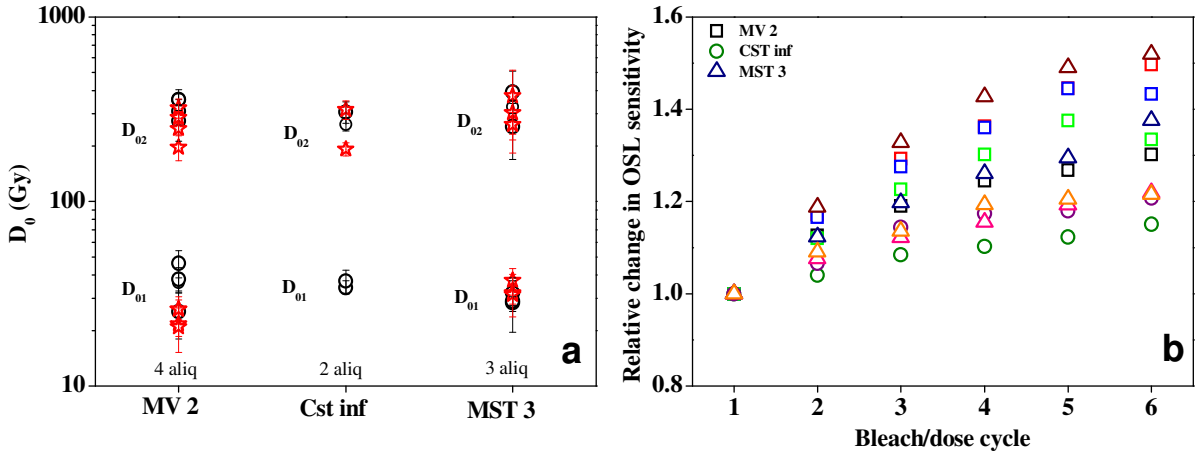

Figure III.13: *(a) Comparison between the saturation characteristics (D_{01}, D_{02}) obtained for dose-response curves constructed after multiple bleach/dose cycles (open stars) and the values obtained for dose-response curves constructed for D_e measurement. The data are obtained from samples collected from Mircea Vodă (MV2), Costineşti (Cst inf) and Mostiştea (MST3). The number of aliquots used is indicated above the sample labels. (b) The relative change in OSL sensitivity as a function of the bleach/dose cycle. The data represent the net OSL signals obtained in each cycle(from the 170 Gy dose) normalized to the OSL signal from the first cycle.*

III.2.5. Growth curve reproducibility

We have also tested the reproducibility of the dose response curve using coarse quartz grains extracted from MV8 (Mircea Vodă). A dose response curve was first constructed up to 15 kGy (represented by circles). A number of regenerative doses were remeasured (repeat points represented by triangles). After constructing this dose response, the sample was bleached, given

a dose of 170 Gy and then the process was repeated. It can be seen that the dose response pattern is the same (stars in Fig. III.14); the dose response was fitted using a double saturating exponential model and the curve saturates. The sensitivity measured by the test dose (T) is also shown as a ratio to the test dose response T_{nat} measured following the first OSL measurement (see Fig. III.14 - inset). T/T_{nat} fluctuates, first decreasing and then increasing as the regenerative dose is increased, but T does not change more than about 30% from the initial value.

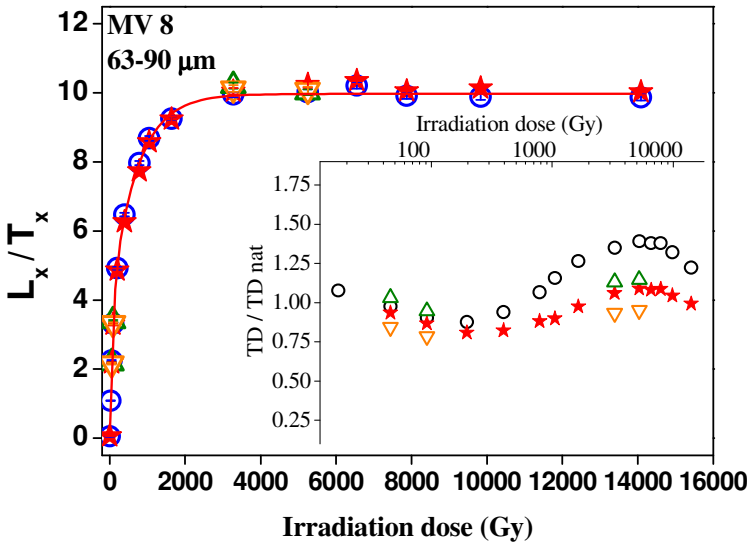

Figure III.14: *Growth curve reproducibility test for a coarse quartz aliquot of sample MV8 (see text for experimental details). The first growth is represented by circles while the second growth is represented by stars. Repeat points for the first and second dose responses are represented by up and down triangles respectively. The inset shows the change in sensitivity monitored by the response to the test dose.*

III.2.6. An infinitely old sample

In order to test whether the difference in dose response curves has an effect when an infinitely old sample is measured, we have constructed the dose response for sample CST_{inf}, collected below palaeosol unit S6 at Costinesti section. This sample is expected to have an age of at least 800 ka and thus one can assume from Fig. III.14 that the natural OSL signals for the 63-90 µm grains are in saturation, as they would have received a dose of > 2.27 kGy. When the same two grain sizes were extracted and measured, once again, the dose response curve for the coarse grains showed negligible growth above 1000 Gy (Fig. III.15), whilst this was observed for

fine quartz only above 4000 Gy (Fig. III.15a). Within 1 standard error, the values of D_e obtained were identical, both being much lower than expected from the geological context of the sample and resulting in an age of ~ 210 Ka, based on the average dose rates for Mostiştea; the natural value of L/T was below the saturation level for both grain sizes. This suggests that there has been loss of OSL signal during burial time. Furthermore, a dose recovery experiment was carried out on fine grains using a dose of 1,170 Gy and this could be recovered within 1% (Fig. III.16).

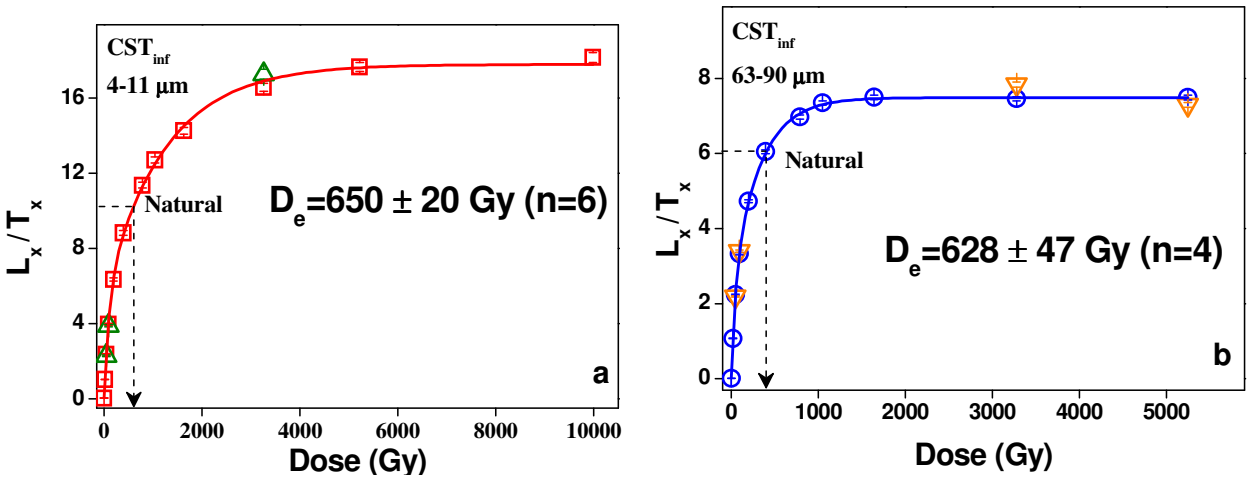

Figure III.15: *Extended dose response curves obtained for sample CST_{inf} using fine (a) and coarse (b) quartz. Recycling points are shown as triangles. The average equivalent dose obtained for each fraction is indicated as well.*

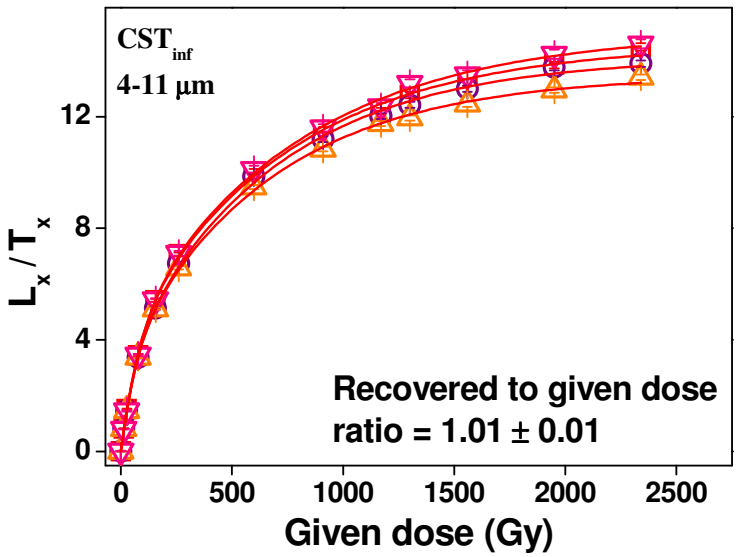

Figure III.16*: Dose-response curves obtained in the dose recovery test using four aliquots of fine-grained quartz of sample CST_{inf}. The average recovered to given dose ratio is also indicated.*

III.2.7. Fading test

In order to test whether OSL signals from fine quartz are affected by fading, four samples of fine grain quartz from Mircea Vodă (MV 4, -6, -9 and -10) were used for fading rate measurement using three aliquots per sample. The measurements were performed following the procedure proposed by Auclair et al. (2003). Table III.4 summarizes the obtained results. The fading rates are similar to the usual values reported for sedimentary quartz and do not indicate any instability of the signal due to fading.

Sample	g_{2days} (%/decade)	average g_{2days} (%/decade)
MV 4	1.70 ± 0.66 1.04 ± 0.66 1.13 ± 0.62	1.55 ± 0.41
MV6	1.21 ± 0.64 1.57 ± 0.71 1.89 ± 0.76	1.29 ± 0.37
MV 9	0.69 ± 0.59 1.17 ± 0.57 0.81 ± 0.48	0.89 ± 0.32
MV 10	1.75 ± 0.99 0.84 ± 1.10 0.85 ± 1.15	1.15 ± 0.63

Table III.4: *Summary of fading rates determined for fine quartz samples collected from the loess section at Mircea Vodă. Fading rates expressed as the percentage of signal lost during a storage period of one decade of time (g-values; Aitken, 1985), were calculated using Eq. (4) of Huntley and Lamothe (2001). The rates are normalised to a measurement delay time of 2 days after irradiation.*

III.3. Discussion and conclusions

Our study of quartz extracted from the loess sequence at Mostistea used the same methodology as the one used in the studies of Timar et al. (2010) and Timar Gabor et al. (2011) for Mircea Voda section. The signals selected for analysis from both grain-size fractions of quartz appear very similar with the ones investigated for samples at Mircea Voda. The dominance of the fast component in the OSL signals is indicated by the decay shape of the CW-OSL and LM-OSL signals. Furthermore, both quartz fractions passed the procedural tests of the single-aliquot regenerative-dose (SAR) protocol (i.e. recycling ratio, recuperation and dose

recovery up to a given dose of 1200 Gy) indicating that the protocol should provide reliable D_e values. High resolution pulse anneal experiments exclude a possible contribution from a thermally unstable component to the OSL signals from both fractions. Additionally, preliminary fading experiments confirm the stability of the investigated signal (Table III.4). However, the age results obtained for the two fractions are generally inconsistent. The age discrepancy resides in the D_e values obtained for the two quartz fractions.

Recently it has been suggested that the SAR protocol might not fully correct for sensitivity change during the measurement of the natural signal (Singhvi et al., 2011). This is currently under testing, however we do not believe it should be the case for the samples investigated in this work based on the good dose recovery and the very good agreement of the quartz fine grains ages to another dosimeter namely feldspar, post IR-IR $_{225}$ protocol (Vasiliniuc et al., submitted –a and -b).

Another issue that remains to be addressed is the observation that the natural signal of an infinitely old sample was found not to be in saturation. This was previously reported by other studies where a higher than exponential growth was observed (see e.g. Lai et al., 2010). This might imply that the laboratory constructed dose response dose not reflect the growth of the signal in nature.

The cause of the different pattern of growth in the dose response at very high doses for the two grain sizes investigated might reside in the possible different origin of the grains (Buggle at al., 2008). However, a different origin of the grains should not justify the difference in equivalent doses that leads to a systematic overestimation of the coarse grains (63-90 μm) to the fine (4-11 μm).

A comparison of the saturation characteristic doses obtained for the two fractions investigated in this study to similar studies world wide is not straightforward, as these values are meaningful only in the case when the growth curve is constructed to doses high enough for the second component to be fully saturated. Such studies are quite few in literature, possible due to the long irradiation time needed. Nonetheless, it is intriguing to note that our obtained values for the fine quartz (4-11μm) fraction (D_{01} = 175 ± 10, D_{02} = 1823 ± 10 (n=6)), are very similar to the values reported by Lowick et al. (2010b) in their study on fine material (D_{01} = 128, D_{02} = 1680 Gy), while the saturation characteristic doses obtained in this study for coarse (63-90 μm) quartz (D_{01} = 55 ± 3, D_{02} = 586 ± 5 (n=5))are close to the values previously reported on coarse material

by Murray et al. (2007) (D_{01} = 44 Gy, D_{02} = 450 Gy for 180-250 μm quartz) respectively Pawley et al. (2011) (D_{01} = 51 Gy, D_{02} = 320 Gy for 125-180 μm quartz). Further research is needed to sustain and explain this observation.

In the case of the samples investigated from Mostistea section all the equivalent doses determined (at least for the 63-90μm) fraction are obtained by interpolating on a region of the dose response where the first exponential function is already in saturation (D_e (63-90 μm) > $2D_{01}$ =110 Gy). We believe that more work is needed for conceptualising the process, independent processes or set of competing processes that generate the double exponential saturating behaviour of quartz OSL in order for these equivalent doses to be considered reliable.

Our results from the quartz-based OSL study at Mostistea indicate that the age discrepancy observed between two grain sizes of quartz may be characteristic for loess deposits in SE Romania. The source of this discrepancy remains yet unexplained. Our data confirm the fact that the linear tem increasingly reported in literature for quartz OSL dose response up to 1000 Gy is the expression of a second later saturating exponential function. The presence of an additional function, besides a single saturating exponential, in the dose response curves constructed for both types of quartz grains, may indicate that there are still unknown processess that influence the characteristics of the signals used for age determination. Therefore, these results suggested that the reliability of the age results obtained from signals with similar saturation characteristics of the dose response curve should be regarded with caution.

CHAPTER IV

Combined IRSL and post-IR OSL dating of Romanian loess using single aliquots of polymineral fine grains

Chapter based on:

Vasiliniuc, S., D.A.G. Vandenberghe, A. Timar-Gabor , C. Panaiotu, C. Cosma, P. Van den haute, submitted. *Combined IRSL and Post-IR OSL dating of Romanian loess using single aliquots of polymineral fine grains.* Quaternary International.

IV. Combined IRSL and post-IR OSL dating of Romanian loess using single aliquots of polymineral fine grains

IV.1. Introduction

As previously discussed in Chapter I, the age discrepancy obtained by Timar et al (2011) for different grain-size fractions of quartz led to significant doubt regarding the chronology of the loess sequence at Mircea Vodă. In this work, an alternative procedure is applied which is aimed to investigate luminescence signals from quartz, but also from feldspar, the alternate dosimeter of choice. A fine mineral mixture is used as sample material with grain size between 4 and 11 µm (polymineral fine grains). The possibility to independently stimulate both minerals (quartz and feldspar) is based on the sensitivity that feldspars have to infrared (IR) stimulation which is absent for quartz (see Chapter II).

A 'double-SAR' protocol (Banerjee et al., 2001; Roberts and Wintle, 2001) is used for equivalent dose (D_e) determination. This protocol involves observing an infrared stimulated luminescence (IRSL) signal from the feldspathic component of the mineral mixture, followed by that of an optically stimulated luminescence signal (post-IR OSL) that is thought to originate mainly with the quartz constituent. We investigated this approach because (i) it may allow obtaining reliable age results while avoiding the chemical separation process during sample preparation, and (ii) the feldspar-IRSL ages may provide an independent age check on the OSL ages previously obtained using silt-sized quartz.

IV.2. Samples and instrumentation

Twelve samples were taken from the loess units corresponding to the last four glacial periods. Nine samples (GLL-071801 to -09) were collected from the L1 loess unit while one sample was collected from each of the three loess units below (GLL-071810 from L2, -12 from

L3 and -13 from L4). A complete description of the study site and sample collection can be found in Timar et al. (2010) and Timar Gabor et al. (2011).

We used archived polymineral fine-grained material (4-11 μm) of samples from the previous study by Timar et al. (2010). The 4-11 μm fraction was isolated using conventional sample preparation techniques (Lang et al., 1996; Frechen et al., 1996) and aliquots were prepared by settling from a 2mg/ml suspension in acetone on aluminium discs.

All luminescence measurements were performed using an automated Risø TL/OSL-DA-12 reader equipped with an infrared (IR; 830 ± 10 nm) laser diode (Bøtter-Jensen and Murray, 1999) and blue (470 ± 30 nm) light emitting diodes (LEDs; Bøtter-Jensen et al., 1999). The UV emission of the luminescence signals was detected through a 7.5 mm thick Hoya U-340 filter.

IV.3. Luminescence investigations

IV.3.1. Experimental details

The double-SAR protocol (Banerjee et al., 2001; Roberts and Wintle, 2001) allows the observation of two luminescence signals in a single SAR cycle. The first stimulation, using IR, releases an IRSL signal that should sample most of the feldspathic component from the mineral mixture; a subsequent stimulation with the blue diodes releases an OSL signal (post-IR OSL) that is expected to be dominated by the quartz component (Roberts and Duller, 2004). As such, the protocol allows derivation of two sets of D_e values.

Table 1 shows the measurement steps and parameters in the protocol as used in this work. Both stimulations were performed for 100 s at 125 ^{o}C. A 10 s preheat treatment was applied before measuring the response to the natural and regenerative doses. A cutheat to 180 ^{o}C was applied prior to the measurement of the response to the test dose (10 Gy, unless stated otherwise) and a stimulation with the blue diodes for 40 s at 280 °C was performed at the end of each cycle (high temperature cleanout; Murray and Wintle, 2003). The signals used in the calculations were derived from the first 2 s of stimulation, minus a background evaluated from the last 10 s.

1. Dose	
2. Preheat to 240 °C, for 10 s	
3. IRSL, 100 s at 125 °C	**→ $L_{x, IRSL}$**
4. OSL, 100 s at 125 °C	**→ $L_{x, post\text{-}IR\ OSL}$**
5. Test dose	
6. Cutheat to 180 °C	
7. IRSL, 100 s at 125 °C	**→ $T_{x, IRSL}$**
8. OSL, 100 s at 125 °C	**→ $T_{x, post\text{-}IR\ OSL}$**
9. OSL, 40 s at 280 °C	

Table IV.1: *The double-SAR measurement protocol.*

IV.3.2. Luminescence characteristics

Fig. IV.1 shows a representative dose response curve of the IRSL and post-IR OSL signal from an aliquot of sample GLL-071806. In both cases, the natural signal is well below saturation. Fig. IV.1 also illustrates that sensitivity changes occurring during repeated SAR cycles are accurately corrected for (i.e. recycling ratios are within 0.9-1.1) and that the curves pass close to the origin (implying that recuperation is negligible). The inset in Fig. IV.1 presents representative decays of IRSL and post-IR OSL signals in comparison with the decay of the OSL signal from calibration quartz. The post-IR OSL signal appears to decay much slowly than the OSL signal from calibration quartz. Timar Gabor et al. (2011; their Fig. IV.3) showed that natural OSL signals of pure 4-11 μm quartz extracted from the same samples are indistinguishable from the calibration quartz signals. Therefore, the slower decay of the post-IR OSL signal cannot be derived entirely from quartz. It may however indicate that a significant contribution from the feldspathic component persists in the post-IR OSL signal.

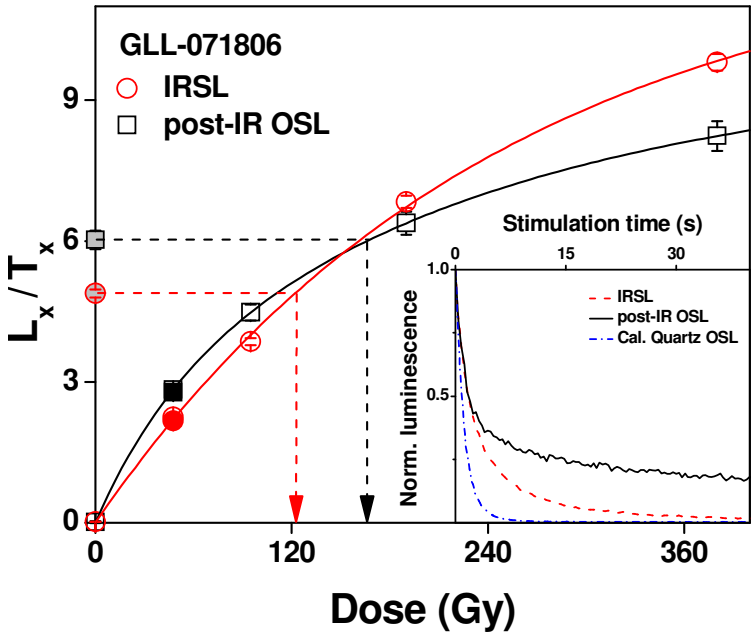

Figure IV.1: *Dose response curves of the IRSL (open circle) and post-IR OSL signal (open square) from one aliquot of sample GLL-071806. The sensitivity-corrected natural signals are shown as grey-filled symbols and recycling points are shown as solid symbols. The solid lines represent the best fit to a single saturating exponential function (IRSL data) and to the sum of two saturating exponential functions (post-IR OSL data). The inset shows representative decay curves of the OSL signal from fine silt-sized (4-11 μm) calibration quartz, and the IRSL and post-IR OSL signals from polymineral fine grains, obtained using sample GLL-071802.*

The ability to recover a known given dose was tested using different preheat treatments on sample GLL-071802. Three aliquots per preheat were bleached for 1 h in a Hönle SOL2 solar simulator. After a pause for 1 h at room temperature, the aliquots were given a dose equal to the estimated natural dose and measured as if this dose was unknown. Fig. IV.2a shows that, across the investigated preheat range (200 – 260 °C, for 10 s), the ratio of recovered to given dose does not vary with preheat treatment, and is within 10 % from unity; the overall average recovered/given dose ratios are 1.02 ± 0.01 and 0.97 ± 0.04 for the IRSL and post-IR OSL signal, respectively. The corresponding recycling ratios lie within 0.9-1.1 (Fig. IV.2b), although it appears to be systematically higher (~5 %) than unity for the IRSL signal and lower (~8 %) for the post-IR OSL signal. The post-IR OSL signal exhibits no recuperation (-0.3 ± 0.1%, on average), while recuperation of the IRSL signal remains below 1.5 % (Fig. IV.2b).

For samples GLL-071803 and -10, a dose recovery test was then performed using a 10 s preheat at 240 °C. The recovered to given dose ratio does not differ by more than 5 %

from unity for both signals of sample GLL-071803 and for the post-IR OSL of sample GLL-071810; a value of 1.3 ± 0.8 was observed for the IR-signal of sample GLL-071810.

The preheat dependence of equivalent dose was investigated for sample GLL-071802. The D_e results together with the corresponding recycling and recuperation are shown in Fig. IV.2(c) and (d), respectively. Both the IRSL and the post-IR OSL D_es appear independent of preheat temperature and result in average values of 41.4 ± 0.8 and 32.1± 0.7 Gy, respectively. Over the examined preheat temperature range, recycling ratios are within 5% of unity and recuperation is below 1%.

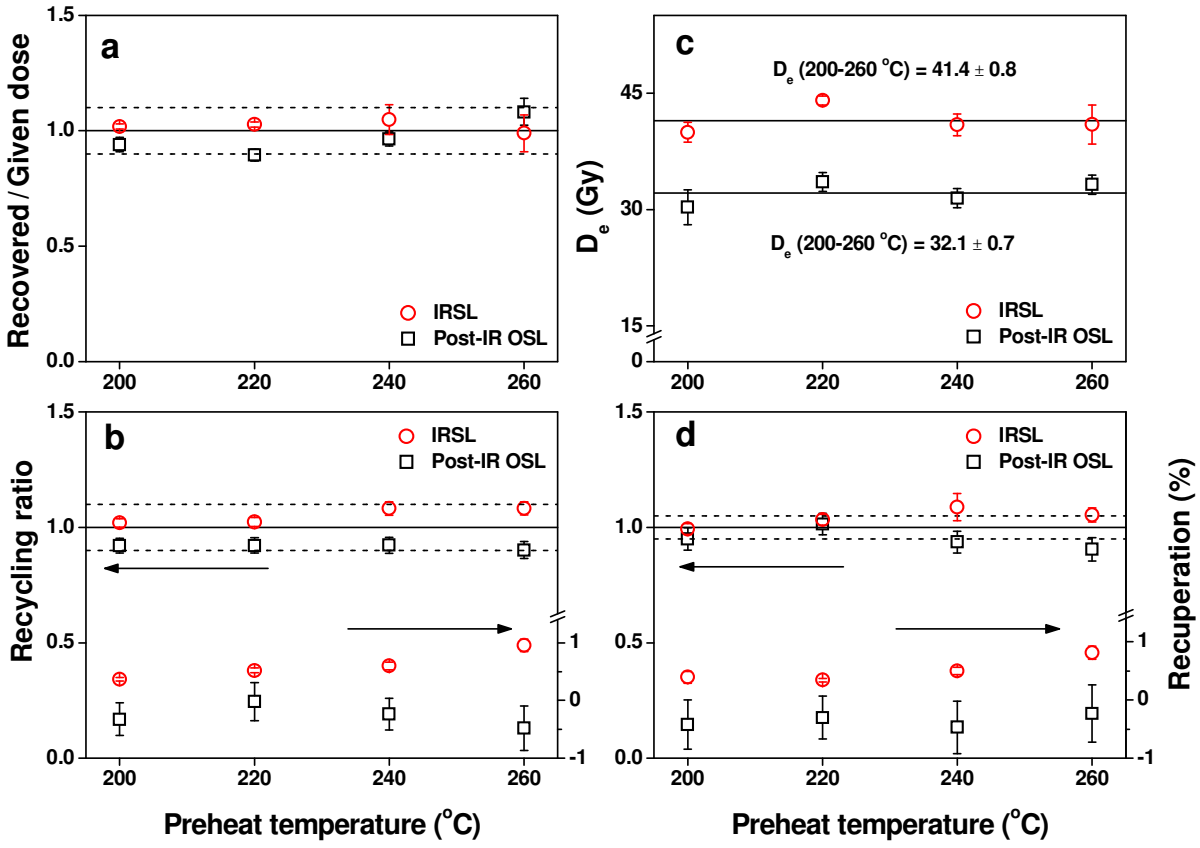

Figure IV.2: *(a) Variation in recovered/given dose ratio as a function of preheat temperature for sample GLL-071802. (b) Recycling ratios and recuperation corresponding to the data in (a). The solid and dashed lines in (a) and (b) highlight the ideal ratio of unity and a ± 10 % deviation, respectively. (c) Variation in equivalent dose (D_e) as a function of preheat temperature for sample GLL-071802. Each data point represents the average of two aliquots. The solid lines (eye guide) highlight the average value across the 200-260 °C preheat temperature range. (d) Recycling ratios and recuperation corresponding to the data in (b). The solid and dashed lines highlight the ideal ratio of unity and a ± 5 % deviation, respectively.*

Based on the above, a preheat temperature of 240 ^{o}C for 10s was chosen for D_e determination. For each sample, at least 5 aliquots were measured and the average values are given in Table IV.2. Except for the two uppermost samples (GLL-071801 and -02), the post-IR OSL signals yielded higher D_e values than the corresponding IRSL signals.

Measurements of the fading rate were performed following the procedure proposed by Auclair et al. (2003), and used the aliquots from the D_e measurements. First, the aliquots were consecutively bleached using the two types of stimulation sources (the IR laser diode and the blue LEDs) for 250 s at 125 ^{o}C. This 'double bleach' was repeated after a 1 h pause. Using the double-SAR protocol the response to a constant regenerative dose (25 or 50 Gy) was then repeatedly measured for various storage times after the preheating of the regenerative dose. A test dose of 10 Gy or 25 Gy was used to correct for sensitivity changes.

The percentage of signal lost during a storage period of one decade of time, usually denoted as 'g' value (Aitken, 1985), was calculated using Eq. (4) of Huntley and Lamothe (2001). Table 2 presents the average fading rates normalised to a measurement delay time of 2 days after irradiation for both the IRSL and the post-IR OSL signal. Compared to the post-IR OSL signal, the IRSL signal of all samples exhibited a higher fading rate; the overall average g-values (n = 71) are 4.0 ± 0.1%/decade and 1.8 ± 0.2%/decade for the IRSL and post-IR OSL signals, respectively. No detectable dependence of the fading rate on depth was observed.

IV.3.3. Age results

Table IV.2 (and caption) summarizes the information relevant to the IRSL and post-IR OSL age calculation. Both the IRSL and the post-IR OSL age results were corrected for anomalous fading using the method proposed by Huntley and Lamothe (2001). For the sake of comparison, the table includes the OSL ages previously obtained by Timar et al. (2010) using silt-sized (4-11 μm) quartz.

Fig. IV.3a plots the fading-corrected IRSL ages versus the corresponding fading-corrected post-IR OSL ages. Except for the two uppermost samples, for which the IRSL ages are significantly older than the post-IR OSL ages (by ~ 50%; see Fig. IV.3a - upper inset), the two sets of ages agree within 5%; this is remarkable as the average g values for the two signals had been shown to differ by a factor of 2 (4.0 ± 0.1 and 1.8 ± 0.2 for IRSL and post-IR OSL,

respectively. A comparison between the uncorrected IRSL and post-IR OSL ages is given in the lower inset in Fig. IV.3a. The uncorrected IRSL ages obtained for the three uppermost samples appear to agree very well with the post-IR OSL ages. For the rest of the samples a significant difference between the two types of age results is observed; the post-IR OSL ages are systematically older than the IRSL ages, with approximately 35 %.

Fig. IV.3b compares the fading-corrected IRSL and post-IR OSL ages with the fine (4-11 µm) quartz OSL ages obtained by Timar et al. (2010; data given in Table IV.2). For all samples, the corrected post-IR OSL and the OSL ages agree well; the same holds for the corrected IRSL ages, except for the two uppermost samples that overestimate the quartz OSL age by ~ 50 % (Fig. IV.3b-inset).

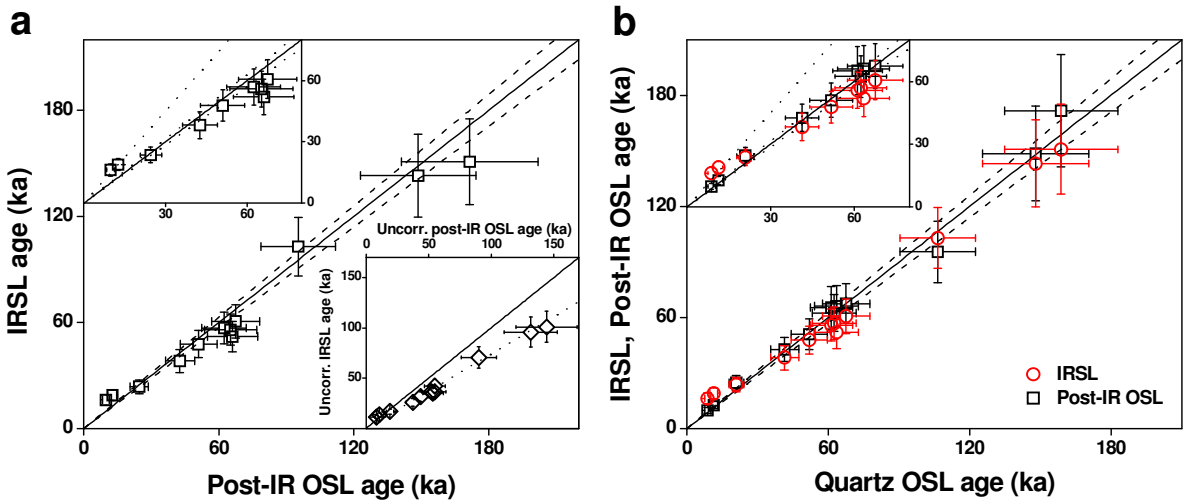

Figure IV.3: *(a) Comparison between fading-corrected IRSL and fading-corrected post-IR OSL ages. (b) Plot of fading-corrected IRSL and post-IR OSL ages against the quartz OSL ages of Timar et al. (2010). The upper insets in (a) and (b) present the age results obtained for samples collected from the L1 loess unit; the lower inset in (a) shows the uncorrected IRSL ages against the uncorrected post-IR OSL ages for all samples investigated. All error bars represent 1 sigma total uncertainty. The solid lines represent the 1:1 relation and the dashed lines bracket a 5 % deviation from unity. The dotted lines (insets) represent a 50 % deviation from unity for the upper insets in (a) and (b) and a 35 % deviation from unity for the lower inset in (a).*

Loess unit	Sample	Depth (m)	Measurement	Dose Rate (Gy/ka)	De (Gy)	$Age_{uncorr.}$ (ka)	g_{2days} (%/decade)	$Age_{corr.}$ (ka)	σ_r (%)	σ_{sys} (%)	σ_{tot} (%)	σ_{tot} (ka)
L1	GLL-071801	0.85	IRSL	3.20 ± 0.05	37 ± 1	12	3.6 ± 0.9	16	11	14	18	3
			Post-IR OSL	3.02 ± 0.05	26 ± 1	9	1.6 ± 0.8	10	4	14	15	1
			Quartz OSL	2.85 ± 0.05	24.9 ± 0.4	9			2	14	15	1
	GLL-071802	1.05	IRSL	3.22 ± 0.06	44 ± 1	14	3.6 ± 0.4	19	6	14	16	3
			Post-IR OSL	3.04 ± 0.06	32 ± 1	11	1.9 ± 0.3	13	6	14	15	2
			Quartz OSL	2.87 ± 0.05	32 ± 1	11			3	14	15	2
	GLL-071803	1.30	IRSL	3.46 ± 0.05	58 ± 1	17	3.6 ± 0.6	24	8	14	17	4
			Post-IR OSL	3.27 ± 0.05	63 ± 2	19	2.7 ± 0.6	25	7	14	16	4
			Quartz OSL	3.08 ± 0.05	64 ± 2	21			3	14	15	3
	GLL-071804	1.85	IRSL	3.14 ± 0.05	81 ± 2	26	4.0 ± 0.7	38	10	14	17	7
			Post-IR OSL	2.96 ± 0.05	111 ± 3	38	1.4 ± 0.3	43	5	14	15	6
			Quartz OSL	2.78 ± 0.04	114 ± 2	41			2	14	14	6
	GLL-071805	2.25	IRSL	3.40 ± 0.07	108 ± 1	32	4.2 ± 0.5	48	7	15	16	8
			Post-IR OSL	3.20 ± 0.07	140 ± 4	44	1.7 ± 0.6	51	7	15	16	8
			Quartz OSL	3.01 ± 0.06	156 ± 3	52			3	15	15	8
	GLL-071806	2.80	IRSL	3.50 ± 0.05	124 ± 3	35	4.6 ± 0.3	56	5	15	16	9
			Post-IR OSL	3.30 ± 0.05	177 ± 8	54	2.1 ± 0.8	65	10	15	18	12
			Quartz OSL	3.10 ± 0.04	190 ± 3	61			2	15	15	9
	GLL-071807	3.75	IRSL	3.58 ± 0.05	131 ± 3	37	4.5 ± 0.3	57	5	15	15	9
			Post-IR OSL	3.37 ± 0.05	177 ± 6	52	1.9 ± 0.4	62	6	15	16	10
			Quartz OSL	3.16 ± 0.05	197 ± 3	62			2	15	15	9
	Continued on next page											

	GLL-071808	4.00	IRSL	3.72 ± 0.05	137 ± 2	37	3.7 ± 0.6	52	8	15	17	9
			Post-IR OSL	3.51 ± 0.05	193 ± 11	55	2.0 ± 0.6	66	9	15	17	11
			Quartz OSL	3.30 ± 0.05	209 ± 3	63			2	15	15	9
	GLL-071809	5.00	IRSL	3.69 ± 0.04	156 ± 6	42	3.7 ± 0.2	61	5	15	15	9
			Post-IR OSL	3.48 ± 0.03	192 ± 7	55	2.2 ± 0.4	68	6	15	16	11
			Quartz OSL	3.28 ± 0.03	221 ± 5	68			2	15	15	10
L2	GLL-071810	8.00	IRSL	3.30 ± 0.05	233 ± 5	71	3.8 ± 0.4	103	6	15	16	16
			Post-IR OSL	3.10 ± 0.05	280 ± 15	90	0.7 ± 0.9	95	9	15	17	17
			Quartz OSL	2.92 ± 0.04	310 ± 9	106			3	15	15	16
L3	GLL-071812	15.00	IRSL	3.29 ± 0.06	315 ± 14	96	4.0 ± 0.4	143	7	15	16	16
			Post-IR OSL	3.10 ± 0.05	408 ± 24	132	1.3 ± 0.6	149	9	15	17	26
			Quartz OSL	2.91 ± 0.05	430 ± 13	147			3	15	15	23
L4	GLL-071813	18.00	IRSL	3.30 ± 0.04	333 ± 11	101	4.0 ± 0.4	151	6	15	16	24
			Post-IR OSL	3.11 ± 0.03	449 ± 36	144	1.9 ± 0.5	172	10	15	18	30
			Quartz OSL	2.92 ± 0.03	467 ± 11	159			3	15	15	24

Table IV.2: *Summary of calculated dose rates, equivalent doses (D_e), uncorrected ages, fading rates (g_{2days}), fading-corrected ages, and random (σ_r), systematic (σ_s) and total uncertainties (σ_{tot}). Dose rates were obtained using the radionuclide activity concentrations reported by Timar et al. (2010; their Table S3) and the conversion factors of Adamiec and Aitken (1998). Correction of alpha, beta and gamma contributions for the effect of moisture used a time-averaged water content of 20 ± 5 % (Balescu et al., 2003). Mean a-values of 0.08 ± 0.02 and 0.06 ± 0.02 were used for IRSL and post-IR OSL respectively (Rees-Jones, 1995). The quartz OSL data are for fine-grained quartz (Timar et al., 2010). Uncertainties in the age results were obtained using the error assessment system proposed by Aitken and Alldred (1972) and Aitken (1976). The uncertainties given for the dose rate, D_e and g_{2days} values are random; all uncertainties represent one sigma. The stratigraphic position of the samples is shown in the left column.*

IV.4. Discussion

This study evaluates the applicability of a double-SAR protocol for dating Romanian loess using polymineral fine grains. Laboratory tests (i.e. recycling ratio, recuperation and dose recovery; see Section IV.3.2) indicate that the protocol should be suitable for D_e determination using both IRSL and post-IR OSL signals. However, both signals exhibit anomalous fading (see Table IV.2), for which correction must be made.

The significant fading rate observed for the post-IR OSL signal indicates that the preceding stimulation with IR diodes does not reduce the contribution from feldspar to a negligible level. This was expected from the shape of the decay curve of this signal in comparison with typical fine silt (4-11 μm) calibration quartz (see Section IV.3.2; inset in Fig. IV.1). Previous studies have indicated that OSL signals from feldspars may be observed even after IR stimulation (see e.g. Duller and Bøtter-Jensen, 1993; Roberts, 2007; Kim et al., 2009). Zhang and Zhou (2007) recommend that the IR stimulation in the double-SAR protocol should be long enough to ensure the isolation of a quartz-dominated post-IR OSL signal; 1000 s duration was found sufficient for their samples.

For the uppermost two samples (GLL-078101 and -02), the fading-corrected IRSL ages are significantly higher than the corrected post-IR OSL ages (Fig. IV.3b); the latter agree well with the quartz-based OSL ages. These two samples were collected from the upper part of the L1 loess unit, which may have been affected by post-depositional soil formation processes (e.g. bioturbation) during the Holocene. Therefore, the apparent inconsistency may be related to incomplete resetting of the IRSL signal during such reworking; it is well known that feldspar IRSL signals bleach more slowly than quartz OSL (see e.g. Thomsen et al., 2008a). Evidence for post-depositional disturbance in the top of L1 has also been presented by Timar Gabor (2010), who observed broad dose distributions in small aliquots of sand-sized (63-90 μm) quartz grains extracted from these same samples.

For the remainder of the samples, the corrected IRSL ages agree well with the corrected post-IR OSL ages (Fig. IV.3a) although the two signals appear to be affected by anomalous fading to different extents (see Table IV.2 and Fig. IV.3a; lower inset). Furthermore, the entire post-IR OSL dataset agrees well with that previously obtained by Timar et al. (2010) using OSL signals from silt-sized quartz. The overall consistency between results obtained for different

dosimeters (feldspar and quartz) increases the reliability of age results obtained using fine grains, at least for the samples collected from loess unit L1. As such, they corroborate the correlation of the weakly developed palaeosol in the L1 unit with MIS3.

The quartz OSL ages for the samples collected from the loess units L2, L3 and L4 have previously been interpreted as underestimates of the true burial age (Timar et al., 2010). The agreement between the OSL and the fading-corrected IRSL ages for these samples is not thought to enhance the reliability of either dataset. Indeed, the fading-correction model is expected to be valid only for samples for which the natural signal falls on the linear region of the dose response curve (Huntley and Lamothe, 2001), a condition which is not met for these samples. As such, both datasets are interpreted as underestimating the true burial age, and their agreement as coincidence.

The excellent agreement between the fading-corrected post-IR OSL ages and the quartz OSL ages (Fig. IV.3b) suggests that it may not be necessary to chemically separate the fine quartz fraction in order to obtain reliable luminescence ages for Romanian loess. A similar finding was recently reported by Schmidt et al. (2010) using polymineral fine grains extracted from Serbian loess.

The results presented here do not necessarily imply that OSL signals from sand-sized quartz yield inaccurate ages. It has been demonstrated that SAR-OSL dating is a reliable chronological tool for sand-sized sediments from a wide variety of depositional environments (see e.g. Murray and Olley, 2002). Instead, the age discrepancy (Timar Gabor et al., 2011) may reflect a hitherto unexplained phenomenon in OSL production and/or an unknown process in loess formation and/or preservation. A comparison between ages obtained using sand-sized quartz and feldspar would be a further test of their accuracy and help identifying the cause for various grain-size fractions yielding deviating ages. Unfortunately, the archived samples contained insufficient sand-sized feldspar grains to facilitate such a comparison.

IV.5. Conclusions

We conclude that application of the double-SAR protocol to polymineral fine grains offers a viable alternative for dating Romanian loess, avoiding the need to isolate pure quartz using chemical procedures. The IRSL and post-IR OSL signals exhibit anomalous fading,

however, and the ages derived from these signals are therefore dependent on the fading correction model. An agreement between ages obtained using feldspar (IRSL), quartz (OSL) and/or mixed (post-IR OSL) signals increases confidence in the dating results. Our results suggest that use of the double-SAR protocol should be restricted to samples from last glacial period.

CHAPTER V

Conventional IRSL dating of Romanian loess using single aliquots of polymineral fine grains

Chapter based on:

Vasiliniuc, S., Vandenberghe, D., Timar-Gabor, A., van den Haute, P., Cosma, C., submitted. *Conventional IRSL dating of Romanian loess using single aliquots of polymineral fine grains.* Radiation Measurements.

Basarin, B., Vandenberghe, D.A.G., Marković, S.B., Catto, N., Hambach, U., **Vasiliniuc, S.,** Derese, C., Roncevic, S., Vasiljević, A., Lj Rajić, Dj., 2011. *The Belotinac section (Southern Serbia) at the southern limit of the European loess belt: initial results.* Quaternary International 240 (1-2), 128-138.

V. Conventional IRSL dating of Romanian loess using single aliquots of polymineral fine grains

V.1. Introduction

This study documents IRSL signals from polymineral fine grains – in the hope that they may allow improvement in our understanding of the discrepancy between the two sets of quartz-based ages (see Section I.5). Since IRSL signals from feldspars saturate at higher doses than OSL signals from quartz (see Section II.4.2), feldspar-based ages could also extend the chronology of stratigraphic units for which quartz-OSL ages are interpreted as underestimates.

A conventional IRSL approach is investigated using a single-aliquot regenerative-dose (SAR) protocol (Murray and Wintle, 2000) involving IR stimulation at 50 ^{o}C and detection in the blue region. The influence of preheat temperature on dose recovery, equivalent dose, fading rates and fading corrected ages are investigated. Age results obtained using both low and high preheat temperature are compared with previously obtained quartz-OSL ages. Moreover, pulse anneal and combined IR/TL experiments (see Section II.4.5) are performed in order to investigate the thermal stability and origin of the signal.

V.2. Materials and methods

This study uses archived material of samples from the previous studies by Timar et al. (2010) and Timar Gabor et al. (2011). The reader is referred to their works for a complete description of the study site and sample collection. The samples are listed in order of depth in Table V1. Polymineral fine grains (4-11 μm) were separated using conventional sample preparation techniques (Lang et al., 1996; Frechen et al., 1996). Part of the material was further prepared for the extraction of fine grained quartz (Timar et al., 2010) while the rest of the material was archived and subsequently used in this study. Aliquots were prepared by settling the polymineral-fine grains in acetone on aluminum discs.

All luminescence measurements were performed using a Risø TL/OSL-DA-15 reader. Infrared stimulation used infrared (IR) LEDs emitting at 875 nm and IRSL signals were detected through a BG39/Corning 7-59 filter combination (Bøtter-Jensen et al. 2003). Our SAR-IRSL protocol involved stimulation with IR diodes for 100 s at 50 °C and used the same thermal treatment prior to measuring the response to both regenerative and test doses (Huot and Lamothe, 2003; Blair et al., 2005). The size of the test dose was 10 Gy in all experiments. Each measurement of the response to the test dose was followed by stimulation with the IR diodes for 40 s at 290 °C. Unless otherwise stated, the signals used for calculations were integrated over the first 1.2 s of stimulation minus a background evaluated from the last 10 s.

V.3. Dose response

A representative SAR dose-response curve is shown in Fig. V.1 for an aliquot of sample GLL-071806. The growth curve can be well represented by the sum of two single saturating exponential functions. In the example given, the corrected natural IRSL signal lies well below the laboratory saturation level, which is valid for all the investigated samples. Fig. V.1 also illustrates the general behaviour of the samples in the SAR-IRSL protocol. Sensitivity changes occurring during the repeated SAR cycles are accurately corrected for, as is indicated by the ability to re-measure points on the dose-response curve (Fig. V.1, open triangles). The dose-response curve passes close to the origin, demonstrating that recuperation is negligible (open circle in Fig. V.1).

V.4. Dose recovery test

V.4.1. Dose recovery test using solar simulator as bleaching agent

A dose recovery test (Wallinga et al., 2000) was carried out for several samples, and using different preheat temperatures and durations. Natural aliquots were bleached for 1 h in a Hönle SOL2 solar simulator, left for one hour at room temperature and given a laboratory dose close to the estimated natural dose; the values are given in Table V.1. This given dose was then immediately measured using the SAR protocol as if it were an unknown dose.

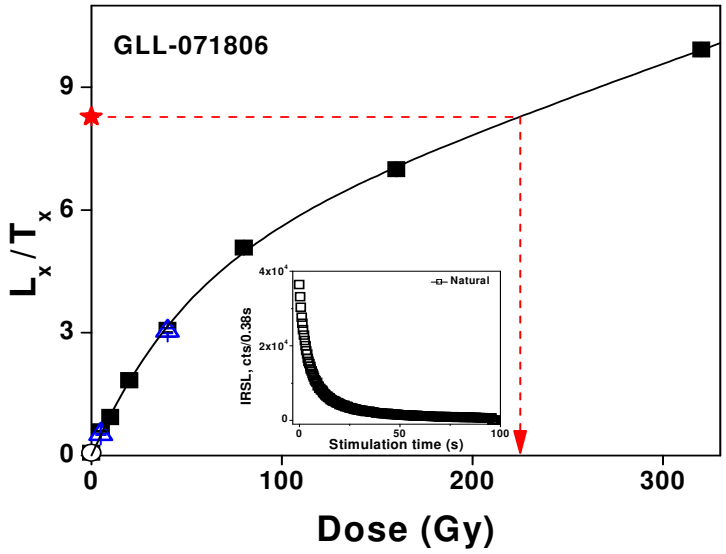

Figure V.1: *Example of a SAR growth curve for one aliquot of sample GLL-071806. A preheat treatment of 60 s at 250 °C was employed. The natural L_x/T_x ratio is shown as a solid star; recycling points are shown as open triangles and the recuperation point as an open circle. The solid line represents the best fit to the sum of two saturating exponential terms. The inset shows an example of a natural decay curve.*

The dose recovery test was first carried for sample GLL-071801, using preheats of 60 s in the range of 80 to 325 °C; the size of the given dose was chosen to equal the natural dose as obtained using a preheat of 60 s at 115°C. Within analytical uncertainty, the given dose can be recovered to within 5% over the entire temperature range, although there may be a tendency for an increasing overestimation with preheat temperature from 180 °C to 250 °C (Fig. V.2a). Fig. V.2b summarises the corresponding recycling ratios and recuperation (expressed as % of the corrected 'natural' IRSL signal). Recycling ratios are within 5% from unity, although the accuracy of the sensitivity correction appears lower at the two highest preheat temperatures. Recuperation increases with preheat temperatures from 220 °C onwards, reaching a value of ~ 7% at 325 °C.

The dose recovery test was then performed for three more samples (GLL-071802,-06 and -09), and for three preheats of 60 s at 80 °C, 115 °C and 250 °C only. This time, the size of the given dose equaled the natural dose as obtained in preliminary experiments that used a preheat of 60 s at 250°C. The results are summarized in Fig. V.2c The overall picture that emerges is that the given dose is increasingly overestimated with both increasing preheat temperature and

sampling depth. Only the preheat treatment of 60 s at 80 °C yields recovered/given dose ratios that fall within 10% of unity for all three samples.

A preheat of 60 s at 250 °C significantly overestimates the given dose, with values of 1.3 ± 0.1, 1.6 ± 0.1 and 2.1 ± 0.3 being found for samples GLL-071802, -06 and -09, respectively. Fig. V.2d demonstrates that this is not associated with corresponding poor recycling ratios or significant recuperation of the signal. Decreasing the duration of the preheat treatment from 60 s to 10 s, did not significantly improve the ability to recover a dose (Fig. V.2c, open symbols).

To test whether the given dose overestimation is due to a residual signal persisting after the bleaching process, the preheat dependence of the residual dose was measured in aliquots of the same samples that had been bleached for 1 h in the SOL 2 solar simulator. The residual dose increases with preheat temperature from ~ 0.2 Gy (for a 60 s preheat at 80 °C) to ~2 Gy (for a 60 s preheat at 250 °C). As the residual dose represents only a small fraction of the given dose, which ranged from ~ 50 to 250 Gy, it cannot account for the observed overestimation.

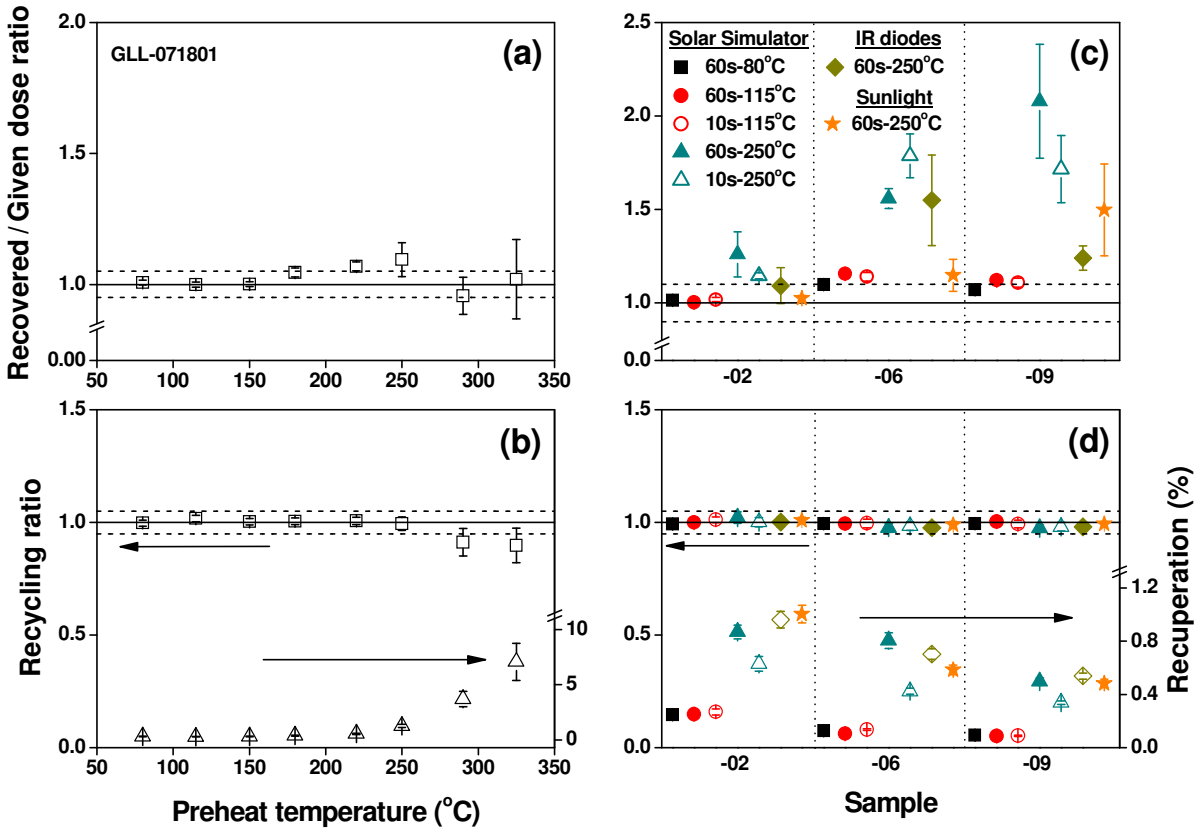

Figure V.2: *(a) Dependence of dose recovery on preheat treatment for sample GLL-071801. (b) Recycling ratios and recuperation corresponding to the results shown in (a). (c) Results of the dose recovery test for samples GLL-071802, -06 and -09 using three preheat temperatures (80, 115 and 250 °C). (d) Recycling ratios and recuperation corresponding to the results shown in (c)*

respectively. The solid and dashed lines (eye guide) highlight the ideal ratio of unity and a ± 5 % (a, b, d) or ± 10 % (c) deviation, respectively. All data points are the average for two to three aliquots and error bars represent one standard error. Residual doses measured using three aliquots per data symbol were subtracted. The dotted lines (c and d) are meant as eye guide to distinguish the results obtained for each sample.

V.4.2. Dose recovery test using other bleaching procedures

Using a preheat treatment for 60 s at 250 ^{o}C, the dose recovery test was repeated with bleaching using infrared light. Six aliquots for each of the samples GLL-071802, -06, -09 were first subjected to a double IR stimulation at room temperature for 250 s. A 1 h pause was inserted between the two bleaching treatments. Half of the aliquots were then treated in the same manner as in the previous dose recovery experiments. The other half were used for residual dose measurements. While the value of the residual dose is observed to increase up to ~ 9 Gy for samples GLL-071806 and -09, a significant overestimation of the given dose persisted (see Fig. V.2c – diamond symbols). Only for sample GLL-071802, the measured to given dose ratio falls within 10 % from unity. However, after an unfiltered 4 h sunlight bleach, the recovered/given dose ratio for the same three samples decreased to 1.03 ± 0.02, 1.15 ± 0.09 and 1.50 ± 0.25, respectively (Fig. V.2c – star symbols). Residual doses persisting after the 4 h sunlight bleaching were found comparable with the doses measured after 1 h in the solar simulator (~2 Gy) and were subtracted from the recovered doses.

V.4.3. Dose recovery test without bleaching

A dose recovery experiment was also performed by giving a 500 Gy laboratory dose on top of the natural dose for the uppermost sample GLL-071801. The experiment was carried out for preheats of 60 s at 115 ^{o}C (D_e ~ 25 Gy) and 250 ^{o}C (D_e ~ 39 Gy), each time using 3 aliquots; recovered/given dose ratios of 1.27 ± 0.03 and 1.84 ± 0.06 were obtained, respectively. These results are unexpectedly poor in comparison with those obtained earlier using the solar simulator as the bleaching agent (see Fig. V.2a). They might indicate a dependence of the luminescence sensitivity on the magnitude of the given dose as discussed below.

V.4.4. Dose recovery as a function of given dose

It was therefore further investigated whether the ability to recover a dose is dependent on the size of the given laboratory dose. Aliquots of samples GLL-071802, -06 and -09 were first bleached for 1 h in the solar simulator. Groups of three aliquots were then given various laboratory doses, and measured using a SAR protocol with a preheat for 60 s at 115°C. Fig. V.3 plots the recovered/given dose ratio as a function of the given dose (expressed as a fraction of the natural dose estimated using this particular preheat). There is a clear tendency for the measured dose to be overestimated as the size of the given dose increases, and the overestimation appears larger for samples collected at greater depths. For all three samples, the protocol is able to accurately measure a given dose equal to the estimated D_e. For all given doses, recycling ratios were consistent with unity and recuperation negligible (< 0.5 %).

A similar influence of the size of the given dose was observed when this dose recovery experiment was repeated for a preheat of 60 s at 250°C. For sample GLL-071802 this was observed to persist, even when 4 h sunlight bleach was used instead of the solar simulator (data not shown).

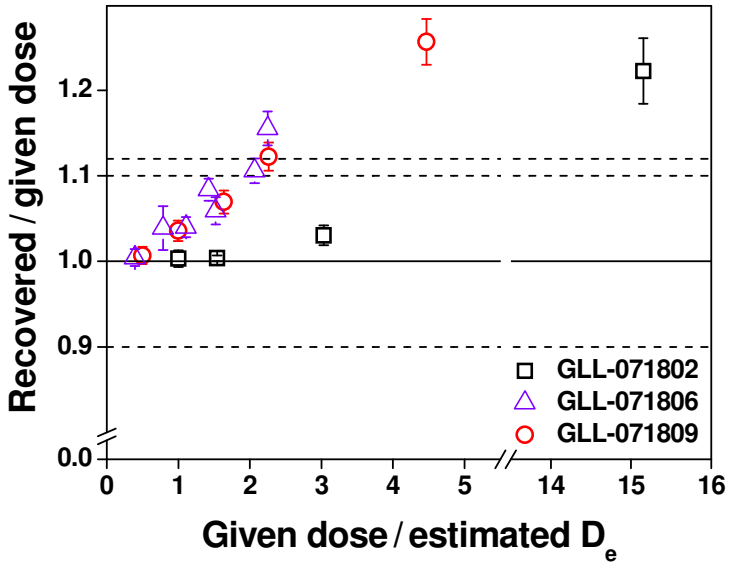

Figure V.3: *Dependence on the size of the given dose (expressed as a fraction of the estimated equivalent dose, D_e) of the recovered to given dose ratio. Error bars represent one standard error. Three aliquots were measured for each data point. The solid and dashed lines highlight the ideal ratio of unity and a ± 10 % deviation*

V.5. Preheat dependence of equivalent dose, fading rate and age

The results from the dose recovery tests (section V.4) suggest that significant initial sensitivity changes occur which are both temperature and dose dependent. It seems logical to expect that the temperature dependence is reflected in measurements of a particular natural dose (or D_e), after correction for anomalous fading. The dependence of the fading-corrected age on the preheat was investigated for samples GLL-071801, -09 and -10. Fig. V.4a shows the dependence of the equivalent dose (D_e) on the preheat temperature. For all three samples, the D_e systematically increases with preheat temperature, and across the 150-225 ^oC range in particular. The recycling ratios are consistent with unity over the entire investigated temperature range (80 – 325 ^oC), confirming that sensitivity changes occurring throughout repeated measurement cycles are accurately corrected for; recuperation is negligible (< 3 %) up to a preheat temperature of 250 ^oC, after which it steadily increases up to as much as ~10 % at the highest preheat temperature of 325 °C (Fig. V.4b).

Fig. V.4c shows the fading rates (*g*-values) measured for the same aliquots that were used to produce the data in Fig. V.4a (i.e. the D_e versus temperature plots). These fading rates were measured following the procedure proposed by Auclair et al. (2003; see also Basarin et al., 2011), calculated following Huntley and Lamothe (2001) and normalised to a measurement delay time of 2 days after irradiation. For all three samples, the fading rate decreases significantly with preheat temperature.

Fig. V.4d shows the fading corrected ages (Huntley and Lamothe, 2001) corresponding to the data shown in Figs V.4a and c. Similarly to the D_e, the fading-corrected ages systematically increase with increasing preheat temperature, and especially in the interval from ~150 °C to ~225 °C. This implies that preheat dependence of the D_e is not entirely counterbalanced by an opposite dependence of the fading rate.

V.6. Age results

One possible explanation for the observed dependence on the preheat of the fading-corrected ages, is initial sensitivity change, as indicated by the dose recovery data (see section V.4). On the other hand, the ability to recover a dose is clearly dependent on the bleaching agent

used to perform the test, which makes it less straightforward to evaluate the suitability of the SAR-measurement parameters for determining natural doses.

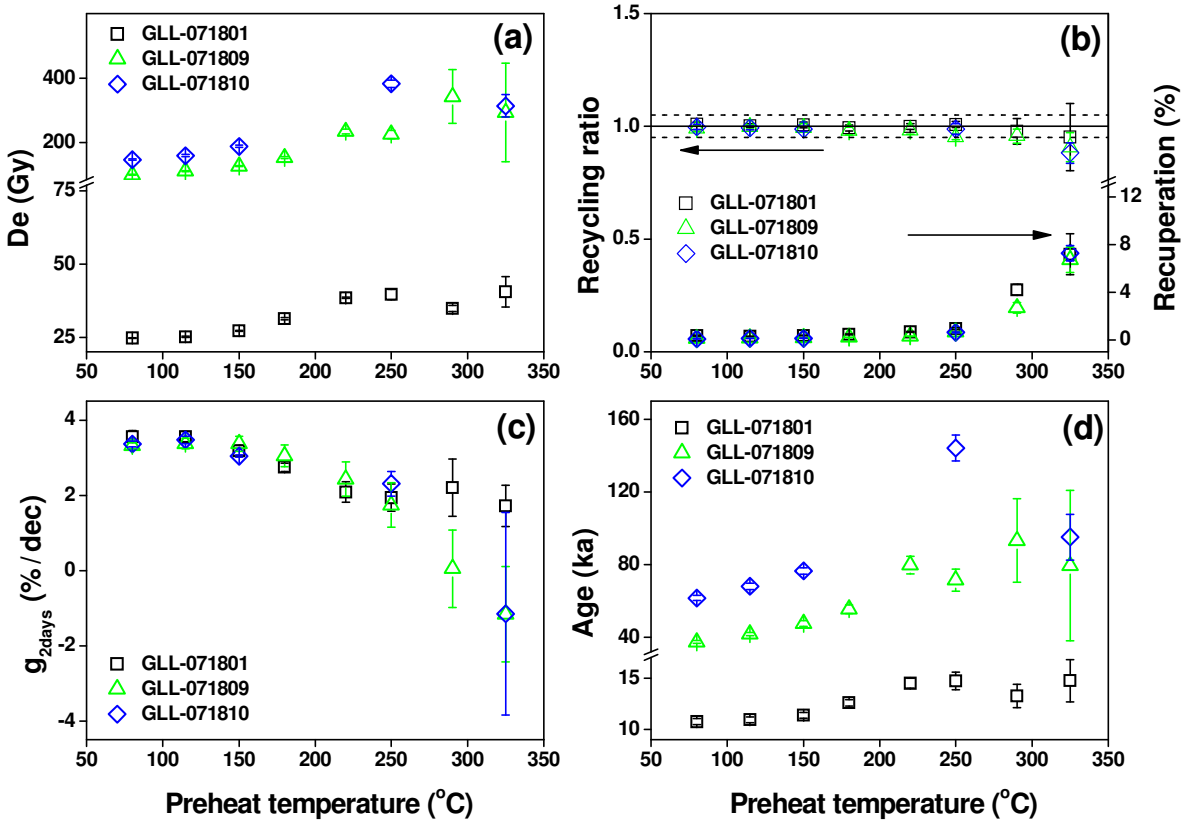

Figure V.4: *Dependence on the preheat temperature of: (a) equivalent dose; (b) recycling ratio and recuperation corresponding to the aliquots measured in (a); (c) fading rate (g_{2days}-value) and (d) fading-corrected ages. Each data point represents the average of at least three aliquots. All error bars represent one standard error. The solid and dashed lines in (b) are eye guides and show the ideal recycling ratio of unity and a ± 5 % deviation, respectively.*

D_e measurements were therefore performed for six aliquots of each sample using a preheat treatment for 60 s at 115 °C. In addition, for several samples, D_e measurements were also performed for three aliquots per sample, using a preheat for 60 s at 250 °C. The measurements of D_e were followed by those of the fading rate. The results are summarized in Table V.1, together with the uncorrected and fading-corrected ages. It can be seen that both sets of fading-corrected ages are entirely consistent with the stratigraphic position of the samples. The ages obtained using the preheat at 250 °C, however, are significantly higher.

In Fig. V.5, the fading-corrected ages are plotted against the SAR-OSL ages obtained by Timar et al. (2010) on silt-sized quartz. For samples collected in the L1 loess unit, excepting the two uppermost samples, the IRSL ages obtained using the preheat at 250 °C are in excellent agreement (within 5 %) with the quartz-based ages (see Fig. V.5 – inset; open circles). As the depth of the samples increases, the quartz-based ages are increasingly overestimated. On the other hand, except for the three uppermost samples, the age results obtained using the preheat at 115 °C are systematically underestimating the quartz-based ages (Fig. V.5 open squares). These results appear consistent with a ~ 35 % underestimation up to the two lowermost samples for which it slightly increases to ~ 47 %. This discrepancy is interpreted as evidence for a contribution from a thermally unstable signal to the regenerated IRSL data, but not the natural. A plot of corrected age versus preheat temperature usually offers the simplest means for identifying thermal instability (see e.g. Murray et al., 2009). However, the occurrence of temperature dependent initial sensitivity changes will upset the diagnostic capacity of such a plot, and alternative investigations are required.

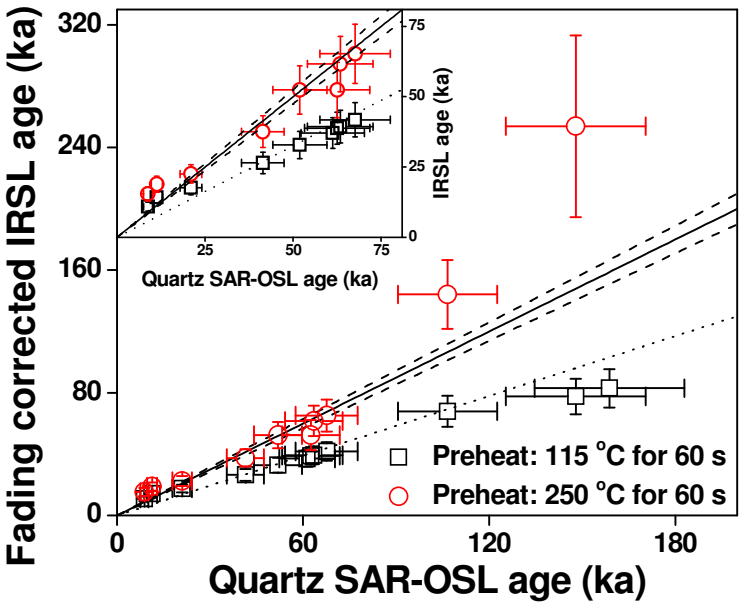

Figure V.5: *Plot of fading corrected IRSL ages against fine silt quartz OSL ages obtained by Timar et al. (2010). Each data point is the average of minimum 3 aliquots measured for each sample. The inset shows the age results for the samples collected in the L1 loess unit. All errors shown are 1σ total uncertainty. The solid line (eye guide) represents the 1:1 relation while the dashed and dotted lines represent a ±5 % and 35 % deviation, respectively.*

Sample	Measurement-Preheat	Dose Rate (Gy/ka)	De (Gy)	$Age_{uncorr.}$ (ka)	g_{2days} (%/decade)	$Age_{corr.}$ (ka)	σ_r (%)	σ_{sys} (%)	σ_{tot} (%)	σ_{tot} (ka)
GLL-071801	IRSL-115	3.20 ± 0.05	25.2 ± 0.2	8	3.6 ± 0.1	11	3	14	14	2
	IRSL-250		41 ± 3	13	1.9 ± 0.4	15	8		16	3
	OSL	2.85 ± 0.05	24.9 ± 0.4	9			2	14	15	1
GLL-071802	IRSL-115	3.22 ± 0.06	33.1 ± 0.2	10	3.4 ± 0.1	14	3	14	14	2
	IRSL-250		49 ± 1	15	2.3 ± 0.3	19	5		15	3
	OSL	2.87 ± 0.05	32 ± 1	11			3	14	15	2
GLL-071803	IRSL-115	3.46 ± 0.05	44.6 ± 0.4	13	3.4 ± 0.2	18	3	14	15	3
	IRSL-250		67 ± 1	19	1.65 ± 0.04	23	2		15	3
	OSL	3.08 ± 0.05	64 ± 2	21			3	14	15	3
GLL-071804	IRSL-115	3.14 ± 0.05	62 ± 1	20	3.1 ± 0.1	26	2	14	15	4
	IRSL-250		105 ± 2	33	1.3 ± 0.3	38	4		15	6
	OSL	2.78 ± 0.04	114 ± 2	41			2	14	14	6
GLL-071805	IRSL-115	3.40 ± 0.07	82 ± 1	24	3.2 ± 0.1	33	3	15	15	5
	IRSL-250		148 ± 5	43	2.0 ± 0.6	52	7		16	9
	OSL	3.01 ± 0.06	156 ± 3	52			3	15	15	8
GLL-071806	IRSL-115	3.50 ± 0.05	94 ± 1	27	3.3 ± 0.1	37	2	15	15	5
	OSL	3.10 ± 0.04	190 ± 3	61			2	15	15	9
GLL-071807	IRSL-115	3.58 ± 0.05	99 ± 2	28	3.6 ± 0.1	39	3	15	15	6
	IRSL-250		174 ± 18	49	0.8 ± 0.5	52	12		19	10
	OSL	3.16 ± 0.05	197 ± 3	62			2	15	15	9
GLL-071808	IRSL-115	3.72 ± 0.05	102 ± 1	27	3.7 ± 0.1	39	2	15	15	6
	IRSL-250		191 ± 5	51	2.0 ± 0.5	62	6		16	10
	OSL	3.30 ± 0.05	209 ± 3	63			2	15	15	9
GLL-071809	IRSL-115	3.69 ± 0.04	111 ± 1	30	3.4 ± 0.1	42	2	15	15	6
	IRSL-250		205 ± 6	56	1.7 ± 0.6	65	7		16	10
	OSL	3.28 ± 0.03	221 ± 5	68			2	15	15	10
GLL-071810	IRSL-115	3.30 ± 0.05	160 ± 3	48	3.5 ± 0.1	68	3	15	15	10
	IRSL-250		382 ± 11	116	2.3 ± 0.3	144	5		15	22
	OSL	2.92 ± 0.04	310 ± 9	106			3	15	15	16
GLL-071812	IRSL-115	3.29 ± 0.06	185 ± 2	56	3.3 ± 0.2	78	3	15	15	12
	IRSL-250		738 ± 132	224	1.3 ± 0.1	254	18		23	59
	OSL	2.91 ± 0.05	430 ± 13	147			3	15	15	23
GLL-071813	IRSL-115	3.30 ± 0.04	194 ± 4	59	3.5 ± 0.1	83	3	15	15	13
	OSL	2.92 ± 0.03	467 ± 11	159			3	15	15	24

Table V.1: *Summary of calculated dose rates, equivalent doses (D_e), uncorrected ages, fading rates (g_{2days}), fading-corrected ages, and random (σ_r), systematic (σ_s) and total uncertainties (σ_{tot}). Dose rates were obtained using the radionuclide activity concentrations reported by Timar et al. (2010; Table S3) and the conversion factors of Adamiec and Aitken (1998). Correction of alpha, beta and gamma contributions for the effect of moisture used a time-averaged water content of 20 ± 5 % (Balescu et al., 2003). A mean a-value of 0.08 ± 0.02 was used (Rees-Jones, 1995). The OSL data for fine-grained quartz are taken from Timar et al. (2010). Uncertainties on the age results were obtained using the error assessment system proposed by Aitken and Alldred (1972) and Aitken (1976). The uncertainties mentioned with the dose rates, D_e's and g_{2days} values are random; all uncertainties represent one sigma.*

V.7. Thermal stability

Further investigations into the thermal stability of the IRSL signal from the polymineral fine grains started by examining the thermoluminescence (TL) glow curves. Fig. V.6 shows the natural and regenerated TL glow curves for sample GLL-071801, which was collected at the top of the sequence. The natural TL curve has no significant signal below 200 °C and is dominated by a pronounced asymmetrical peak at ~ 250 °C with a small shoulder around 320 °C and a tail spreading up to 500 °C. In the regenerated TL signal that received no thermal pre-treatment, two additional low-temperature peaks occur at ~ 90 °C and 130 °C. If a preheat treatment at 115 °C is used, the regenerated TL signal appears as a broad peak, rising from ~ 100 °C. This signal appears to have, besides the components observed in the natural signal, some additional components in the range 150 – 200 °C. After a preheat of 60 s at 250 °C, the regenerated TL signal consists of clearly visible peak at ~ 320 and a less pronounced peak at ~ 430 °C as a tail of the 320 °C peak. Sample GLL-071813, which is the lowermost sample that was collected from the sequence, displayed a very similar TL behaviour.

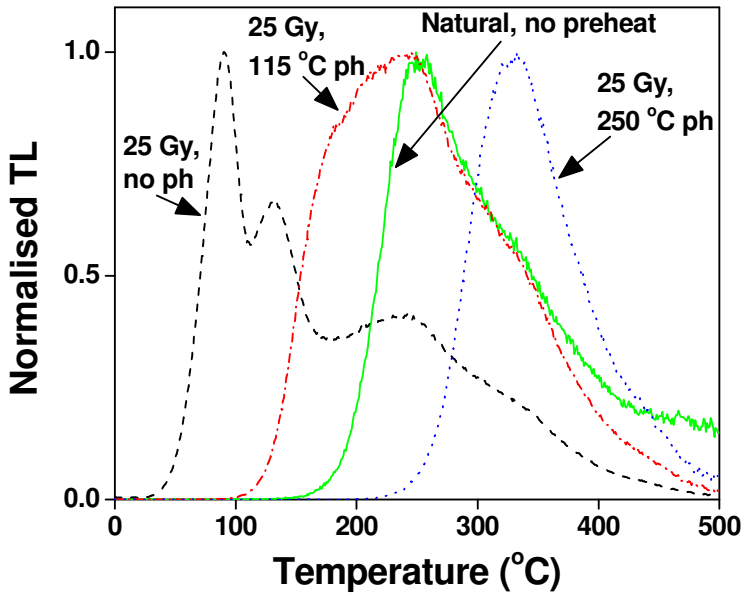

Figure V.6: *TL signals normalised to the maximum intensity values. All signals were measured using one aliquot of sample GLL-071801: natural without preheating (solid line), 25 Gy regenerative dose without preheating (dashed line), 25 Gy regenerative dose followed by preheating at 115 °C for 60 s (dash-dot line) and 25 Gy regenerative dose followed by preheating at 250 °C for 60 s (dotted line).*

As observed in Fig. V.6, a preheat of 60 s at 115°C does not remove all the low temperature TL peaks that have been observed in the regenerated signal. If the remaining components are IR sensitive, they might contribute to the measured IRSL and upset the age determination. Similar to Murray et al. (2009), this was examined by documenting the effect of prior IR stimulation on TL and relating the observations to the pulse anneal characteristics of the IRSL signal.

Fig. V.7a presents the regenerated TL signal that remains after exposure to IR for various stimulation durations (experimental details are given in the caption). The TL signal remaining after a preheating to 115 ^{o}C for 60 s is bleachable by IR from ~ 140 ^{o}C up to a temperature of ~ 400 ^{o}C; exposure to IR does not seem to have an effect on the temperature region between 400 °C and 500 °C. Fig. V.7b plots the difference between the TL signal without prior IR stimulation and the signals following IR stimulation (i.e. the 'lost TL'). The lost TL signal has the shape of a broad peak (a multiplet) with the maximum intensity at ~ 250 ^{o}C. Thus, the TL component at 250 ^{o}C appears the most IR sensitive. However, there is a significant loss from the components in the 150-200 ^{o}C range. Significant phototransfer into the 130 ^{o}C TL peak is observed with increasing stimulation duration. The same observations were made for sample GLL-071813.

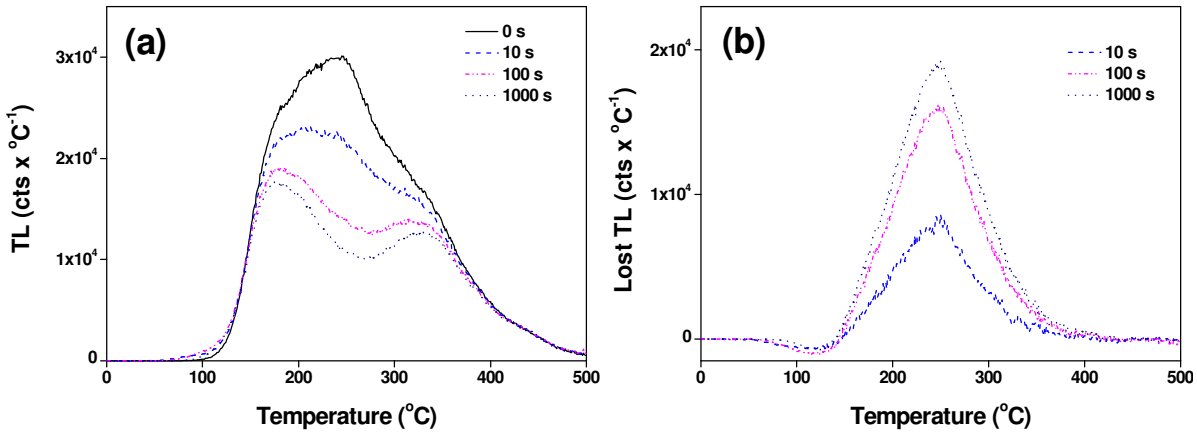

Figure V.7: *(a) effect of prior IR on TL. An aliquot of polymineral fine grains of sample GLL-071801 was repeatedly heated (to 500 ^{o}C) and irradiated (25 Gy) until a stable TL signal was reached. The aliquot was then given a 25 Gy dose, preheated to 115 ^{o}C for 60 s and the TL signal measured after various times (0, 2, 4, 10, 40, 100, 200, 500 and 1000 s) of exposure to IR. The background was subtracted using a second TL signal measured immediately following first one. The measurements for 0, 4 and 40 s were repeated and yielded reproducible results. (b) TL lost as a result of IR stimulation. The curves were obtained by subtracting the TL curves after IR stimulation from the curved observed without stimulation.*

The data indicate that the regenerated IR signal might contain a contribution from low temperature TL components (between 150 and 200 ^{o}C), and pulse anneal experiments were performed to verify this.

A multiple-aliquot pulse anneal measurement was performed, similar to that employed by Banerjee et al. (2001). Sixteen natural aliquots of sample GLL-071801 were each heated for 10 s to a different temperature in between 80 °C and 380 ^{o}C and were then stimulated using the IR diodes for 100 s at 50 ^{o}C to measure the natural IRSL signal. The aliquots were then given a 10 Gy test dose, heated to 90 ^{o}C and stimulated at 50 ^{o}C for 100 s to measure the test dose signal. The sensitivity-corrected signals are plotted as open squares in Fig. V.8. A second set of aliquots was bleached for 1 h in the solar simulator; after a pause for 1 h at room temperature, they were given a regeneration dose of 10 Gy and measured as the set of natural aliquots (Fig. V.8 - open triangles). There is no decrease in the natural IRSL when heated up to 180°C for 10 s, while the regenerated IRSL starts to decrease with preheats in excess of 140°C; both the natural and the regenerated signal are fully eroded by a thermal treatment of 10s at 380 °C. Pulse-anneal data for the regenerated IRSL signal were also obtained using a single aliquot of sample GLL-071801 (Fig. V.8; open circles).

In this experiment, the aliquot was heated to 500 ^{o}C, given a 10 Gy, preheated for 10 s to a temperature between 80 and 450 ^{o}C and measured to give L_x.; this was followed by a measurement of the response to a 10 Gy test dose after a fixed preheat of 90 ^{o}C for 10 s. The reproducibility of the measurements was confirmed by repeating the measurements for preheat temperatures of 100 °C, 200 °C and 300 ^{o}C (Fig V.8; filled circles). The sensitivity-corrected regenerated IRSL signal starts to decrease from a preheat of 10 s at 130 °C onwards and the signal is depleted by more than 10% at a temperatures of ~ 160 ^{o}C. The single-aliquot pulse anneal experiment was also performed for samples GLL-0718-06 and -13, and yielded identical results. The pulse anneal experiments show that the regenerated signal is thermally less stable than the natural. Also, they demonstrate that there may be some contribution from TL components below 200 ^{o}C since the majority of the signal seems to be associated with a temperature region in the TL glow curve that extends from ~150 °C to ~300 °C. The derivative of the regenerated single-aliquot pulse-anneal data shows a peak at ~230°C (see inset to Fig. V.8). A small IRSL signal remains after preheating to 300 °C, and may be associated with the IR

bleachable TL peak at ~320 °C. The IRSL signal is completely thermally eroded by a preheat of 10 s to 380 °C and, above ~ 400 °C, no TL is reduced by exposure to IR (Fig. V.7).

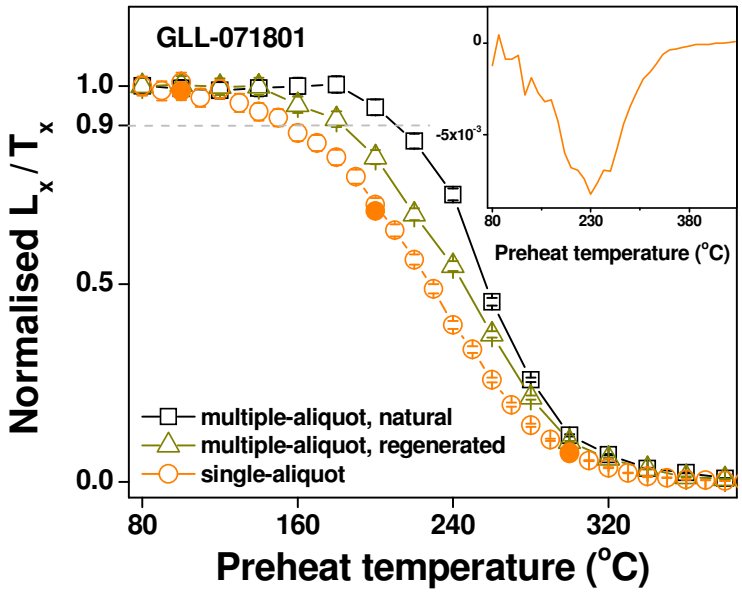

Figure V.8: *Pulse anneal curves representing the variation of the sensitivity corrected IRSL signal with preheat temperature (see text for more details on the measurement procedure). The dashed line is meant as an eye guide and indicates a reduction of the IRSL signal by 10 %. The inset shows the first order derivative of the single-aliquot data.*

V.8. Comparative SAR IRSL investigations using Serbian loess

Three samples (GLL-090830, -34, -37) collected from the loess-palaeosol sequence at Belotinac (Southern Serbia) were investigated in order to obtain a preliminary chronology (Basarin et al., 2011). Sample GLL-090830 was collected from the lower part of the uppermost loess layer L1L1L1 (the notations follow the stratigraphic scheme proposed by Marković et al., 2008). Samples GLL-090834 and -37 were collected from the upper part of the well-developed palaeosol L1S1 and from the lower part of a sandy layer at the base of the profile, respectively. Using the SAR protocol outlined in Section V.2 IRSL investigations were performed following the same approach as for the Romanian loess.

V.8.1. Dose response

Fig. V.9 shows a typical growth curve for one of the samples (GLL-090834); it was measured using a preheat of 60s at 250°C. The growth of the signal with dose is represented best by the sum of a single saturating exponential and a linear component. The growth curve passes very close to the origin (i.e. recuperation is negligible) and the correction for sensitivity changes appears to work well (recycling ratio is equal to unity).

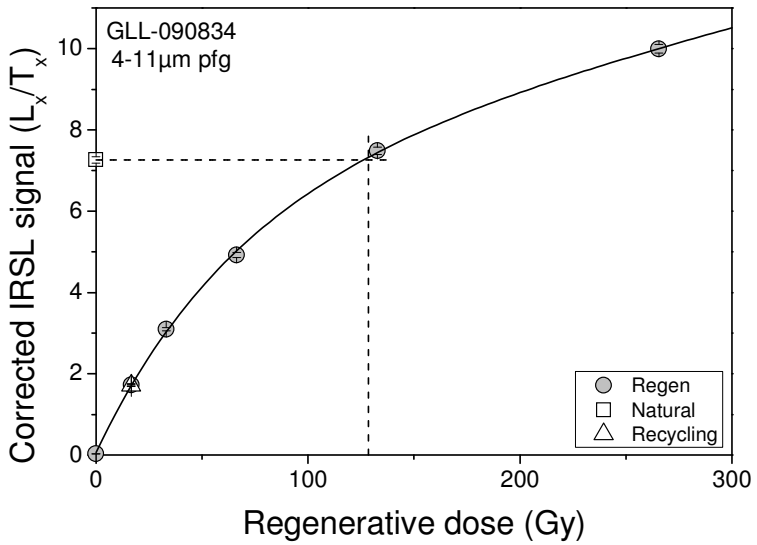

Figure V.9: *SAR-IRSL dose-response curve for a single aliquot of polymineral fine-grains extracted from sample GLL-090834; it was measured using a preheat of 60s at 250°C. The dose-response (solid line) is represented best by the sum of a single saturating exponential and a linear component. The recycling point is shown as an open triangle. The equivalent dose is obtained by interpolating the corrected natural IRSL signal (open square) on the sensitivity-corrected growth curve.*

V.8.2. Dose recovery test

The dose recovery test was performed for all three samples using 1 h bleaching in the solar simulator (see section V.4.1 for experimental details). Using a preheat for 60s at 250°C, the average measured to given dose ratios (± 1 standard error) are 1.33 ± 0.03, 1.5 ± 0.3 and 1.6 ± 0.3 for samples GLL-090830, -34 and -37, respectively. The results are shown in Fig. V.10a. Fig. V.10b shows the corresponding values for the recycling ratio and recuperation; it demonstrates that, despite the poor recovery, sensitivity changes occurring throughout the

measurement procedure are accurately corrected for (recycling ratios are consistent with unity), and recuperation is negligible (< 0.5 % of the sensitivity corrected natural IRSL signal).

We tested whether the given dose overestimation is due to a residual dose by measuring aliquots that had been bleached for one hour in the SOL 2 solar simulator. The residual dose amounts to 2-3 Gy, which is insignificant compared to the given doses of ~100-170Gy (Fig. 2a, inset). It is concluded that the poor dose recovery is not due to the effects of incomplete resetting (which includes thermal transfer), but is likely to originate with an initial sensitivity change, which is not corrected for using the SAR protocol.

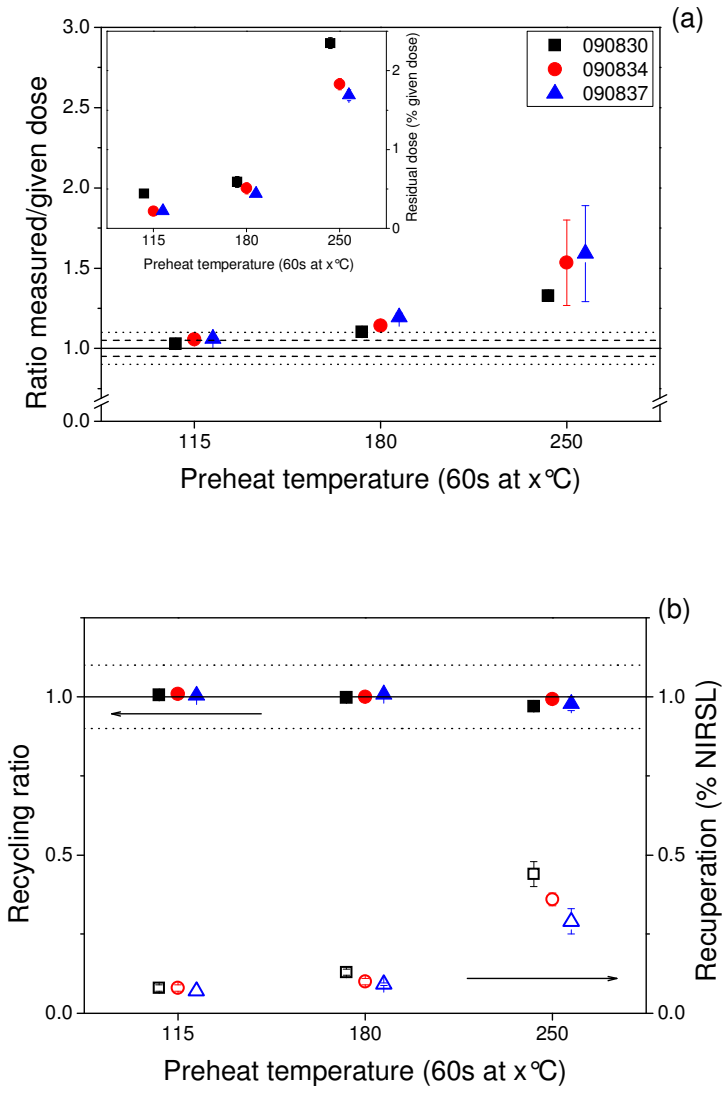

Figure V.10: *Summary of dose recovery data. Each datapoint represents the average ± 1 standard error of three measurements. (a) Ratio of measured to given dose as a function of*

preheat temperature. The dashed and dotted lines (eye guides) bracket, respectively, a 5% and 10% deviation of the ratio from unity. The inset plots the dose measured in bleached aliquots as a function of preheat temperature; the dose is expressed as a percentage of the known laboratory dose given in the dose recovery test. (b) Corresponding values for the recycling ratio and recuperation. The solid and dashed lines (eye guides) indicate a value for the recycling ratio of 1.0 ± 0.1.

Assuming that preheating is the main cause for the initial change in sensitivity, it can be expected that the effect can be reduced (or overcome) using preheat treatments that are less stringent. Therefore, the dose recovery test was repeated for preheats of 60s at 180°C and 60s at 115°C. The results, included in Fig. V.10a, show that the given dose is increasingly overestimated with increasing preheat temperature. Only the lowest preheat of 60s at 115°C allows determining the given dose reasonably accurate (i.e. to within 5%). The average measured to given dose ratios (± 1 standard error) obtained using this thermal pretreatment are 1.03 ± 0.01, 1.057 ± 0.005 and 1.06 ± 0.01 for samples GLL-090830, -34 and -37, respectively; the overall average (± 1 standard error) is 1.05 ± 0.01. Fig. V.10b demonstrates that the recycling ratio shows no variation with preheat and comfortably falls within the 1.0±0.1 range. The recuperated signal appears to increase with preheat temperature, but is negligible (< 0.5%) over the entire range. The inset to Fig. V.10a shows the preheat dependence of the dose measured in aliquots that received a 1 hour bleach using the SOL 2 solar simulator. The increase in residual dose with preheat temperature can be explained through thermal transfer and/or initial sensitivity change; it should be noted that, at all three investigated preheat temperatures, the residual dose represents only a small fraction of the given dose.

V.8.3. Preheat dependence of equivalent dose

If the dependence of dose recovery with preheat temperature is due to an initial sensitivity change, it seems logic to expect it in measurements of equivalent dose (D_e) as well. This was investigated by measuring the D_e for each sample using preheat temperatures of 115°C, 180°C and 250°C. The D_e shows the same trend with preheat temperature as the measured/given dose ratio, but the magnitude of its dependence appears higher (Fig. V.11). It remains to be investigated whether a dependence of fading rate on preheat, as observed by Murray et al.

(2009), might account for this. Also in this experiment were recycling ratios close to unity and did recuperation not exceed about ~0.5% of the corrected natural IRSL signal (data not shown).

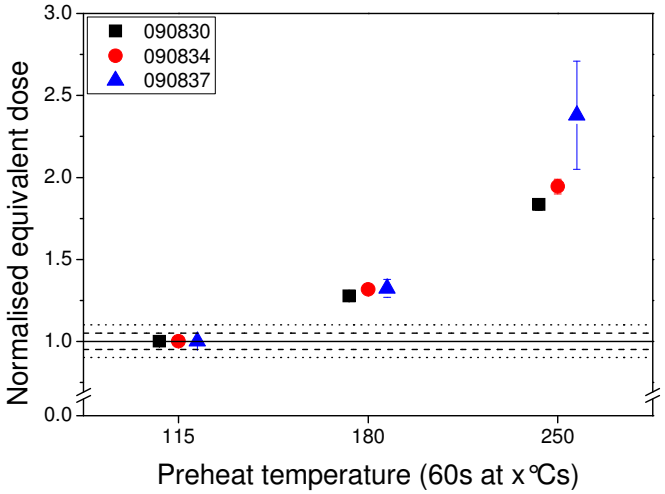

Figure V.11: *Dependence of equivalent dose on preheat temperature; the data have been normalised to the value measured at 115°C. Each datapoint represents the average ± 1 standard error of three measurements. The dashed and dotted lines (eye guides) bracket, respectively, a 5% and 10% deviation from unity.*

V.9. Discussion

Although recent studies on IRSL signals from sand-sized K-feldspar show that they are thermally stable up to a temperature of ~230 °C (e.g. Murray et al., 2009), it seems from the above that the signals from the investigated polymineral-fine grains may have unstable, low temperature sources. Indeed, regenerated TL signals appear to have multiple low temperature components as shown in Section V.7 - Fig. V.6. This distribution of TL components is often encountered in previous studies of feldspars (Duller, 1997). Strickertsson (1985) observed a similar shape for the glow curve of K-feldspar with two low temperature (at 95 and 128 °C) and four high temperature peaks (at 223, 299, 384 and 470 °C). Murray et al. (2009) also observed low temperature components at ~ 100-130 °C and higher temperature components at ~ 310 °C and 400 °C. They also showed phototransfer of charge during IR stimulation to a trap around 230 °C. For other representative studies that provide similar TL characteristics for feldspars and polymineral-fine grains one may refer to Duller and Bøtter-Jensen (1993), Bøtter-Jensen et al. (1993) or Rees-Jones and Tite (1994).

Combined IR/TL experiments indicate that low preheat treatments such as 115 ^{o}C are not able to completely remove all the thermally unstable components in the regenerated signal (see Fig. V.7a and b). Furthermore pulse anneal data indicate that these persisting components appear to influence the thermal stability of the IRSL signal (Fig. V.8). This contribution will not occur in the natural IRSL signals because of the short lifetime of the associated trap (see e.g. Strickertsson, 1988), but it will appear in the regenerated IRSL signals when no preheat is applied. Li and Wintle (1992) reached a similar conclusion for 4-11 μm polymineral extracts from Chinese loess.

Therefore, the observed dependence of D_e on the preheat treatment applied (see Section V.5 - Fig. V.4a) and, consequently, age underestimation when a low preheat is used (see Fig. V.4d) are caused by the low temperature contributions to the IRSL signal. This is further supported by the similar observations made using Serbian loess discussed in Section V.8.3 and the recent studies of Schmidt et al. (2010 and 2011) using Serbian and German loess, respectively. Due to the limited dataset and the absence of an independent age control, the initial age results for the Belotinac section, obtained using a low preheat temperature (Basarin et al., 2011), can not be considered as underestimates. Further investigations into this matter are underway.

The necessity of higher preheat treatments (e.g. 210-230 ^{o}C) to remove thermally unstable components has been suggested by several previous studies on TL and IRSL signals from loess or pure feldspars (see e.g. Wintle, 1985; Li, 1991 or Duller, 1994). A significant number of previous IRSL studies applied a preheat treatment to 250 ^{o}C for 60 s (see e.g. Huot and Lamothe, 2003; Buylaert et al., 2007). Buylaert et al. (submitted) advise the use of a preheat temperature above 200 ^{o}C in order to isolate a thermally stable signal from modern dust samples from China.

Our dose recovery experiments using a preheat to 250 ^{o}C for 60 s indicated the occurrence of significant initial sensitivity changes that the SAR protocol is unable to correct for (Sections V.4 and V.8.2; Figs. V.2c and V.10a). However, the fading corrected age results obtained for the loess sequence at Mircea Vodă using this preheat treatment are in good agreement with previously reported quartz-OSL ages for samples collected in the uppermost loess unit L1 (Fig. V.5). Furthermore, as the quartz-OSL age results corresponding to the samples collected from the deeper loess units were interpreted as age underestimates (Timar et

al., 2010), the older IRSL age results obtained for these samples are not unexpected. Since the ability to recover a given dose was observed to depend on the bleaching agent (see Section V.4 Fig. V.2c), it is considered that the age agreement obtained with the quartz-OSL results may not be a laboratory artifact.

The apparent discrepancy between the results of the dose recovery test using different preheat and bleach treatments needs further investigations. It however underlines the important role of the dose recovery test as an indicator of the performance of the applied SAR protocol. Initial sensitivity changes appear to be dependent also on the size of the given dose (see Fig. V.3). The single-aliquot regenerative and added dose (SARA) protocol is a procedure that is known to take into account initial sensitivity change occurring between the measurement of the natural signal and the corresponding test dose signal (Mejdahl and Bøtter-Jensen, 1994; Buylaert et al., 2006). However, this procedure assumes that any changes in sensitivity occurring throughout the measurements are dose-independent, which is not the case here.

V.10. Conclusions

At this stage of our investigation, the chronology of the loess-palaeosol sequence near Mircea Vodă is not improved. Age results obtained from polymineral fine grains using conventional IRSL signals appear to be affected by thermal instability, initial sensitivity changes, and/or a combination of both phenomena. The initial age results proposed for the loess-palaeosol sequence at Belotinac should be interpreted with caution.

Further investigations using the recently reported Post-IR IRSL (Buylaert et al., 2009) dating using higher stimulation temperatures are hoped to provide a solution for the age discrepancy between different grain-size fractions of quartz reported by Timar Gabor et al. (2011).

CHAPTER VI

Testing the potential of elevated temperature post-IR IRSL signals for dating Romanian loess

Chapter based on:

Vasiliniuc, S., D.A.G. Vandenberghe, A. Timar-Gabor , C. Panaiotu, C. Cosma, P. Van den haute, submitted. *Testing the potential of elevated temperature post-IR IRSL signals for dating Romanian loess.* Quaternary Geochronology, proceedings of LED 2011.

VI.Testing the potential of elevated temperature post-IR IRSL signals for dating Romanian loess

VI.1. Introduction

We continue our attempts to obtain a reliable chronology for Romanian loess using luminescence signals from feldspars. Since the conventional IRSL approach seems unable to provide accurate results (see Chapter V) we now focus on a recently developed alternative method – post-IR IRSL.

Thomsen et al. (2008a) observed that using elevated temperature IR stimulation immediately after the IR stimulation at 50 ^{o}C results in lower fading rates. This was confirmed by later studies where post-IR IRSL signals were shown to pass laboratory tests and provide accurate age results (Buylaert et al., 2009; Thiel et al., 2011b). Furthermore recent studies show that, besides having a lower fading rate, the post-IR IRSL signal is also thermally more stable than the IRSL signal obtained using a single IR stimulation at 50 ^{o}C (Thomsen et al.,2011; Li and Li, 2011).

In this study we test the potential of elevated temperature IRSL signals in a post-IR IRSL SAR protocol. The luminescence characteristics of IRSL and post-IR IRSL signals are documented using two preheat/stimulation temperature combinations in a SAR-based methodology. Dose response characteristics and laboratory tests are presented together with fading measurements. Finally, age results based on the elevated temperature post-IR IRSL are discussed in comparison with the ages obtained using IRSL measured at 50 ^{o}C and quartz OSL ages.

VI.2. Samples and experimental details

In this study we used 8 samples, considered as representative for the loess-palaeosol sequence near Mircea Vodă: five samples (GLL-071802, -03, -06, -07, -09) collected from the uppermost loess unit (L1), and three samples (GLL-071810, -12, -13) collected from the loess

units below L2, L3 and L4, respectively. The reader is referred to the recent works of Timar et al. (2010) and Timar Gabor et al. (2011) for a detailed description of the study site and sample collection. Polymineral fine grains (4-11 μm) were separated using conventional sample preparation techniques (Lang et al., 1996; Frechen et al., 1996). Part of the material was further prepared for the extraction of fine grained quartz (Timar et al., 2010). The rest of the material was archived and subsequently used in this study. Aliquots were prepared by settling the polymineral, fine grains in acetone on aluminium discs.

All luminescence measurements were performed using a Risø TL/OSL-DA-15 reader. Infrared stimulation used IR LEDs emitting at 875 nm (Bøtter-Jensen et al. 2003) and IRSL signals were detected through a Schott BG39/Corning 7-59 filter combination passing light between 320 and 450 nm (Thomsen et al., 2008a). Unless otherwise stated, a constant test dose of 10 Gy was given and a heating rate of 5 ^{o}C/s in a nitrogen atmosphere was employed.

The post-IR IRSL signals were documented using the modified SAR protocol given in Table VI.1, based on that developed for quartz by Murray and Wintle (2000). Two preheat - post-IR IR stimulation temperature combinations were used. In the first, a 60 s preheat treatment at 250 ^{o}C was followed by 100 s IR stimulation at 50 ^{o}C (IR_{50}) and a second 100 s stimulation at 225 ^{o}C (post-IR IR_{225}). This is identical to the protocol chosen by Buylaert et al. (2009), who applied it to a wide range of sedimentary feldspar. The second post-IR IRSL protocol involved a 60 s preheat treatment at 325 ^{o}C and an elevated temperature IR stimulation at 300 ^{o}C (post-IR IR_{300}) following the IR_{50} stimulation. This protocol is similar to that of Thiel et al. (2011b) who chose a preheat temperature of 320 ^{o}C and post-IR IR temperature of 290 ^{o}C and time of 100 s in their study of loess from a section in Austria. These temperatures were also used by Stevens et al. (2011) in their protocol for polymineral fine grains for loess from the Carpathian Basin. They were able to obtain post-IR IRSL ages that were greater than the OSL ages for quartz extracted from the same fine grain fraction. In our study, the initial preheat temperatures were 25 ^{o}C higher than the temperature selected for the post-IR IRSL measurements in order to remove the isothermal TL signal that would otherwise be observed. The thermal treatment used prior to measuring the response to the regenerative and test doses was identical (Huot and Lamothe, 2003; Blair et al., 2005). To reduce recuperation, each measurement of the response to the test dose was followed by a high-temperature optical stimulation with IR (Murray and Wintle, 2003) performed by stimulating with the IR LEDs for 40 s either at 290 °C or 340 ^{o}C. The signals used

for all calculations (IR_{50} and post-IR IR_T) were integrated over the first 1.2 s of stimulation time minus a background evaluated from the last 10 s.

SAR protocol		Variable temperature	Measured IRSL
1.	Dose		
2.	Preheat, 60 s	250 or 325 °C	
3.	IRSL, 100 s at 50 °C		IR_{50}
4.	IRSL, 100 s $\rightarrow L_x$	225 or 300 °C	post-IR IR_T
5.	Test dose		
6.	Preheat, 60 s	250 or 325 °C	
7.	IRSL, 100 s at 50 °C		IR_{50}
8.	IRSL, 100 s $\rightarrow T_x$	225 or 300 °C	post-IR IR_T
9.	IRSL, 40 s	290 or 340 °C	
10.	Return to step 1		

Table VI.1: *The SAR protocol used for IRSL and post-IR IRSL measurements.*

VI.3. Luminescence characteristics

VI.3.1. Evaluation of the IR_{50} and post-IR IR_T signals

Fig. VI.1 shows representative decay curves for both IR_{50} and post-IR IR_T signals recorded on an aliquot of sample GLL-071806, obtained using a single cycle of the protocol in Table VI.1. Prior to measuring these signals, the aliquot was subjected to repeated cycles of heating to 500 °C and irradiation with 25 Gy in order to obtain a constant sensitivity. The aliquot was then given a dose of 25 Gy. The intensity of the IR_{50} signal after a preheat at 250 °C is slightly stronger than that of the post-IR IR_{225} (Fig. VI.1a); this is in contrast to the findings of Buylaert et al. (2009) who reported that for all their samples, the post-IR IR_{225} was ~ 2.5 times brighter than the prior IRSL at 50 °C. Nevertheless the two signals have similar decay rates (see Fig. VI.1a-inset). On the other hand, the intensity post-IR IR_{300} signal is significantly stronger than the intensity of the corresponding IR_{50} signal measured after a preheat at 325 °C (Fig. VI.1b). The latter is also observed to have a slower decay rate and to have a significant background level relative to its initial intensity (see Fig. VI.1b-inset). This is due to the weak signal remaining after the thermal erosion caused by preheating at 325 °C for 100 s. Significant

thermal erosion is expected from the pulse annealing studies carried out on IRSL from loess (Li and Wintle, 1992); these show almost total loss of signal after heating to 325 ^{o}C at 5 ^{o}C/s and then immediate cooling. A negligible signal was detected during 1.9 s before the IR diodes were switched on (Fig. VI.1a and b) indicating no isothermal thermoluminescence (ITL) contribution to the post-IR IR_T signals.

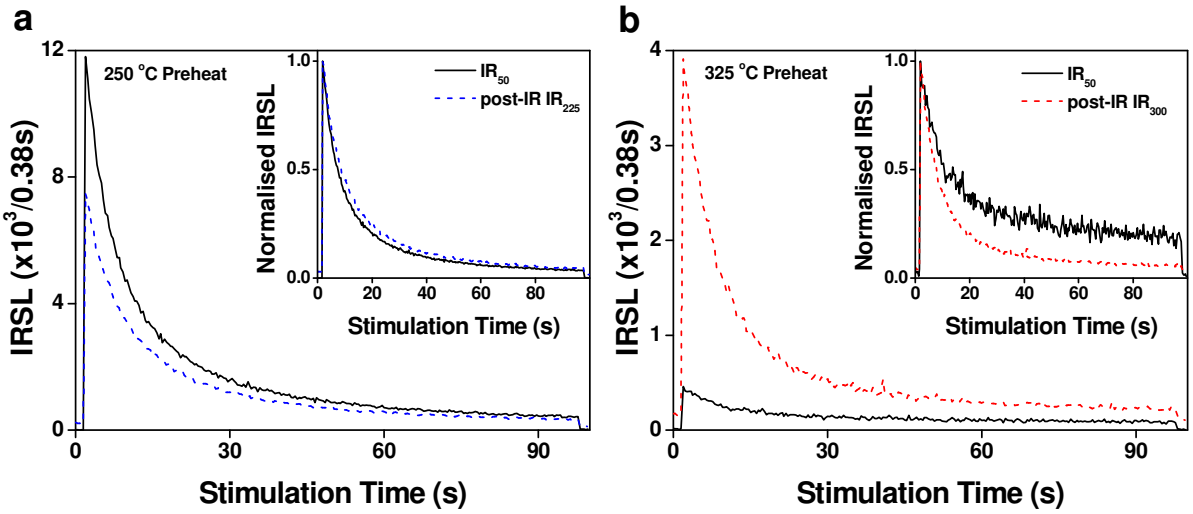

Figure VI.1: *Representative decay curves for (a) IR_{50} and post-IR IR_{225} (measured after an initial preheat at 250 ^{o}C) and (b) IR_{50} and post-IR IR_{300} (measured after an initial preheat at 325 ^{o}C). The insets in (a) and (b) show the same signals but normalized to their maximum intensity.*

VI.3.2 SAR protocol

Typical dose response curves (L_x/T_x versus dose) for four samples (GLL-071806, - -10, -12 and -13) collected from different loess units (L1, L2, L3 and L4, respectively) are presented in Fig. VI.2 with maximum regenerative doses of 420, 760, 1,480 and 2000 (for -12), 4,000 and 12000 (for -13) Gy, respectively. Different growth patterns are observed between the IR_{50} signal and corresponding post-IR IR_T signal, independent from the depth of the samples. For the samples collected from the two uppermost loess units, the natural signal is well below saturation for both types of signal and preheat treatments (Fig. VI.2a and b). The same holds for the IR_{50} signal recorded using the sample collected from the L3 unit (GLL-071812). However, the post-IR IR_T natural signal is very close to the saturation level (~90 %) as shown by open square symbols in Fig. VI.2c and d.

Fig. VI.2e and f show dose response curves up to 4 kGy for the sample collected from the L4 loess unit (GLL-071813). When a 250 ^{o}C preheat is used, the natural post-IR IR_{225} signal corresponds to the saturating part of the curve, while the corresponding IR_{50} signal is still below saturation (~80% of saturation level). Interestingly, when a preheat treatment at 325 ^{o}C is applied the IR_{50} signal is lying very close to the saturation level of the curve (95 ± 20 %), whereas the post-IR IR_{300} signal lies above the saturation level (109 ± 81 %). Such behaviour has been previously reported in quartz OSL investigations, but not in IRSL studies using feldspar or polymineral fine grains. Nevertheless, for some of the aliquots of sample GLL-071813, the natural post-IR IR_{300} does lie very close to, or in, the saturating region (~100 ± 10 %) of the dose response curve (see Fig. VI.2f-inset). The observation that the natural post-IR IR_T signals are in, or close to, saturation (Fig. VI.2e and f) indicates that the fading rates measured in section VI.3.4 may be a laboratory artefact.

The accurate correction of sensitivity change during repeated SAR cycles was monitored by repeating the measurement of the first regenerative dose after the largest dose had been given (see Fig. VI.2 – solid symbols). All the investigated samples exhibit recycling ratios within 10 % from unity independent of the signal used (Table VI.2). Furthermore, a negligible amount of signal was observed to be transferred between measurement cycles by means of recuperation (< 3 % of the sensitivity-corrected natural signal).

VI.3.3. Dose recovery

Dose recovery tests (Wallinga et al., 2000) were performed using three aliquots per sample for both post-IR IR_T protocols. Separate aliquots were used to determine the residual doses that may persist after bleaching. The test was performed for six samples from different depths (see Table VI.2). The aliquots were first bleached for 1 h using a Hönle SOL2 solar simulator.

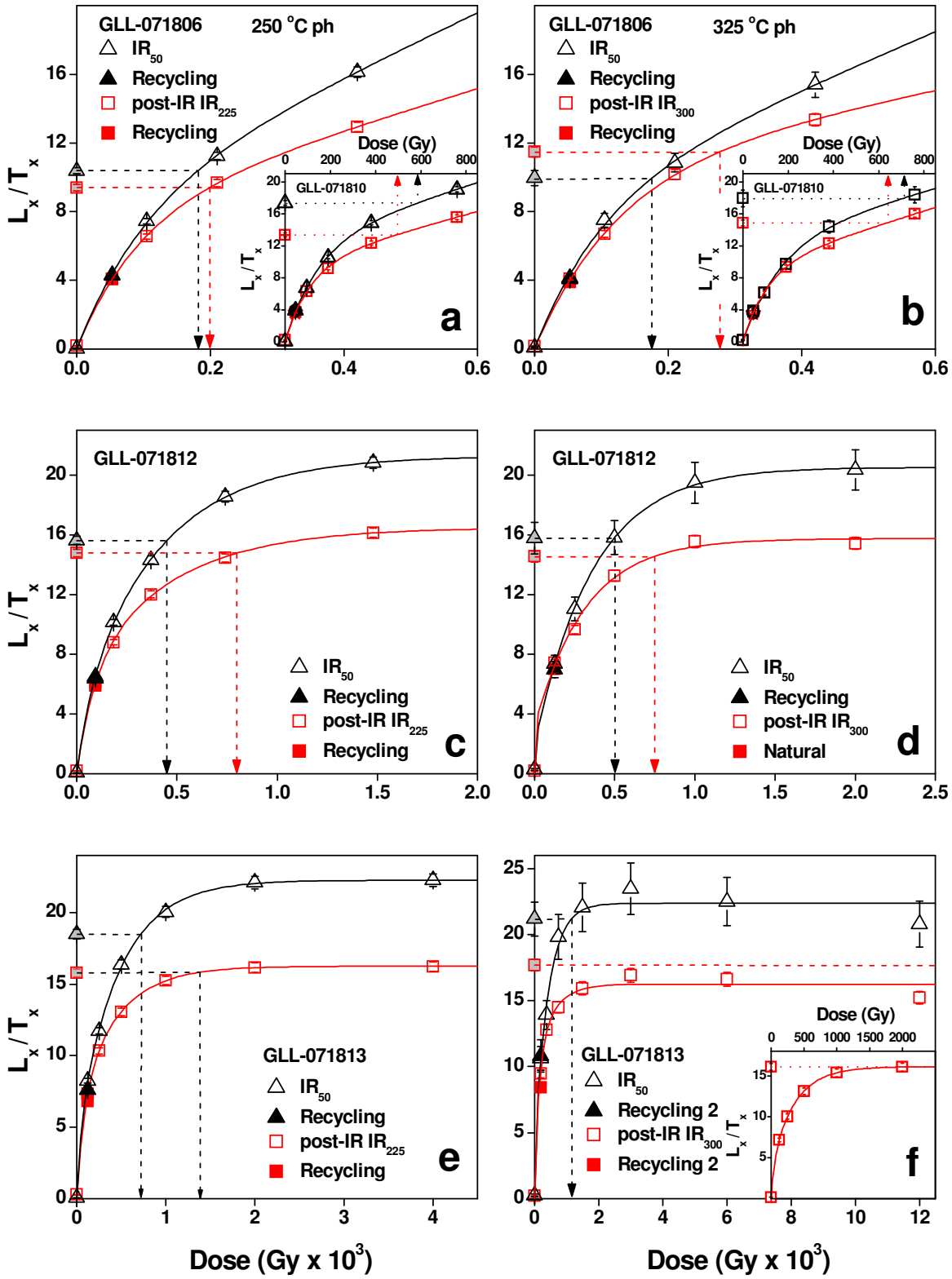

Figure VI.2: *Examples of dose response curves of signals obtained using the two SAR protocols: IR_{50} and post-IR IR_{225} (a,c,e); IR_{50} and post-IR IR_{300} (b,d,f). The signals were measured using aliquots of samples collected from different loess units: GLL-071806 (a,b); GLL-071810 (insets*

in a and b); GLL-071812 (c,d) and GLL-071813 (e,f). The sensitivity-corrected natural signals are shown as grey-filled symbols and recycling points are shown as solid symbols. The solid lines represent the best fit to: the sum of a single saturating exponential and a linear term (a,b) and the sum of two saturating exponential functions (c,d,e,f).

After a delay of 1 h, a dose approximately equal to the measured post-IR IR_T D_e (values given in Table VI.3) was then given and subsequently measured using the corresponding post-IR IR_T protocol. Residual doses persisting after the 1 h bleach in the solar simulator were measured using maximum regenerative doses of 20, 40, 60, 80 and 200 (for GLL-071812 and -13), Gy respectively. The residual doses range from 3.8±0.3 Gy to 17.0±0.4 Gy for post-IR IR_{225} and from 11.3±0.3 Gy to 33.2±1.1 Gy for post-IR IR_{300} (Table VI.2), with there being a trend for increasing residual signal with increasing equivalent dose; thus, they are less than, or equal to, 6 % of the D_e measured using the post-IR IR_{225} signal and between 2 and 19 % of the D_e for the post-IR IR_{300}. For the IR_{50} signals from both post-IR IR_T protocols, the measured residual doses reach a maximum of 3 % from the corresponding D_e value. The doses obtained for the six samples are plotted in Fig. VI.3 and the average recovered/given dose ratios obtained after subtraction of residual doses are given in Table VI.2. For the uppermost sample (GLL-071802) a recovered/given dose ratio of 1.06 ± 0.02 was obtained using the IR_{50} signal after preheating at 250 ^{o}C. However, for the rest of the samples, the recovered/given dose ratio appears significantly and systematically larger than unity with the apparent trend of the overestimation showing increase with depth (see Table VI.2 and Fig. VI.3a). For samples collected from the upper two loess units (L1 and L2), the recovered/given dose ratios obtained using the post-IR IR_{225} signal appear very close to unity (within 5 %; Table VI.2). For the two samples collected from L3 and L4 an overestimation of the given dose is observed, especially for sample GLL-071813 from the lowermost loess unit.

Different results were obtained from the dose recovery test using the signals obtained after preheating at 325 ^{o}C. The recovered/given dose ratios obtained using the IR_{50} signal, for all six samples, appear generally consistent with 10 % deviation from unity (Fig. VI.3b). For sample GLL-071813, the saturation characteristics of the dose response curve influence the accuracy of the measurement for this sample as discussed below. Using the post-IR IR_{300} signal, the recovered/given dose ratio falls within 5 % from unity for the four samples collected from the upper two loess units (Fig. VI.3b).

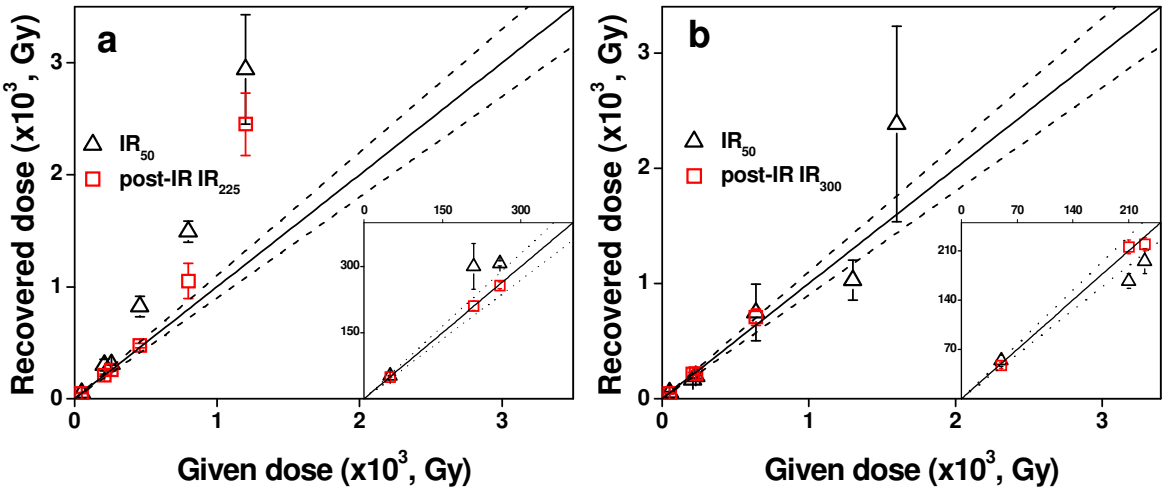

Figure VI.3: *Summary of dose recovery test for the post-IR IR_{225} and corresponding IR_{50} (a) and post-IR IR_{300} and corresponding IR_{50} (b). Error bars represent one standard error. The solid lines represent the 1:1 relation and the dashed lines bracket a 10 % deviation from unity. The insets show the results for samples from the loess unit L1.*

The measurement of the recovered dose for the samples collected in L3 and L4 was hampered by the saturation characteristics of the dose response curves.

Fig. VI.4 shows the dose response curves for the dose recovery tests for the IR_{50} and corresponding post-IR IR_T signals measured for the two lowermost investigated samples (GLL-071812 and -13). While for sample GLL-071812 the signals (IR_{50} and post-IR IR_{225}) measured after irradiation with the given dose (see Table VI.2) and preheating at 250 ^{o}C are still below the saturation level of the curve (Fig. VI.4a), for sample GLL-071813, the same signals appear to correspond to the saturation level of the curve (Fig. VI.4b). Interpolation of the signals in this region of the curve is not expected to be accurate (Murray and Funder, 2003; Wintle and Murray, 2006).The latter situation is also observed for the IR_{50} signals measured after preheating at 325 ^{o}C for sample GLL-071813. However, the post-IR IR_{300} signals appear above the saturation level of the curve for both samples (Figs. VI.4c and d), making the recovery of the given dose impossible (shown by X in Table VI.2).

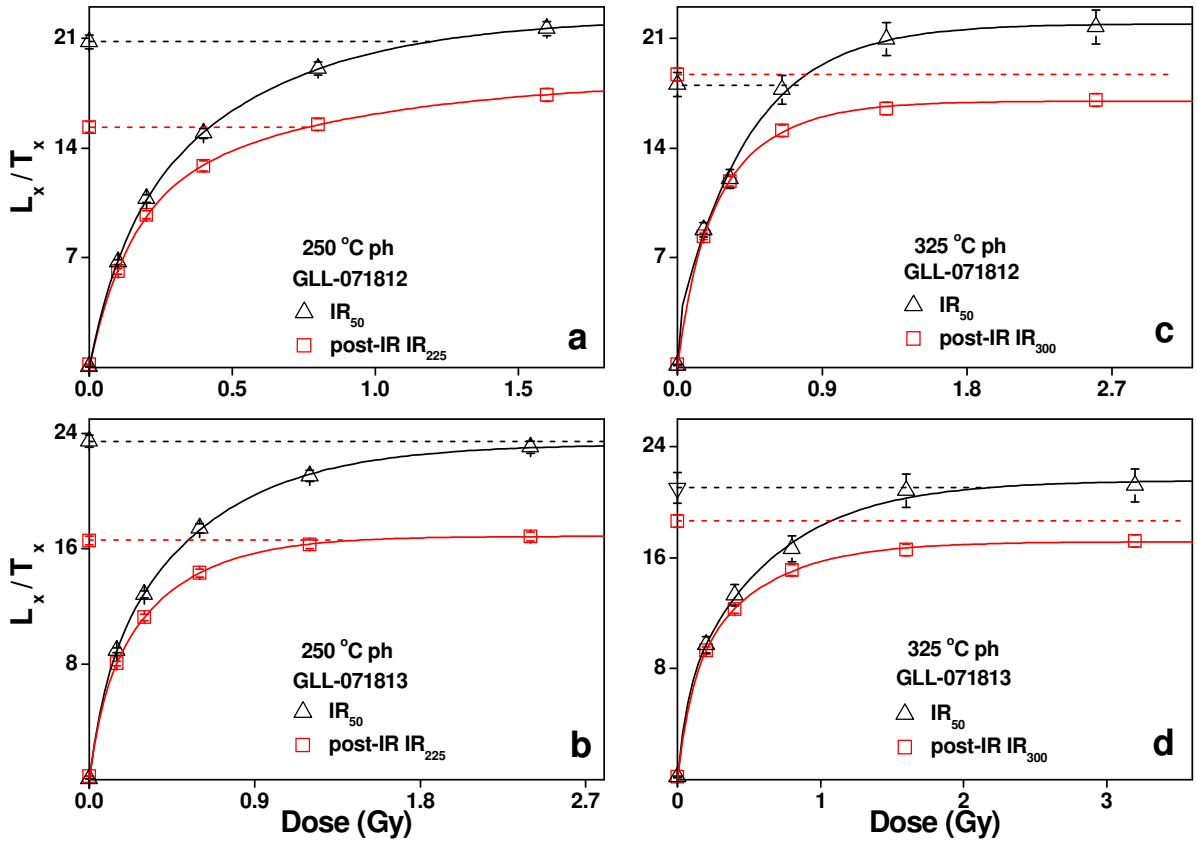

Figure VI.4: *Dose response curves obtained in dose recovery tests for the two lowermost collected samples: GLL-071812 (a,c) and GLL-071813 (b,d). The sensitivity corrected signals corresponding to the given dose are represented by horizontal dashed lines. The solid lines represent the best fit to the sum of two saturating exponential functions.*

We note that for all samples and investigated signals in the dose recovery measurements, the recycling ratio was within 10 % of unity, while recuperation was below 3 %.

Loess Unit	Sample	Depth (m)	IRSL signal	Recycling ratio	Given dose (Gy)	Recovered/ given dose	Residual dose (Gy)
L1	**GLL-071802**	1.05	**post-IR IR_{225}**	0.99 ± 0.02	50	0.99 ± 0.03	3.8 ± 0.3
	n=3		**IR_{50}**	1.01 ± 0.02		1.06 ± 0.02	1.6 ± 0.1
			post-IR IR_{300}	1.02 ± 0.03	50	0.95 ± 0.08	11.3 ± 0.3
			IR_{50}	0.96 ± 0.09		1.08 ± 0.16	5.5 ± 0.5
	GLL-071803	1.30	**post-IR IR_{225}**	0.98 ± 0.01			
	n=6		**IR_{50}**	1.01 ± 0.01			
			post-IR IR_{300}	0.99 ± 0.02			
			IR_{50}	1.01 ± 0.05			
	GLL-071806	2.80	**post-IR IR_{225}**	0.96 ± 0.01	210	1.00 ± 0.05	9.9 ± 0.3
	n=6		**IR_{50}**	0.96 ± 0.01		1.43 ± 0.25	2.9 ± 0.1
			post-IR IR_{300}	0.93 ± 0.03	210	1.03 ± 0.05	23.8 ± 1.0
			IR_{50}	0.96 ± 0.07		0.80 ± 0.11	10.2 ± 1.6
	GLL-071807	3.75	**post-IR IR_{225}**	0.97 ± 0.01			
	n=6		**IR_{50}**	0.97 ± 0.01			
			post-IR IR_{300}	0.96 ± 0.02			
			IR_{50}	0.95 ± 0.05			
	GLL-071809	5	**post-IR IR_{225}**	0.97 ± 0.02	260	0.99 ± 0.03	10.1 ± 0.3
	n=3		**IR_{50}**	1.01 ± 0.02		1.34 ± 0.03	2.9 ± 0.1
			post-IR IR_{300}	1.01 ± 0.03	230	0.95 ± 0.04	20.5 ± 0.7
			IR_{50}	0.91 ± 0.06		0.85 ± 0.08	11.9 ± 3.9
L2	**GLL-071810**	8	**post-IR IR_{225}**	0.98 ± 0.02	460	1.03 ± 0.04	12.7 ± 1.3
	n=3		**IR_{50}**	0.98 ± 0.02		1.79 ± 0.20	3.4 ± 0.3
			post-IR IR_{300}	0.96 ± 0.03	640	1.10 ± 0.11	30.1 ± 0.8
			IR_{50}	0.90 ± 0.11		1.17 ± 0.38	13.3 ± 1.1
L3	**GLL-071812**	15	**post-IR IR_{225}**	0.97 ± 0.01	800	1.31 ± 0.20	14.1 ± 0.7
	n=6		**IR_{50}**	0.97 ± 0.01		1.87 ± 0.11	3.9 ± 0.2
			post-IR IR_{300}	0.97 ± 0.03	1300	X	30.2 ± 1.4
			IR_{50}	0.90 ± 0.05		0.79 ± 0.13	11.8 ± 1.4
L4	**GLL-071813**	18	**post-IR IR_{225}**	0.96 ± 0.01	1200	2.04 ± 0.23	17.0 ± 0.4
	n=6		**IR_{50}**	0.95 ± 0.01		2.45 ± 0.41	4.3 ± 0.2
			post-IR IR_{300}	0.94 ± 0.02	1600	X	33.2 ± 1.1
			IR_{50}	0.86 ± 0.05		1.49 ± 0.53	13 ± 0.9

Table VI.2: *Summary of recycling ratio, dose recovery and residual doses. Recycling ratio datasets were obtained from the SAR D_e measurements. The number of aliquots included in the average recycling ratio is indicated below each sample code. Recovered per given dose ratio and residual dose values represent the average of 3 aliquots per sample. All errors represent one standard error. The stratigraphic position of the samples is indicated in the left column.*

VI.3.4 Fading measurements

Following the method proposed by Auclair et al. (2003), fading measurements were performed using the same aliquots that were used for D_e determinations. The aliquots were first bleached using 100 s IR stimulation at 50 ^oC coupled with a second 100 s IR stimulation at 250 or 325 ^oC, depending on the post-IR IR_T protocol used in the previous D_e measurement of the aliquots. This bleach treatment was repeated after 1 h pause. The aliquots were then repeatedly given a constant dose of 50 Gy and the L_x/T_x was measured after different delay times (from ~ 0.2 h to a few tens of hours) inserted after preheating. A 20 Gy test dose was used for all fading measurements. Table VI.3 contains the obtained g-values (percentage of the signal lost per decade of time – Aitken, 1985) calculated using Eq. (4) of Huntley and Lamothe (2001) and normalised to a measurement delay time of 2 days after irradiation.

The overall (n = 39) average fading rate for all eight samples is 1.1 ± 0.1 %/decade for the post-IR IR_{225} signal, which is more than 50 % smaller than the value obtained for the corresponding IR_{50} signal (2.7 ± 0.1 %/decade). An overall average of 0.5 ± 0.2 %/decade is obtained for the post-IR IR_{300} signal. The values for the post-IR IR_T signals are very small, but appear to be statistically significant, though they are at odds with the finding in section VI.3.2 that the natural signals for the two oldest samples are in, or close to, saturation. The average value of -1.2 ± 0.4 %/decade for the IR_{50} signal related to the post-IR IR_{300} signal (obtained from the data in Table VI.2) is the result of low signals (Fig. VI.1b) and poor reproducibility relating to the preheat having been carried out at 350 °C.

VI.4. Age results

Table VI.3 contains a summary of the dose rates, equivalent doses, fading rates and age results for all eight samples. For the post-IR IR_T measurements, no aliquot was rejected due to a recycling ratio exceeding the accepted range of ± 10 % from unity. The same holds for the IR_{50} signal recorded after a 250 ^oC preheat treatment. However, the IR_{50} signal recorded after a preheat at 325 ^oC exhibited poor recycling ratios some for aliquots, though the D_e values for these aliquots were included in the average D_e given in Table VI.3. Residual doses measured after 1 h bleach using a solar simulator were not subtracted from the average equivalent doses.

The works of Stevens et al. (2011) and Thiel et al. (2011b) indicate that signal resetting in nature may be different than under the stimulation conditions in the laboratory, and thus making this correction may be inappropriate.

Since the observed fading rates may be a laboratory artefact, the uncorrected post-IR IR_{225} and post-IR IR_{300} ages (shown highlighted in Table VI.3) were selected for further discussion. In Fig. VI.5 these ages are plotted against corresponding IR_{50} ages, corrected for fading in the case of measurement after the 250 °C preheat and uncorrected when measured after the 325 °C preheat. An agreement within 10 % is observed between the two sets of ages for all the investigated samples for the post-IR IR_{225} ages, whereas the post-IR IR_{300} age results appear systematically older than the IR_{50} ages.

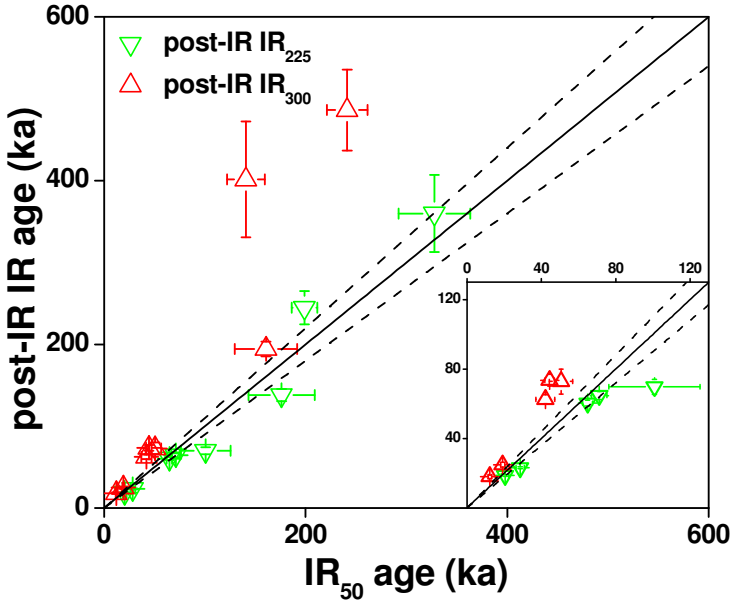

Figure VI.5: *Plot of uncorrected post-IR IR_T ages against the corresponding IR_{50} ages. The IR_{50} ages obtained using a preheat at 250 °C were corrected for fading, the IR_{50} ages obtained using a preheat at 325 °C were not corrected for fading. Error bars represent 1σ random uncertainty. The inset shows the data corresponding to samples collected from the loess unit L1.*

The four sets of ages shown highlighted in Table VI.3 are further compared with the previously reported silt-sized quartz OSL ages (Timar et al., 2010). Fig. VI.6a presents the fading-corrected IR_{50} ages obtained using a preheat at 250 °C (open symbols) and the uncorrected IR_{50} ages obtained using a preheat at 325 °C (closed symbols) plotted as a function of the OSL ages. Apart from the youngest sample (GLL-071802), the fading-corrected IR_{50} ages

obtained for samples from loess unit L1 (see Table VI.3), are in general agreement (within 10 %) with the quartz OSL ages. For sample GLL-071802 the IR_{50} age is with ~ 70 % older than the OSL age. The ages obtained for the three oldest samples, taken from L2, L3 and L4, appear systematically older than the quartz OSL ages.

The uncorrected IR_{50} ages obtained using a preheat at 325 ^{o}C (filled symbols in Fig. VI.6a) appear to agree well with the quartz OSL ages for all samples in the uppermost loess unit L1. Furthermore, within 2σ the agreement persists also for samples from the deeper loess units; they are observed to be younger than the fading-corrected IR_{50} ages obtained using a preheat at 250 ^{o}C (open symbols in Fig. VI.6a).

In Fig. VI.6b the uncorrected post-IR IR_T ages are plotted as a function of the quartz-OSL ages. For sample GLL-071802, the two post-IR IR_T ages are larger than the quartz OSL age with ~ 65 %. For the remainder of the samples in L1, an excellent agreement is observed (within 5 %) between the uncorrected ages for both post-IR IR_T signals and the silt-sized quartz OSL ages. For samples collected from the deeper loess units, the post-IR IR_T ages appear increasingly older than the quartz OSL ages; the post-IR IR_{300} ages (upward triangles in Fig. VI.6b) are generally older than the post-IR IR_{225} ages (downward triangles in Fig. VI.6b).

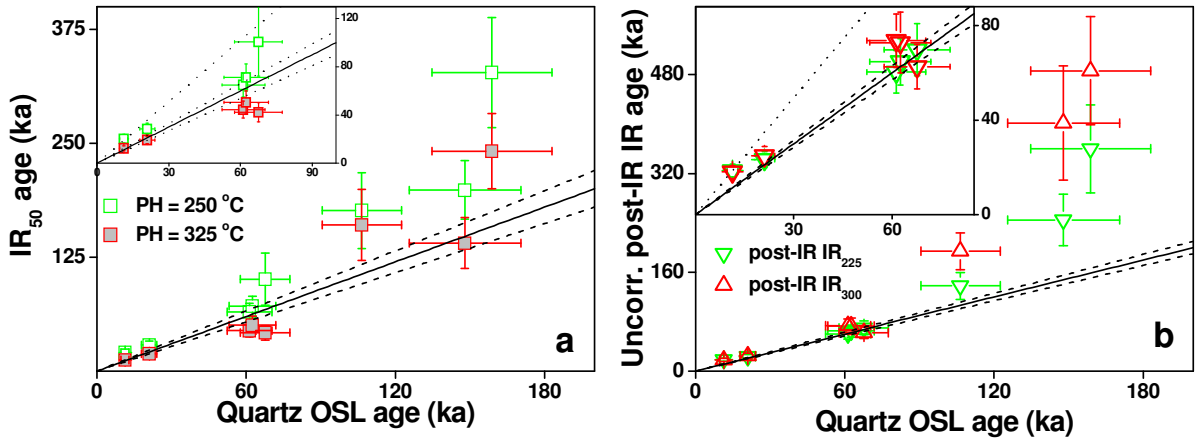

Figure VI.6: *(a) Plot of the IR_{50} ages used in Fig. VI.5 as a function of silt-sized quartz OSL ages obtained by Timar et al., 2010. (b) Plot of the post-IR IR_T ages used in Fig.* VI.*5 against the same quartz OSL ages. All errors shown are 1σ total uncertainty. The insets show the data corresponding to samples collected from the loess unit L1.*

Sample GLL-	Depth (m)	Dose rate (Gy/ka)	IRSL signal	D_e (Gy)	$Age_{uncorr.}$ (ka)	g_{2days} (%/decade)	$Age_{corrr.}$ (ka)	σ_r (%)	σ_{sys} (%)
071802	1.05	3.22 ± 0.06	**post-IR IR_{225}**	60 ± 1 $_{(n=3)}$	**19 ± 3**	0.6 ± 0.2	19 ± 3	2	14
			IR_{50}	55 ± 5	17 ± 3	2.1 ± 0.1	**20 ± 4**	10	
			post-IR IR_{300}	58 ± 3	**18 ± 3**	0.6 ± 0.4	19 ± 3	6	
			IR_{50}	40 ± 3	**12 ± 2**	-2.1 ± 0.5		7	
071803	1.30	3.46 ± 0.05	**post-IR IR_{225}**	80 ± 1 $_{(n=6)}$	**23 ± 3**	1.3 ± 0.2	26 ± 4	2	14
			IR_{50}	76 ± 4	22 ± 3	2.9 ± 0.4	**29 ± 5**	8	
			post-IR IR_{300}	86 ± 5	**25 ± 4**	0.6 ± 0.4	26 ± 4	6	
			IR_{50}	66 ± 4	**19 ± 3**	0.9 ± 0.9		6	
071806	2.80	3.50 ± 0.05	**post-IR IR_{225}**	212 ± 5 $_{(n=6)}$	**60 ± 9**	1.2 ± 0.2	67 ± 10	3	15
			IR_{50}	175 ± 5	50 ± 7	2.8 ± 0.2	**65 ± 10**	4	
			post-IR IR_{300}	285 ± 11	**74 ± 11**	-0.4 ± 0.5	74 ± 11	5	
			IR_{50}	156 ± 9	**45 ± 7**	-3.1 ± 1.5		6	
071807	3.75	3.58 ± 0.05	**post-IR IR_{225}**	232 ± 7 $_{(n=6)}$	**65 ± 10**	1.1 ± 0.2	71 ± 11	4	15
			IR_{50}	202 ± 11	56 ± 9	2.5 ± 0.1	**71 ± 11**	6	
			post-IR IR_{300}	261 ± 26	**73 ± 13**	1.1 ± 0.5	80 ± 15	10	
			IR_{50}	182 ± 22	**51 ± 10**	-1.8 ± 0.6		12	
071809	5	3.69 ± 0.04	**post-IR IR_{225}**	257 ± 16 $_{(n=3)}$	**70 ± 11**	0.8 ± 0.1	75 ± 12	6	15
			IR_{50}	290 ± 70	79 ± 22	2.6 ± 0.2	**101 ± 29**	24	
			post-IR IR_{300}	231 ± 9	**63 ± 9**	0.6 ± 0.1	66 ± 10	4	
			IR_{50}	156 ± 19	**42 ± 8**	-2.1 ± 1.7		12	
071810	8	3.30 ± 0.05	**post-IR IR_{225}**	454 ± 24 $_{(n=3)}$	**138 ± 22**	1.3 ± 0.1	156 ± 24	5	15
			IR_{50}	433 ± 80	131 ± 31	3.0 ± 0.2	**176 ± 42**	19	
			post-IR IR_{300}	640 ± 27	**194 ± 30**	1.5 ± 0.7	224 ± 38	5	
			IR_{50}	529 ± 102	**161 ± 39**	-0.5 ± 0.8		19	
071812	15	3.29 ± 0.06	**post-IR IR_{225}**	805 ± 65 $_{(n=6)}$	**245 ± 42**	1.0 ± 0.2	269 ± 46	8	15
			IR_{50}	517 ± 29	157 ± 25	2.4 ± 0.2	**199 ± 32**	6	
			post-IR IR_{300}	1321 ± 231	**401 ± 92**	0.7 ± 0.4	429 ± 100	18	
			IR_{50}	463 ± 61	**141 ± 28**	-1.3 ± 0.9		13	
071813	18	3.30 ± 0.04	**post-IR IR_{225}**	1188 ± 155 $_{(n=6)}$	**360 ± 71**	1.5 ± 0.3	415 ± 83	13	15
			IR_{50}	812 ± 85 $_{(n=6)}$	246 ± 45	2.9 ± 0.2	**328 ± 60**	11	
			post-IR IR_{300}	1604 ± 162 $_{(n=3)}$	**486 ± 88**	-0.3 ± 0.4	491 ± 89	10	
			IR_{50}	796 ± 66 $_{(n=5)}$	**241 ± 41**	-0.5 ± 0.4		8	

Table VI.3: *Summary of calculated dose rates, equivalent doses (D_e), uncorrected ages, fading rates (g_{2days}), fading-corrected ages, random (σ_r) and systematic (σ_s) uncertainties. Dose rates were obtained using the radionuclide activity concentrations from Timar et al. (2010; their Table S3) and the conversion factors of Adamiec and Aitken (1998). Correction of alpha, beta and gamma contributions for the effect of moisture used a time-averaged water content of 20 ± 5 % (Balescu et al., 2003). A mean a-value of 0.08 ± 0.02 was used (Rees-Jones, 1995). The error assessment system proposed by Aitken and Alldred (1972) and Aitken (1976) was used in calculating uncertainties on the age results. The number of aliquots included in the average De value is given between brackets. The random uncertainty is mentioned with dose rates, D_e and*

g_{2days}. Uncertainties mentioned with the age results (uncorrected and corrected for fading) are overall uncertainties. Random uncertainties for the IR_{50} signal measured after signal include fading rate uncertainty. All uncertainties represent one sigma. The stratigraphic position of the samples is indicated in the left column.

VI.5. Summary of IRSL and post-IR_T results

This paper evaluates the performance and dating potential of two post-IR IR_T protocols using polymineral fine grains extracted from the Romanian loess-palaeosol sequence near Mircea Vodă. The post-IR IR_{225} signal is observed to successfully pass the SAR performance tests in terms of recycling ratio, recuperation and dose recovery (Table VI.2). As found by Buylaert et al. (2009) and Thiel et al. (2010), the fading rates measured for this signal are significantly smaller than the values obtained for the corresponding IR_{50} signal (Table VI.3). Therefore, the post-IR IR_{225} signal appears be suitable for obtaining reliable age results for the investigated samples. Furthermore, both the natural and laboratory-induced signals were observed to correspond to the saturating region of the dose response curve (Figs. VI.2e and VI.4b). This indicates that the observed fading is probably an artefact of the measurement procedure, thus excluding the need for fading correction. A similar observation was recently reported by Thiel et al. (2011b) using a post-IR IR_T signal stimulated at 290 ^oC for loess older than 750 ka from Austria.

For samples collected from the loess units L1 and L2, the post-IR IR_{300} signal seems to have a similar dating potential as the post-IR IR_{225} (Table VI.3). In addition, the fading rates measured for this signal appear even lower than for the post-IR IR_{225} signal (Table VI.3). However, for some of the measured aliquots of the lowermost sample (GLL-071813), the natural signal appears to fall above the saturation level of the dose response curve (Fig. VI.2f). The same behaviour was observed in dose recovery measurements for samples GLL-071812 and -13 (Figs. VI.4c and d). It appears that artificial irradiation with large doses leads to initial sensitivity changes that the SAR protocol is unable to correct for. Several studies report a similar behaviour for quartz OSL signals (Yoshida et al., 2000; Bailey et al., 2005), but we have no knowledge of a similar observation in IRSL dating. Further investigations are necessary in order to document this anomalous behaviour and therefore, we refrain from further discussion of the age results obtained using the post-IR IR_{300} signal.

The two IRSL signals stimulated at 50 ^{o}C (after preheats at either 250 °C or 325 °C), appear to have different characteristics. A poor performance in the dose recovery test was observed when a preheat at 250 ^{o}C is applied (Fig. VI.3a). This was not unexpected as our previous investigations using conventional IR_{50} indicated the occurrence of temperature-dependent initial sensitivity changes (Vasiliniuc et al., submitted-c). On the other hand, for the IR_{50} signal measured after preheating at 325 ^{o}C, the dose recovery test is successfully passed (Fig. VI.3b). Furthermore, the two signals appear to be affected by anomalous fading to different extents (see Table VI.3). The overall average fading rate for the IR_{50} signal measured after preheating at 325 ^{o}C (-1.2 ± 0.4 %/decade) indicates that this signal may not be affected by anomalous fading. Our previous investigations using conventional IR stimulation at 50 ^{o}C (Vasiliniuc et al., submitted-c) indicated that fading rates decrease with the increase of preheat temperature. This was also observed for two K-feldspar samples by Murray et al. (2009). However our results indicate that a negative fading rate for the IR_{50} recorded after a preheat at 325 ^{o}C may be systematic (except sample GLL-071803, the rest of the samples exhibit a negative average fading rate; see Table VI.3). On the other hand, the IR_{50} signal obtained after preheating at 250 ^{o}C is indeed affected by fading (overall average g-value: 2.7 ± 0.1 %/decade). The fading-corrected ages obtained using this signal appear to agree with the previously reported silt-sized quartz OSL ages (Fig. VI.6a) for samples in the uppermost loess unit. The agreement is considered a coincidence since the D_e values obtained for this signal are offset by initial sensitivity changes as indicated by the dose recovery test (Fig. VI.3a; Table VI.3).

The uncorrected age results obtained using the IR_{50} signal after preheating at 325 ^{o}C are generally agreeing with the quartz OSL ages for all investigated samples (see Section VI.4; Fig. VI.6a). However this agreement is not considered reliable for the following reasons: (i) the uncorrected IR_{50} age results appear consistent with the silt-sized quartz ages for samples expected to have ages older than 250 ka (Timar et al., 2010) and (ii) the $D_e$values obtained using this signal are generally lower than the D_e values obtained for the other investigated signals (IR_{50} and post-IR IR_T). It may be that due to the small intensity of the signal, our fading measurements were not able to accurately constrain the fading rate for this signal. Further measurements of this signal on a large number of aliquots are therefore necessary in order to document fading and the cause of the small D_e values obtained.

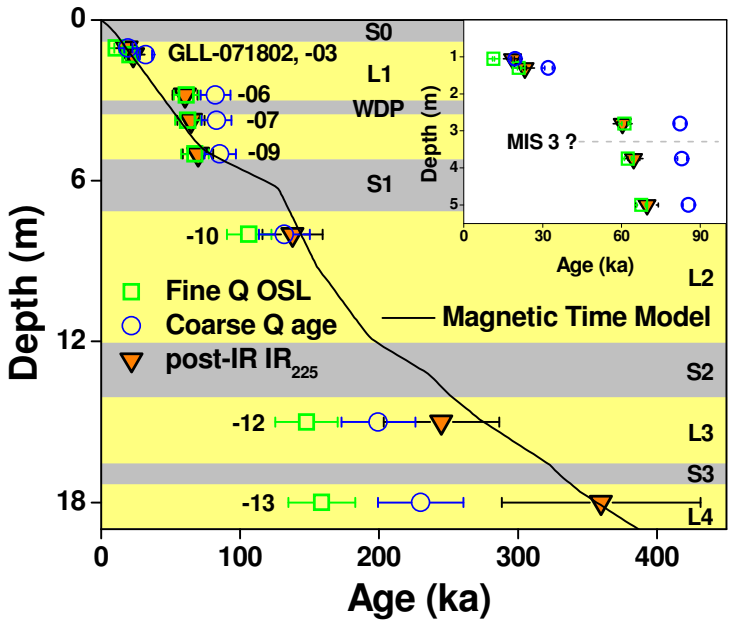

Figure VI.7: *Summary of uncorrected post-IR IR_{225} ages versus depth. The silt- and sand-sized quartz OSL ages and palaeomagnetic time-depth model (Timar et al., 2010 and Timar Gabor et al., 2011) are shown as well. The error bars 1σ total uncertainty. The inset shows the results (1σ random uncertainty) obtained for the uppermost loess unit L1.*

VI.6. Discussion of post-IR IR_{225} ages

In Fig. VI.7 the uncorrected post-IR IR_{225} ages, are presented, together with the two sets of OSL ages obtained by Timar et al. (2010) and Timar-Gabor et al., (2011) using either silt-sized (4-11µm) and fine sandy (63-90 µm) quartz, together with the magnetic time-depth model proposed by Timar et al. (2010). As shown in Fig. VI.6b, the post-IR IR_{225} age results obtained for the samples in L1 and L2 are generally consistent with the silt-sized quartz OSL ages, whereas for the samples collected from L3 and L4 the ages based on both types of quartz grain-size are increasingly underestimated. However, the ages based on the coarser quartz fraction (63-90 µm) appear consistent within one and two standard errors with the post-IR IR_{225} ages for samples GLL-071812 and -13 respectively. Nevertheless, considering the possible limitations of quartz-based SAR-OSL dating of older samples (Murray et al., 2007), the observed underestimation of quartz-based ages is not surprising.

Balescu et al. (2010) dated a sample collected from the loess unit L3 at the same depth as sample GLL-071812 using conventional IRSL applied on coarse-grained alkaline feldspars. Their age of 279 ± 41 ka is in excellent agreement with the post-IR IR_{225} age obtained in this study (245 ± 46 ka). This independent result, together with the age of ~ 270 ka suggested by the magnetic time-depth model (Timar et al., 2010), support an older depositional age for the material collected at this depth than the age obtained for the 63-90 μm quartz fraction (Timar Gabor et al. 2011). Due to interpolation of the natural signal close to or in the saturating region of the dose response curve (Fig. VI.2e), the accuracy of the age obtained for sample GLL-071813 is questionable (Wintle and Murray, 2006) and the post-IR IR_{225} age of 360±71 ka is interpreted as a minimum age.

An underestimation of the silt-sized quartz OSL age obtained by Timar et al. (2010) for sample GLL-071802 was also observed when it was compared with the IRSL signal for polymineral fine grains stimulated at 125 ^{o}C and detected in the UV region (Vasiliniuc et al., submitted-b). As IRSL signals are more difficult to bleach in nature than OSL signals from quartz (Godfrey-Smith et al., 1988; Thomsen et al., 2008a), a possible explanation for apparent underestimation of the quartz OSL ages may be incomplete resetting of the IRSL signals for the polymineral fine grains. One possible cause of incomplete resetting may be soil formation processes (such as bioturbation) during the Holocene (Timar Gabor, 2010).

It is considered that the post-IR IR_{225} ages (uncorrected for fading) are reliable and may be used as an independent age control. As such, they provide additional support for the silt-sized quartz OSL chronology over the last interglacial-glacial period. These datasets allocate the weak palaeosol in L1 and three uppermost palaeosols in the section (S1, S2 and S3; see Timar et al., 2010) to MIS 3, 5, 7 and 9 respectively. In addition, the change in sedimentation rate observed by Timar et al. (2010) to coincide with the transition from MIS 4 to MIS 3 is considered reliable/accurate.

VI.7. Conclusions

The two post-IR IR_T signals investigated in this paper appear not to suffer from anomalous fading and, in theory, either may be used to obtain ages for Romanian loess deposits without the need for any correction factor. However, of the two signals, the ages obtained from

the post-IR IR_{225} signal are in agreement with the OSL ages for silt-sized quartz for samples collected from the uppermost loess unit L1 and with independent age control for samples collected deeper down the section (in L2, L3 and L4). The post-IR IR_{300} signal appears to suffer from dose dependent initial sensitivity changes that hamper its use for the oldest samples investigated. Use of the post-IR IR_{225} signal uncorrected for fading is recommended for dating these deposits.

The IRSL signals obtained for stimulation at 50 ^{o}C do not provide reliable age results due to either initial sensitivity changes or, as in the case of measurements made after a preheat applied at 325 °C, inappropriate fading measurement.

SUMMARY AND CONCLUSIONS

Summary and Conclusions

Summary

One of the aims of this PhD project was to extend the quartz OSL investigations in order to see whether the discrepant behaviour observed at Mircea Vodă (Timar et al., 2010 and Timar Gabor et al., 2011) is a general feature of loess in the region. Our study of quartz extracted from the loess sequence at Mostiştea used the same methodology as that used in the studies of Timar et al. (2010) and Timar Gabor et al., (2011). The signals selected for analysis from both grain-size fractions of quartz appear very similar to the ones investigated for samples at Mircea Vodă. The dominance of the fast component in the OSL signals is indicated by the decay shape of the CW-OSL signal and by LM-OSL comparisons with calibration quartz. Furthermore, both quartz fractions passed the procedural tests of the single-aliquot regenerative-dose (SAR) protocol (i.e. recycling ratio, recuperation and dose recovery) indicating that the protocol should provide reliable D_e values. However, the age results obtained for the two fractions are generally inconsistent; similarly to the results obtained by Timar Gabor et al. (2011) at Mircea Vodă (i.e. the sand-sized quartz ages are generally older than the silt-sized quartz ages). The age discrepancy resides in the D_e values obtained for the two quartz fractions.

High resolution anneal experiments exclude a possible contribution from a thermally unstable component to the OSL signals from both fractions. Furthermore, the possibility of incomplete bleaching of the OSL signal in the sand-sized quartz does not seem to hold as residual doses up to more than 100 Gy are needed to compensate for the difference in D_e.

The only difference between the two quartz fractions is in the saturation characteristics of the dose response curves. For both fractions the dose response curves are best fitted with the sum of two saturating exponential terms. Moreover, for each of the quartz fractions the saturation characteristics are independent of the age or the sample. However, the characteristic saturation dose values for the two exponential functions that fit the dose-response curves are significantly higher for the silt-sized fraction than for the sand-sized fraction. Since the equivalent doses of our samples (at least for the coarse grains) are obtained by interpolating on a region of the dose

response curve where the first exponential component is already in saturation, the reliability of using this region of the dose response curve for quartz SAR-OSL dating is questionable.

The main objective of this work was to use luminescence signals from feldspars in order to establish an accurate chronology for Romanian loess. Three different measurement procedures were applied to polymineral fine grains extracted from the loess sequence at Mircea Vodă: double-SAR, conventional IRSL and post-IR IRSL. These are all based on the SAR protocol, the most robust measurement routine available at the moment.

The two signals obtained using the double-SAR protocol, IRSL and post-IR OSL, successfully passed laboratory tests, indicating that the protocol is suitable for D_e determination for both signals. However, the optical separation of the contributions from quartz and feldspar does not appear to be total. The IRSL and post-IR OSL signals exhibit anomalous fading, and the ages derived from these signals are therefore dependent on the fading correction model. Further improvements in the protocol may be achieved by finding the optimum measurement conditions in order to have a better separation of the two contributions. Nevertheless, a general agreement was obtained between the fading corrected age results obtained with both IRSL and post-IR OSL signals and the silt-sized quartz OSL ages obtained by Timar et al. (2010). However, since the quartz OSL ages were interpreted as underestimates for material deposited before the last interglacial period, this agreement is considered valid only for samples collected from the uppermost loess unit L1. The chronology of the loess sequence near Mircea Vodă could not be extended beyond the last glacial period due to limitations of the fading correction method.

The further application of conventional IRSL procedure (IR stimulation at 50 ^{o}C) to date polymineral fine grains extracted from Romanian loess was rather problematic. Dose recovery experiments indicate that the SAR protocol is unable to recover a known given dose when high temperature preheats are employed. This corroborated the need to use signals obtained after low preheat treatments. However, age results obtained using a preheat at 115 ^{o}C for 60 s were significantly underestimating the previously obtained silt-sized quartz OSL ages. Pulse anneal and combined IR/TL experiments indicated that the underestimation is caused by a thermally unstable contribution to the regenerated signals.

It is considered that the conventional IRSL approach is not able to provide accurate depositional ages for Romanian loess due to initial sensitivity changes that occur when a high preheat treatment is applied and/or to contributions from thermally unstable components

observed after low preheats. Furthermore, initial results obtained for polymineral fine grains extracted from the loess sequence at Belotinac (Serbia) indicate that this problem may not be specific to Romanian loess.

The third procedure that we applied is based on the recently proposed post-IR IRSL protocol. The two post-IR IR_T signals were documented using a modified SAR protocol. The post-IR IR_{225} signal is observed to successfully pass the SAR performance tests in terms of recycling ratio, recuperation and dose recovery. Furthermore, both natural and regenerated signals were observed to correspond to the saturating region of the dose-response curve, indicating that the small fading rate determined for this signal is probably an artefact of the measurement procedure.

The post-IR IR_{300} signal appears to have similar results in the SAR performance tests, and an even smaller fading rate than the post-IR IR_{225} signal. However this signal appears to suffer from dose dependent initial sensitivity changes that cause the observation of both natural and laboratory induced signals above the saturation level of the dose response curve. Since this anomalous behaviour is not understood, we are questioning the accuracy of the post-IR IR_{300} ages.

The ages obtained from the post-IR IR_{225} signal are in agreement with the OSL ages for silt-sized quartz for samples collected from the uppermost loess unit L1 and with independent age control for samples collected deeper down the section (in L2, L3 and L4).

The two IRSL signals stimulated at 50 ^{o}C (after preheats at either 250 °C or 325 °C), appear unsuitable for dating. On the one hand the signal obtained after preheating to 250 ^{o}C has poor performance in the dose recovery test, as expected from our previous conventional IRSL investigations. On the other hand, the thermal erosion due to the high preheat at 325 ^{o}C leads to inappropriate fading measurement.

Conclusions

Methodological

The results from the quartz-based OSL study at Mostiştea indicate that the age discrepancy observed between two grain sizes of quartz may be characteristic for loess deposits in SE Romania. The presence of an additional function, besides a single saturating exponential, in the dose response curves constructed for both types of quartz grains, may indicate that there are still unknown processess that influence the characteristics of the signals used for age determination. Therefore, these results suggested that the reliability of the age results obtained from signals with similar saturation characteristics of the dose response curve should be regarded with caution.

The experiments using polymineral fine grains extracted from the loess sequence near Mircea Vodă allowed evaluation of the potential of IRSL signals to establish an accurate chronology for this sequence.

The use of the double SAR protocol appears to be a suitable alternative for dating Romanian loess, avoiding the need to isolate pure quartz using chemical procedures. Although the IRSL and post-IR OSL signals exhibit anomalous fading, and the ages derived from these signals are therefore dependent on the fading correction model, an agreement between ages obtained using feldspar (IRSL), quartz (OSL) and/or mixed (post-IR OSL) signals increases confidence in the dating results. However, the chronology of the loess sequence near Mircea Vodă could not be extended beyond the last glacial period due to limitations of the fading correction method.

The further application of conventional IRSL procedure to date polymineral fine grains extracted from Romanian loess was rather problematic. Although previous studies on feldspars indicate that preheating may not be necessary in order to isolate a thermally stable signal, our work shows that this is not valid for the samples investigated. Moreover, our experiments show that the use of a high preheat treatment is hampered by initial sensitivity changes. Initial results for Serbian loess indicate that the problem may be more general.

The recently developed post-IR IRSL protocol was also tested using polymineral fine grains. Our observations support the previous studies reporting that the post-IR IR_T signals

obtained using an elevated stimulation temperature may not suffer from fading. Methodologically, the post-IR IR_{225} signal is considered the best alternative to date these samples as it passes all procedural checks. This is confirmed by the agreement between the uncorrected post-IR IR_{225} age results and the OSL ages for silt-sized quartz for samples collected from the uppermost loess unit L1 and with independent age control for samples collected deeper down the section (in L2, L3 and L4). The post-IR IR_{300}, however, appears to suffer from dose dependent initial sensitivity changes that hamper its use for the oldest samples investigated.

It is therefore considered that the post-IR IR_{225} signal may provide the necessary insights to clarify the age discrepancy observed in the quartz OSL studies. The use of this signal for the samples collected at Mostiştea would throw more light onto this problem.

Chronological

The age discrepancy between the silt- and sand-sized quartz grains investigated at Mostiştea appears larger than the one obtained for the loess section near Mircea Vodă.

Using alternative procedures to investigate luminescence signals from feldspars, such as the double-SAR and post-IR IRSL protocol, an independent age control was obtained for the loess sequence at Mircea Vodă. The feldspar-based age results obtained using polymineral fine grains agree with the silt-sized chronology for samples collected from the uppermost loess unit L1. This agreement increases the confidence in the reliability of silt-sized quartz as a dosimeter for the last glacial period. It further confirms that the uppermost palaeosol unit S1 has formed during MIS 5 and that the change in sedimentation rate observed for the L1 unit corresponds to the formation of a weakly developed palaeosol during MIS 3. Furthermore, the post-IR IR_{225} ages correlate the formation of the lower palaeosols, S2 and S3, during MIS 7 and 9 respectively.

Our work brings further evidence that the S1 and S2 units can no longer be thought of as interstadial soils that developed during the Last Glacial, indicating that the chronostratigraphical framework proposed by Conea (1969) is not accurate. Furthermore, the obtained age results are further confirming the potential of luminescence dating to detect variations in dust transport and deposition and also to assess the reliability of proxy-based methods.

A further direction of study would be to extend the post-IR IRSL investigations to other representative loess sequences in Romania. The promising results obtained using these signals may allow an extended chronological correlation of loess deposition in this region.

REFERENCES

References

Adamiec, G., Aitken, M., 1998. Dose-rate conversion factors: update. Ancient TL 16, 37-50.

Aitken, M.J., 1976. Thermoluminescent age evaluation and assessment of error limits: a revised system. Archaeometry 18, 233-238.

Aitken, M.J., 1985. Thermoluminescence Dating. Academic Press, London.

Aitken, M.J., 1998. An Introduction to Optical Dating. The dating of Quaternary Sediments by the Use of Photon-stimulated Luminescence. Oxford University Press, Oxford.

Aitken, M.J., Alldred, J.C., 1972. The assessment of error limits in thermoluminescence dating. Archaeometry 14, 257-267.

Auclair, M., Lamothe, M., Huot, S., 2003. Measurement of anomalous fading for feldspar IRSL using SAR. Radiation Measurements 37, 487-492.

Bailey, R.M., Armitage, S.J., Stokes, S., 2005. An investigation of pulsed-irradiation regeneration of quartz OSL and its implications for the precision and accuracy of optical dating. Radiation Measurements 39, 347-359.

Balescu, S., Lamothe, M., Mercier, N., Huot, S., Balteanu, D., Billiard, A., Hus, J., 2003. Luminescence chronology of Pleistocene loess deposits from Romania: testing methods of age correction for anomalous fading in alkali feldspars. Quaternary Science Reviews 22, 967-973.

Balescu, S., Lamothe, M., Panaiotu, C., Panaiotu, C., 2010. La chronologie IRSL des séquences loessiques de l'Est de La Roumanie. Quaternaire 21, 115-126.

Ballarini, M., Wallinga, J., Wintle, A.G., Bos, A.J.J., 2007. A modified SAR protocol for optical dating of individual grains from young quartz samples. Radiation Measurements 42, 360-369.

Banerjee, D., Murray, A.S., Bøtter-Jensen, L., Lang, A., 2001. Equivalent dose estimation using a single aliquot of polymineral fine grains. Radiation Measurements 33, 73-94.

Basarin, B., Vandenberghe, D.A.G., Marković, S.B., Catto, N., Hambach, U., **Vasiliniuc, S.,** Derese, C., Roncevic, S., Vasiljević, A., Lj Rajić, Dj., 2011. The Belotinac section (Southern Serbia) at the southern limit of the European loess belt: initial results. Quaternary International 240 (1-2), 128-138.

Bateman, M.D., Boulter, C.H., Carr, A.S., Frederick, C.D., Peter, D., Wilder, M., 2007. Detecting post-depositional sediment disturbances in sandy deposits using optical luminescence. Quaternary Geochronology 2, 57-64.

Berger, G.W., Chen, R., 2011. Error analysis and modeling of double saturating exponential dose response curves from SAR OSL dating. Ancient TL 29, 9-14.

Blair, M.W., Yukihara, E.G., McKeever, S.W.S., 2005. Experiences with single-aliquot OSL procedures using coarse-grain feldspars. Radiation Measurements 37, 361-374.

Bøtter-Jensen, L., Jungner, H., Mejdahl, V., 1993. Recent developments of OSL techniques for dating quartz and feldspars. Radiation Protection Dosimetry 47, 643-648.

Bøtter-Jensen, L., Murray, A.S., 1999. Developments in optically stimulated luminescence techniques for dating and retrospective dosimetry. Radiation Protection Dosimetry 84, 307-315.

Bøtter-Jensen, L., Duller, G.A.T., Murray, A.S., Banerjee, D., 1999. Blue light emitting diodes for optical stimulation of quartz in retrospective dosimetry and dating. Radiation Protection Dosimetry 84, 335-340.

Bøtter-Jensen, L., McKeever, S.W.S., Wintle, A.G., 2003. Optically Stimulated Luminescence Dosimetry. Elsevier Science, The Netherlands.

Bøtter-Jensen, L., Andersen, C.E., Duller, G.A.T., Murray A.S., 2003. Developments in radiation, stimulation and observation facilities in luminescence measurements. Radiation Measurements 37, 535-541.

Buggle, B., Glaser, B., Zöller, L., Hambach, U., Marković, S., Glaser, I., Gerasimenko, N., 2008. Geochemical characterisation and origin of Southeastern and Eastern European loesses (Serbia, Romania, Ukraine). Quaternary Science Reviews 27, 1058-1075.

Buggle, B., Hambach, U., Glaser, B., Gerasimenko, N., Marković, S., Glaser, I., Zöller, L., 2009. Stratigraphy, and spatial and temporal paleoclimatic trends in Southeastern/Eastern European loess paleosol sequences. Quaternary International 196, 86-106.

Buylaert, J.P., Murray, A.S., Huot, S., Vriend, M.G., Vandenberghe, D., De Corte, F., Van den haute P., 2006. A comparison of quartz OSL and isothermal TL measurements on Chinese loess. Radiation Protection Dosimetry 119 (1-4), 474-478.

Buylaert, J.P., Vandenberghe, D., Murray, A.S., Huot, S., De Corte, F., Van den haute P., 2007. Luminescence dating of old (>70 ka) Chinese loess: a comparison of single aliquot OSL and IRSL measurements. Quaternary Geochronology 2, 9-14.

Buylaert, J.P., Murray, A.S., Vandenberghe, D., Vriend, M., De Corte, F., Van den haute, P., 2008. Optical dating of Chinese loess using sand-sized quartz: establishing a time frame for Late Pleistocene climate changes in the western part of the Chinese Loess Plateau. Quaternary Geochronology 3, 99-113.

Buylaert, J.P, Murray, A.S., Thomsen, K.J., Jain, M., 2009. Testing the potential of an elevated temperature IRSL signal from K-feldspar. Radiation Measurements 44, 560-565.

Buylaert, J.P., Huot, S., Murray, A.S., van den Haute, P., 2011. Infrared stimulated luminescence dating of an Eemian (MIS 5e) site in Denmark using K-feldspar. Boreas 40, 46-56.

Buylaert, J.-P., Thiel, C., Murray, A.S., Vandenberghe, D.A.G., Yi, S., Lu, H., submitted for publication. IRSL and post-IR IRSL residual doses recorded in modern dust samples from the Chinese loess plateau. Geochronometria.

Choi, J.H., Murray, A.S., Cheong, C.S., Hong, D.G., Chang, H.W., 2003. The resolution of stratigraphic inconsistency in the luminescence ages of marine terrace sediments from Korea. Quaternary Science Reviews 22, 1201-1206.

Codrea, V., 1998. Geologia Cuaternarului. Noţiuni de bază. (Quaternary Geology. Basic notions) Babeş-Bolyai University, Cluj Napoca.

Conea, A., 1969. Profils de loess en Roumanie. La stratigraphy des loess d'Europe. In: Fink J, ed., Bulletin de l'Association Française pour l'étude du Quaternaire. Suppl. INQUA: 127-134.

Conea, A., 1970. Formaţiuni Cuaternare în Dobrogea (loessuri şi paleosoluri) (Quaternary units in Dobrogea). Editura Academiei RSR, Bucureşti: 234 pp (in Romanian).

Duller, G.A.T., 1994. A new method for the analysis of infrared stimulated luminescence data from potassium feldspars. Radiation Measurements 23, 675-682.

Duller, G.A.T., 1997. Behavioural studies of stimulated luminescence from feldspars. Radiation Measurements 27, 663-694.

Duller, G.A.T., 2003. Distinguishing quartz and feldspar in single grain luminescence measurements. Radiation Measurements 37, 161-165.

Duller G.A.T., Wintle, A.G., 1991. On infrared stimulated luminescence at elevated temperatures. Nuclear Tracks and Radiation Measurements 18, 379-384.

Duller, G.A.T., Bøtter-Jensen, L., 1993. Luminescence from potassium feldspars stimulated by infrared and green light. Radiation Protection Dosimetry 47, 683-688.

Fan, A., Li, S-H., Li B., 2011. Observation of unstable fast component in OSL of quartz. Radiation Measurements 46, 21-28

Frechen, M., Schweitzer, U., Zander, A., 1996. Improvements in sample preparation for the fine grain technique. Ancient TL 14, 15-17.

Frechen, M., Oches, E.A., Kohfeld, K.E., 2003. Loess in Europe – mass accumulation rates during the Last Glacial Period. Quaternary Science Reviews 22, 1835-1857.

Frechen, M., 2011. Loess in Eurasia. Quaternary International 234, 1-3.

Godfrey-Smith, D.I., Huntley, D.J., Chen, W.-H., 1988. Optical dating studies of quartz and feldspar sediment extracts. Quaternary Science Reviews 7, 373-380.

Haase, D., Fink. J., Haase, G., Ruske, R., Pecsi M., Richter, H., Altermann, M., Jager, K.-D., 2007. Loess in Europe – its spatial distribution based on a European Loess Map, scale 1:2,500,000. Quaternary Science Reviews 26, 1301-1312.

Huntley, D.J., 2006. An explanation of the power-law decay of luminescence. Journal of Physics: Condensed Matter, 18, 1359-1365.

Huntley, D.J., Lamothe, M., 2001. Ubiquity of anomalous fading in K-feldspars and the measurement and correction for it in optical dating. Canadian Journal of Earth Sciences 38, 1093-1106.

Huntley, D.J., Lian, O.B., 2006. Some observations on tunnelling of trapped electrons in feldspars and their implications for optical dating. Quaternary Science Reviews 25, 2503-2512.

Huot, S., Lamothe, M., 2003. Variability of infrared stimulated luminescence properties from fractured feldspar grains. Radiation Measurements 37, 499-503.

Hütt, G., Jaek, I., Tchonka, J.,1988. Optical dating: K-feldspars optical response stimulation spectra. Quaternary Science Reviews 7, 381-385.

Jain, M., Singhvi, A.K., 2001. Limits to depletion of blue-green light stimulated luminescence in feldspars: implications for quartz dating. Radiation Measurements 33, 883-892.

Jain, M., Murray, A.S., Bøtter-Jensen, L., 2003. Characterisation of blue-light stimulated luminescence components in different quartz samples: implications for dose measurement. Radiation Measurements 37, 441-449.

Jain, M., Ankjaergaard K., 2011. Towards a non-fading signal in feldspar: Insight into charge transport and tunnelling from time-resolved optically stimulated luminescence. Radiation Measurements 46, 292-309.

Kars, R.H., Wallinga, J., Cohen K.M., 2008. A new approach towards anomalous fading correction for feldspar IRSL dating – tests on samples in field saturation. Radiation Measurements 43, 786-790.

Kars, R.H., Wallinga, J., 2009. IRSL dating of K-feldspars: Modelling natural dose response curves to deal with anomalous fading and trap competition. Radiation Measurements 44, 594-599.

Kim, J.C., Roberts, H.M., Duller, G.A.T., Lee, Y.I., Yi, S.B., 2009. Assessment of diagnostic tests for evaluating the reliability of SAR (De) values from polymineral and quartz fine grains. Radiation Measurements 44, 149-157.

Krbetschek M.R., Götze J., Dietrich, A., Trautmann, T., 1997. Spectral information from minerals relevant for luminescence dating. Radiation Measurements 27, 695-748.

Kukla, G.J, Bender, M.L., Beaulieu, J-L., 2002. Last interglacial climates. Quaternary Research 58, 2-13.

Lai, Z.P., 2006. Testing the use of an OSL standardised growth curve (SGC) for D_e determination on quartz from the Chinese Loess Plateau. Radiation Measurements 41, 9-16.

Lai, Z.P., Brückner, H., Zöller, L., Fülling, A., 2007. Existence of a common growth curve for silt-sized quartz OSL of loess from different continents. Radiation Measurements 42, 1432-1440.

Lai, Z.P., Brückner, H., Fülling, A., Zöller, L., 2008. Effects of thermal treatment on the growth curve shape for OSL of quartz extracted from Chinese loess. Radiation Measurements 43, 763-766.

Lai, Z.P., 2010. Chronology and the upper dating limit for loess samples from Luochuan section in the Chinese Loess Plateau using quartz OSL SAR protocol. J. Asian Earth Science, 37, 176-185.

Lamothe, M., Auclair, M., 1997. Assessing the datability of young sediments by IRSL using an intrinsic laboratory protocol. Radiation Measurements 27, 107-118.

Lamothe, M., Auclair, M., 1999. A solution to anomalous fading and age shortfalls in optical dating of feldspar minerals. Earth and Planetary Science Letters 171, 319-323.

Lamothe, M., Auclair, M., 2000. The *fadia* method: a new approach in luminescence dating using the analysis of single feldspars grains. Radiation Measurements 32, 433-438.

Lamothe, M., Auclair, M., Hamzaoui, C., Huot, S., 2003. Towards a prediction of long-term anomalous fading of feldspar minerals. Radiation Measurements 37, 493-498.

Lang, A., Lindauer, S., Kuhn, R., Wagner, G.A., 1996. Procedures used for optically and infrared stimulated luminescence dating of sediments in Heidelberg. Ancient TL 14, 7-11.

Li, S.-H., 1991. Removal of the thermally unstable signal in optical dating of K-feldspar. Ancient TL 9 (2), 26-29.

Li, S.-H., Wintle, A.G., 1992. A global view of luminescence signals from loess. Quaternary Sci. Rev. 11, 133-137.

Li, B., Li, S.-H., 2006. Comparison of D_e estimates using the fast component and the medium component of quartz OSL. Radiation Measurements 41, 125-136.

Li, B., Li, S.-H., 2011. Thermal stability of infrared stimulated luminescence of sedimentary K-feldspar. Radiation Measurements 46, 29-36.

Lisiecki, L.E., Raymo, M.E., 2005. A Pliocene Pleistocene stack of 57 globally distributed benthic d18O records, Paleoceanography 20, PA1003, doi:10.1029/2004PA001071.

Lowick, S.E., Preusser, F., Pini, R., Ravazzi, C., 2010a. Underestimation of fine grain quartz OSL dating towards the Eemian: comparison with palynostratigraphy from Azzano Decimo, northeastern Italy. Quaternary Geochronology 5, 583-590.

Lowick, S.E., Preusser, F., Wintle, A.G., 2010b. Investigating quartz optically stimulated luminescence dose-response curves at high doses. Radiation Measurements 45, 975-984.

Lowick, S.E., Preusser, F., 2011. Investigating age underestimation in the high dose region of optically stimulated luminescence using fine grain quartz. Quaternary Geochronology 6, 33-41.

Maher, B.A., 2011. The magnetic properties of Quaternary aeolian dusts and sediments, and their palaeoclimatic significance. Aeolian Research 3, 87-144.

Marković, S.B., Bokhorst, M.P., Vandenberghe, J., McCoy, W.D., Oches, E.A., Hambach, U., Zöller, L., Stevens, T., Machalett, B., 2008. Late Pleistocene loess-palaeosol sequences in the Vojvodina region, north Serbia. Journal of Quaternary Science 23, 73-84.

Marković, S.B., Hambach, U., Catto, N., Jovanovic M., Buggle, B., Machalett, B., Zöller, L., Glaser, B., Frechen, M., 2009. Middle and Late Pleistocene loess sequences at Batajnica, Vojvodina, Serbia. Quaternary International 198, 255-266.

Mejdahl, V., 1979. Thermoluminescence dating: beta dose attenuation in quartz grains. Archaeometry 21, 61-67.

Mejdahl, V., Bøtter-Jensen, L., 1994. Luminescence dating of archaeological materials using a new technique based on single aliquot measurements. Quaternary Science Reviews. 7, 551–554.

Moska, P., Murray A.S., 2006. Stability of the quartz fast-component in insensitive samples. Radiation Measurements 41, 878-885.

Murray, A.S., Wintle, A.G., 2000. Luminescence dating of quartz using an improved single-aliquot regenerative-dose protocol. Radiation Measurements 32, 57-73.

Murray, A.S., Olley, J.M., 2002. Precision and accuracy in the optically stimulated luminescence dating of sedimentary quartz: a status review. Geochronometria 21, 1-16.

Murray, A.S., Wintle, A.G., 2003. The single aliquot regenerative dose protocol: potential for improvements in reliability. Radiation Measurements 37, 377-381.

Murray, A.S., Funder, S., 2003. Optically stimulated luminescence dating of a Danish Eemian coastal marine deposit: a test of accuracy. Quaternary Science Reviews 22, 1177-1183.

Murray, A.S., Svendsen, J.I., Mangerud, J., Astakhov, V.I., 2007. Quartz OSL age of an Eemian site on the Sula River, Northern Russia. Quaternary Geochronology 2, 107-109.

Murray, A., Buylaert, J-P., Henriksen, M., Svendsen, J-I., Mangerud, J., 2008. Testing the reliability of quartz OSL ages beyond the Eemian. Radiation Measurements 43, 776-780.

Murray, A.S., Buylaert, J.-P., Thomsen, K.J., Jain, M., 2009. The effect of preheating on the IRSL signal from feldspar. Radiation Measurements 44, 554-559.

Necula, C., Panaiotu, C., 2008. Application of dynamic programming to the dating of a loess palaesol sequence. Romanian Reports in Physics 60, 157-171.

Panaiotu, C.G., Panaiotu, E.C., Grama, A., Necula, C., 2001. Paleoclimatic record from loess-paleosol profile in Southeastern Romania. Physics and Chemistry of the Earth A (11-12), 893-898.

Panaiotu, C.E., Balescu, S., Lamothe, M., Panaiotu, C.G., Necula, C., Grama, A., 2004. Astronomical and luminescence dating of Lower Danubian loess (Romania). Geophysical Research Abstracts 6, 02900.

Pawley, S.M., Toms, P., Armitage, S.J., Rose, J., 2010. Quartz luminescence dating of Anglian Stage (MIS 12) fluvial sediments: Comparison of SAR age estimates to the terrace chronology of the Middle Thames valley, UK. Quaternary Geochronology 5, 569-582.

Pecsi, M., 1995. The role of principles and methods in loess-palaeosol investigations. GeoJournal 36, 117-131.

Poolton, N.R.J., Bøtter-Jensen, L., Johnsen, O., 1995. Thermo-optical properties of optically stimulated luminescence in feldspars. Radiation Measurements 24, 531-534.

Poolton, N.R.J., Wallinga, J., Murray A.S., Bulur, E., Bøtter-Jensen L., 2002a. Electrons in feldspar I: on the wavefunction of electrons trapped at simple lattice defects. Physics and Chemistry of Minerals 29, 210-216.

Poolton, N.R.J., Ozanyan K.B., Wallinga, J., Murray A.S., Bøtter-Jensen L., 2002b. Electrons in feldspar II: a consideration of the influence of conduction band-tail states on luminescence processes. Physics and Chemistry of Minerals 29, 217-225.

Poolton, N.R.J., Kars, R.H., Wallinga, J., Bos, A.J.J., 2009. Direct evidence for the participation of band-tails and excited-state tunnelling in the luminescence of irradiated feldspars. Journal of Physics: Condensed Matter 21, doi:10.1088/0953-8984/21/48/485505.

Porter, S.C., 2001. Chinese loess record of monsoon climate during the last glacial-interglacial cycle. Earth-Science Reviews 54, 115-128.

Prescott J.R., Hutton, J.T., 1994. Cosmic ray contributions to dose rates for luminescence and ESR dating: large depths and long-term time variations. Radiation Measurements 23, 497-500.

Prescott, J.R., Robertson G.B., 1997. Sediment dating by luminescence: a review. Radiation Measurements 27, 893-922.

Preusser, F., Chithambo, M.L., Götte, T., Martini, M., Ramseyer, K., Sendezera, E.J., Susino, G.J., Wintle, A.G., 2009. Quartz as a natural luminescence dosimeter. Earth-Science Reviews 97, 184-214.

Pye, K., 1995. The nature, origin and accumulation of loess. Quaternary Science Reviews 14, 653-667.

Rees-Jones, J., 1995. Optical dating of young sediments using fine-grain quartz. Ancient TL 13, 9-14.

Rees-Jones, J., Tite, M.S., 1994. Recuperation of IRSL after bleaching and consequences for dating young sediment. Radiation Measurements 23, 569-574.

Roberts, H.M., 2007. Assessing the effectiveness of the double-SAR protocol in isolating a luminescence signal dominated by quartz. Radiation Measurements 42, 1627-1636.

Roberts, H.M., 2008. The development and application of luminescence dating to loess deposits: a perspective on the past, present and future. Boreas 37, 483-507.

Roberts, H.M., Wintle, A.G., 2001. Equivalent dose determinations for polymineralic fine-grains using SAR protocol: application to a Holocene sequence of the Chinese Loess Plateau. Quaternary Science Reviews 20, 859-863.

Roberts, H.M., Duller, G.A.T., 2004. Standardised growth curves for optical dating of sediment using multiple-grain aliquots. Radiation Measurements 38, 241-252.

Schmidt, E.D., Machalett, B., Marković, S.B., Tsukamoto, S., Frechen, M., 2010. Luminescence chronology of the upper part of the Stari Slankamen loess sequence (Vojvodina, Serbia). Quaternary Geochronology 5, 137-142.

Schmidt, E.D., Frechen, M., Murray, A.S., Tsukamoto, S., Bittmann F., 2011. Luminescence chronology of the loess record from the Tönchesberg section: A comparison using quartz and feldspar as dosimeter to extend the age range beyond the Eemian. Quaternary International 234, 10-22.

Shackleton, N.J., Berger, A., Peltier, W.R., 1990. An alternative astronomical calibration of the lower Pleistocene timescale based on ODP Site 677. Transactions of the Royal Society of Edinburgh: Earth Sciences 81, 251-261.

Shen, Z., Mauz, B., 2011. Estimating the equivalent dose of late Pleistocene fine silt quartz from the Lower Mississippi Valley using a standardized OSL growth curve. Radiation Measurements 46, 649-664.

Singhvi, A.K., Stokes, S. C., Chauhan, N., Nagar, Y., C., Jaiswal, M.J., 2011. Changes in natural OSL sensitivity during single aliquot regeneration procedure and their implications for equivalent dose determination. Geochronometria 38, 231-241.

Smalley, I., 1995. Making the material: the formation of silt-sized primary mineral particles for loess deposits. Quaternary Science Reviews 14, 645-651.

Smalley, I.J., Jefferson, I.F., Dijkstra, T.A., Derbyshire, E., 2001. Some major events in the development of the scientific study of loess. Earth-Science Reviews 54, 5-18.

Smalley, I., Marković, S., Svirčev, Z., 2011. Loess is [almost totally formed by] the accumulation of dust. Quaternary International 240, 4-11.

Spooner, N.A., 1992. Optical dating: preliminary results on the anomalous fading of luminescence from feldspars. Quaternary Science Reviews 11, 139-145.

Spooner, N.A., 1994. The anomalous fading of infrared-stimulated luminescence from feldspars. Radiation Measurements 23, 625-632.

Steffen, D., Preusser, F., Schlunegger, F., 2009. OSL quartz age underestimation due to unstable signal components. Quaternary Geochronology 4, 353-362.

Stevens, T., Thomas, D.S.G., Armitage, S.J., Lunn, H.R., Lu, H., 2007. Reinterpreting climate proxy records from Late Quaternary Chinese loess: A detailed OSL investigation. Earth-Science Reviews 80, 111-136.

Stevens, T., Marković, S.B., Zech, M., Hambach, U., Sümegi, P., 2011. Dust deposition and climate in the Carpathian Basin over an independently dated last glacial-interglacial cycle. Quaternary Science Reviews 30, 662-681.

Strickertsson, K., 1985. The thermoluminescence of potassium feldspars - glow curve characteristics and initial rise measurements. Nuclear Tracks and Radiation Measurements 10, 613-617.

Sugisaki, S., Buylaert, J-P., Murray, A., Tsukamoto, S., Nogi, Y., Miura, H., Sakai, S., Iijima, K., Sakamoto, T., 2010. High resolution OSL dating back to MIS 5e in the central Sea of Okhotsk. Quaternary Geochronology 5, 293-298.

Templer, R.H., 1986. The localised transition model of anomalous fading. Radiation Protection Dosimetry 17, 493-497.

Thiel, C., Coltori, M., Tsukamoto, S., Frechen, M., 2010. Geochronology for some key sites along the coasts of Sardinia. Quaternary International 222, 36-47.

Thiel, C., Terhorst, B., Jaburová, I., Buylaert, J.P., Murray, A.S., Fladerer, F.A., Damm, B., Frechen, M., Ottner, F., 2011a. Sedimentation and erosion processes in Middle to Late Pleistocene sequences in the brickyard Langenlois/Lower Austria. Geomorphology doi:10.1016/j.geomorph.2011.02.011.

Thiel, C., Buylaert, J.P., Murray, A., Terhorst, B., Hofer, I.., Tsukamoto, S., Frechen, M., 2011b. Luminescence dating of the Stratzing loess profile (Austria) - Testing the potential of an elevated temperature post-IR IRSL protocol. Quaternary International 234, 23-31.

Thomsen, K.J., Murray, A.S., Jain, M., Bøtter-Jensen, L., 2008a. Laboratory fading rates of various luminescence signals from feldspar-rich sediment extracts. Radiation Measurements 43, 1474-1486.

Thomsen, K.J., Bøtter-Jensen, L., Jain, M., Denby, P.M., Murray A.S., 2008b. Recent instrumental developments for trapped electron dosimetry. Radiation Measurements 43, 414-421.

Thomsen, K.J., Murray, A.S., Jain, M., 2011. Stability of IRSL sigals from sedimentary K-feldspar samples. Geochronometria 38, 1-13.

Timar-Gabor A., 2010. Retrospective luminescence dosimetry: applications in archaeology, geology and environmental studies [PhD thesis]: Babeş-Bolyai University in Cluj Napoca, Romania.

Timar, A., Vandenberghe, D., Panaiotu, E.C., Panaiotu, C.G., Necula, C., Cosma, C., Van den haute, P., 2010. Optical dating of Romanian loess using fine-grained quartz. Quaternary Geochronology 5, 143-148.

Timar-Gabor, A.I., Vandenberghe, D.A.G., **Vasiliniuc, S.,** Panaiotu, C.E., Panaiotu, C.G., Dimofte, D., Cosma, C., 2011. Optical dating of Romanian loess: a comparison between sand-sized and silt-sized quartz. Quaternary International 240, 62-70.

Vandenberghe, D., De Corte, F., Buylaert, J.-P., Kučera, J., Van den haute, P., 2008. On the internal radioactivity in quartz. Radiation Measurements 41, 768-773.

Vasiliniuc, S., D.A.G. Vandenberghe, A. Timar-Gabor , C. Panaiotu, C. Cosma, P. Van den haute, submitted-a. Testing the potential of elevated temperature post-IR IRSL signals for dating Romanian loess. Quaternary Geochronology, LED 2011 proceedings.

Vasiliniuc, S., D.A.G. Vandenberghe, A. Timar-Gabor , C. Panaiotu, C. Cosma, P. Van den haute, submitted-b. Combined IRSL and Post-IR OSL dating of Romanian loess using single aliquots of polymineral fine grains. Quaternary International.

Vasiliniuc, S., Vandenberghe, D., Timar-Gabor, A., van den Haute, P., Cosma, C., submitted-c. Conventional IRSL dating of Romanian loess using single aliquots of polymineral fine grains. Radiation Measurements.

Visocekas, R. 1985. Tunneling radiative recombination in labradorite: its association with anomalous fading of thermoluminescence. Nuclear Tracks and Radiation Measurements10, 521-529.

Visocekas, R., 2002. Tunnelling in afterglow, its coexistence and interweaving with thermally stimulated luminescence. Radiation Protection Dosimetry 100, 45-54.

Visocekas, R., Spooner, N.A., Zink, A., Blanc, P. 1994. Tunnel afterglow, fading and infrared emission in thermolominescence of feldspars. Radiation Measurements 23, 377-385.

Wallinga, J., Duller, G.A.T., 2000. The effect of optical absorption on the infrared stimulated luminescence age obtained on coarse-grain feldspars. Quaternary Science Reviews 19, 1035-1042.

Wallinga, J., Murray, A., Duller, G., 2000. Underestimation of equivalent dose in single-aliquot optical dating of feldspars caused by preheating. Radiation Measurements 32, 691-695.

Wintle, A.G., 1973. Anomalous fading of thermoluminescence in mineral samples. Nature 245, 143-144.

Wintle, A.G. 1977. Detailed study of a thermoluminescent mineral exhibiting anomalous fading. Journal of Luminescence 15, 385-393.

Wintle, A.G., 1985. Stability of TL signals in fine grains from loess. Nucl. Tracks 10, 725-730.

Wintle, A.G., 1990. A review of current research on TL dating of loess. Quaternary Science Reviews 9, 385-397.

Wintle, A.G. (ed.), 2008. Special Issue: Luminescence dating of Quaternary sediments. Boreas 37, 469-677.

Wintle, A.G., 2010. Future directions of luminescence dating of quartz. Geochronometria 37, 1-7.

Wintle, A.G., Murray, A.S., 2006. A review of quartz optically stimulated luminescence characteristics and their relevance in single-aliquot regeneration dating protocols. Radiation Measurements 41, 369-391.

Yoshida, H., Roberts, R.G., Olley, J.M., Laslett, G.M., Galbraith, R.F., 2000. Extending the age range of optical dating using single 'supergrains' of quartz. Radiation Measurements 32, 439-446.

Zhang, J.F., Zhou, L.P., 2007. Optimisation of the ‘double SAR’ protocol procedure for polymineral fine grains. Radiation Measurements 42, 1475-1482.

Zöller, L., 2010. New approaches to European loess: a stratigraphic and methodical review of the past decade. Central European Journal of Geosciences 2, 19-31.

Acknowledgments

This thesis would never have taken shape without the contribution of many persons to whom I will try to acknowledge within the following lines.

First of all, I want to express my gratitude to Prof. Dr. Constantin Cosma for opening the road of scientific research and encouraging me to take the first steps. I am grateful for his guidance during the past five years and the efforts he paid for the development of the luminescence research group.

My grateful acknowledgement goes also to Prof. Dr. Peter van den haute for his efforts to establish the joint PhD collaboration with Ghent University and for the discussions that we had during my stay in Ghent. I found his experienced points of view very inspiring.

Dr. Alida Timar Gabor is the one person that has significantly contributed, as an informal promoter, to my academic life. I thank her for all the help during this period, for giving me the initial background on luminescence, taking me to meet the loess community at Loessfest in Novi Sad and much more. I am grateful to her mature advice and many encouragements in the periods when I was in difficulty and also for the great time that we had together. I wish her a successful career with many students to guide ahead.

I would also like to express my gratitude to Dr. Dimitri Vandenberghe. His guidance during my stay at Ghent University allowed me to fulfill the objectives of my work. I thank him for his patience in discussing the many subjects that I had trouble understanding and also for adding flavor to my life in Ghent. I consider him a reference for my future and hope that he will be able to inspire many researchers in the field of luminescence dating.

My humble gratefulness goes to Prof.Dr. Ann Grace Wintle for being so helpful and opened to newcomers and kindly accepting to review my work during the preparation of the thesis. I thank her for her inspiring thoughts and stimulating discussions and for accepting our invitation to Cluj Napoca.

I express my appreciation to Conf. Dr. Cristian Panaiotu for his support in the sampling campaign and providing us access to unpublished data, as well as for the helpful discussions and suggestions regarding Romanian loess deposits.

I also want to thank Prof. Dr. Andrew Murray and Dr. Jan-Pieter Buylaert for the stimulating discussion during the UK meeting in Oxford.

I would like to thank my colleagues in Cluj Napoca: Dr. Robert Begy for his help in maintaining the infrastructure of the laboratory, Dr. Mircea Moldovan and Dr. Alexandra Dinu for always offering advice, and Daniela Constantin for her enthusiasm. I wish them all a successful future.

I also want to thank Dr. Cilia Derese for her guidance in sample preparation at Ghent Luminescence Laboratory and for the great company during the UK meeting in Oxford.

I thank Dragan Popov for his warm company during the Loessfest conference in Novi Sad and the other scientific meetings we attended together.

In the end, my deepest appreciation goes to my family, soon to be family and close friends. Their constant love and support gave me the ambition to go further.